Advancing Electroanalytical Methods for Monitoring Chemical Messenger Release

Paul Logan Walsh

A dissertation submitted to the faculty of the University of North Carolina at Chapel Hill in partial fulfillment of the requirements for the degree of Doctor of Philosophy in the Department of Chemistry (Analytical).

Chapel Hill
2012

Approved by:

Dr. R. Mark Wightman

Dr. James Jorgenson

Dr. Royce Murray

Dr. Dorothy Erie

Dr. Mark Zylka

Abstract

PAUL L. WALSH: Advancing Electroanalytical Methods for Monitoring Chemical Messenger Release
(Under the direction of Dr. R. Mark Wightman)

Chemical communication between cells within the body has been long recognized as an integral part of understanding how the human body functions, especially within the central and peripheral nervous system. Electrochemistry at microelectrodes in tissue slices extracted from the body has become a method of choice for probing the release, reuptake, and overall function of chemical messengers. Here, fast-scan cyclic voltammetry (FSCV) and constant potential amperometry at carbon-fiber microelectrodes is used in various different types of tissues such as the adrenal gland and the spinal cord in order to detect and quantify the release of various chemical messengers including epinephrine, norepinephrine, and adenosine. Pharmacological manipulation of these signals allows for further analysis of the origins of these signals as well as their overall function in integral bodily functions. Work performed on the adrenal gland gave new insight into the exocytotic release characteristics of the hormones epinephrine and norepinephrine which had never been carried out in intact tissue. Also, extensive studies on the methods used to probe the release of these hormones were performed, and allowed for the distinction of electrical stimulation of two different cell types, both the neurons which innervate the tissue, and the chromaffin cells which release the neuromodulators detected with this technology. Moving the detection of adenosine by FSCV into lamina II of the spinal cord allowed for determination of enzymatic activity of ectonucleotidases. Furthermore, it provided new proof of adenosine as an antinociceptive neurotransmitter, and gave evidence for an adenosinergic tone in these circuits with the first ever detection of adenosine transients

anywhere in the nervous system. Also, total tissue analysis of various brain regions by high performance liquid chromatography (HPLC) is used to determine fundamental difference or similarities in different strains of animals, animals which have been genetically altered, or animals which have been treated with drugs. Finally, the coating of Ag/AgCl reference electrodes with Nafion for chronic implantation is discussed. These studies use fundamental analytical tools to advance our understanding of the nervous system, and shows new methods of answering long standing biological questions.

To Mom and Dad, Cathleen E. and Kevin M. Walsh

Words can never express my appreciation for all that you have done for me in my life.
You always taught me to find something I love and figure out a way to make a living at it.
This dissertation is just the start of that journey.

Acknowledgements

There are numerous people who have contributed to both the work presented here and the rest of my life over the last 5 years. There's no way a few pages can show my appreciation to all of you, but I'll try anyways. First and foremost I would like to thank my advisor, R. Mark Wightman. Your guidance and support have shaped me into the scientist I am today. While we may not have always agreed, you always made me feel like a colleague and never a subordinate, and pushed me to do my best. The rest of the Wightman lab deserves a huge thank you as well. To Jelena, Keith, and Brian, thank you for all the training and encouragement my first two years. I couldn't have taken over the cell group alone without all you taught me. To Justin, Natalie, Anna, Richard, Pasha, Nii, Khristy, Parry, Rinchen, Fabio, Beth, Zoe, Tommy, Jinwoo, Jenny and Elyse, thanks for your support, encouragement, friendship, and fun times at conferences. Many thanks to Nina for placing all my orders and putting up with me stealing the P card from her.

I would have gotten nowhere with any of this work if it wasn't for my collaborators. A huge thank you to Mark Zylka for allowing some analytical chemist to come and invade his electrophysiology lab so he could measure adenosine in the spinal cord. To Sarah Street, I've never been prouder to be co-author on a paper with anyone. I'll always remember all those long days we spent looking for transients together. Your passion for science, seeking the right answer, and the people around you are something I admire. I would also like to thank the rest of the Zylka lab for your helpful thoughts, questions, and comments. A big thanks to Tommy for helping us design the early experiments with adenosine. Thank you to

Zoe, Thorfinn, and Elyse for taking tissue punches for me for all of my HPLC experiments, and to Ben Philpot and C.J. Malanga for letting me tag onto such an amazing paper.

Names fewer who read this dissertation will recognize who also deserve my gratitude are Corey Lowen and Jay Chandler, my high school chemistry teachers, who first sparked my interest and showed me that I am good enough to take my passion this far. Also, all of my professors at the University of Mary Washington, and especially Charles Sharpless and Raymond Scott, my first research advisors who taught me how to accomplish things on my own by throwing me in a room with an instrument and a user guide and telling me to have fun.

There have been way too many friends and family members that have been there for me through thick and thin and helped me keep my sanity through this thing we call graduate school for me to mention them all by name here. Thank you to you all, especially my tennis buddies who helped me rekindle the other love of my life and coming oh so close to becoming State Champions. Thanks to Nick and Jordan for late night video games. Thanks to Joel for always being able to cheer me up with a phone call. Thanks to Anna for making me run half marathons with her. (There's only a hint of sarcasm there). Thanks to my extended family for all the fun Walsh Weekends in July. They were always a welcomed respite from the day-to-day grind at the lab in the summer.

Finally, a huge thank you to my mom and dad, Cathy and Kevin. I'm sure you know how much I appreciate all your support (both emotional and financial), but it's worth repeating: thank you and I love you.

Table of Contents

List of Tables

List of Figures

List of Abbreviations and Symbols

*	Probability Less Than 0.05
**	Probability Less Than 0.01
***	Probability Less Than 0.001
4-DAMP	4-Diphenylacetoxy-N-(2-chloroethyl)piperidine hydrochloride
A_1R	Adenosine A1 Receptor
ACh	Acetylcholine
AChR	Acetylcholine Receptor
aCSF	Artificial Cerebrospinal Fluid
ADO	Adenosine
Ag/AgCl	Silver-Silver Chloride Reference Electrode
AMP	Adenosine Monophosphate
ATP	Adenosine Triphosphate
ATR	Atropine
BBS	Bicarbonate Buffered Saline
BNST	Bed Nucleus of the Stria Terminalis
CD73	Ecto-5'-nucleotidase
CFM	Carbon-fiber microelectode

COX	Carbenoxolone
CPu	Caudate Putamen
CV	Cyclic Voltammogram or Cyclic Voltammetry
DA	Dopamine
DIP	Dipyridamole
DOPAC	3,4-Dihydroxyphenylacetic Acid
dKO	Double Knockout
DRN	Dorsal Raphe Nucleus
E	Epinephrine
E_{app}	Applied Potential
ECD	Electrochemical Detection or Electrochemical Detector
EDTA	Ethylenediaminetetra-Acetic Acid
EDS	Energy-Dispersive X-Ray Spectroscopy
EGTA	Ethylene Glycol Tetraacetic Acid
FSCV	Fast-Scan Cyclic Voltammetry
HEX	Hexamethonium
HPLC	High-Performance Liquid Chromatography
HQ	Hydroquinone

mAChR	Muscarinic Acetylcholine Receptor
mOsM	Milliosmolar
n	Number of Replicates
NAc	Nucleus Accumbens
nAChR	Nicotinic Acetylcholine Receptor
NE	Norepinephrine
NOS	Nitric Oxide Synthase
NT5E	Ecto-5'-nucleotidase
p	Probability
P-55	Thornel ® 55 Carbon Fiber
PAP	Prostatic Acid Phosphatase
PBS	Phosphate Buffered Saline
PNMT	Phenylethanolamine N-Methyltransferase
psi	Pounds Per Square Inch
Q	Charge
SEM	Scanning Electron Microscopy
SEM	Standard Error of the Mean
SNr	Substantia Nigra Reticulata

$t_{1/2}$	Full-Width at Half Height
T-650	Thornell ® 650 Carbon Fiber
TH	Tyrosine Hydroxylase
THG	Thapsigargin
Tris	Trizma ® Hydrochloride
TTX	Tetrodotoxin
VGCC	Voltage-Gated Calcium Channel
VTA	Ventral Tegmental Area
WT	Wild-Type

Chapter I

Probing Synaptic Mechanisms in Tissue Slices with Electrochemistry

Introduction

Electrochemistry at carbon-fiber microelectrodes has been recognized as a useful tool for studying electroactive neurotransmitters in living tissue since it was first demonstrated by Ralph Adams in the 1970s (Gonon et al., 1978). Carbon-fiber microelectrodes are widely used for these kinds of studies due to their large potential window, their favorable surface properties for analyzing biogenic amines, excellent sensitivity, and low noise. Furthermore, the small size of carbon-fiber microelectrodes provides excellent spatial resolution when implanted into tissue, as well as small, stable background currents when using fast scan rates during voltammetric studies. Additionally, the small size of the carbon-fiber results in little to no tissue damage compared to other methods for measuring neurotransmitters like microdialysis (Jaquins-Gerstl and Michael, 2009). While electrochemistry gives a wealth of information when it is used in whole animal studies, the use of electrochemistry at the single cell level as well as in tissue slices has profound implications for looking at the mechanisms involved in the release and uptake of neurotransmitters at the synaptic level.

Previous reviews have covered the use of electrochemical methods, especially fast-scan cyclic voltammetry for the detection of electroactive neurotransmitters in whole animal studies including freely moving animals, and individual cells for the study of vesicular events (Travis and Wightman, 1998, Robinson et al., 2008, Kim et al., 2011). In this chapter, the

various methods for neurotransmitter release and production will be discussed, as well as the various electrochemical methods used at microelectrodes to detect and quantify these chemical messengers. The focus will include the use of these electrochemical methods in tissue slices from various parts of the central and peripheral nervous system including the brain, spinal cord, and adrenal gland. There are many advantages to using tissue slice preparations including the ability to visualize the tissue underneath a microscope ensuring accurate and precise placement of the sensor, and localized and acute stimulation of the tissue being studied which allows for synapses close to the electrode to be studied. Also, when making tissue slices all inputs and outputs are severed, allowing for pharmacological manipulation of the specific region being studied without interference from afferent brain regions. Finally, applications of these methods for the study of synaptic mechanisms and transgenic disease state animal models for the quantification of neurotransmitter release will be covered.

Chemical Messenger Release and Production in Tissue Slices

Exocytosis

Katz first discovered the quantization of neurotransmitters at the neuromuscular junction in the 1950s (del Castillo and Katz, 1954). Exocytosis is the process by which individual vesicles, packets of chemical messengers, are released by a cell into the extracellular space. Figure 1.1 is a diagram which shows the various major steps of the exocytotic process. Catecholaminergic vesicles are packaged with neurotransmitters via active transport through the vesicular transporter coupled to a proton pump which allows the neurotransmitter to be loaded into the vesicle against its electrochemical gradient (Chaudhry et al., 2008). The vesicle is then segregated into different pools near the cell membrane including the readily (or immediately) releasable pool, the slowly releasable pool, both of

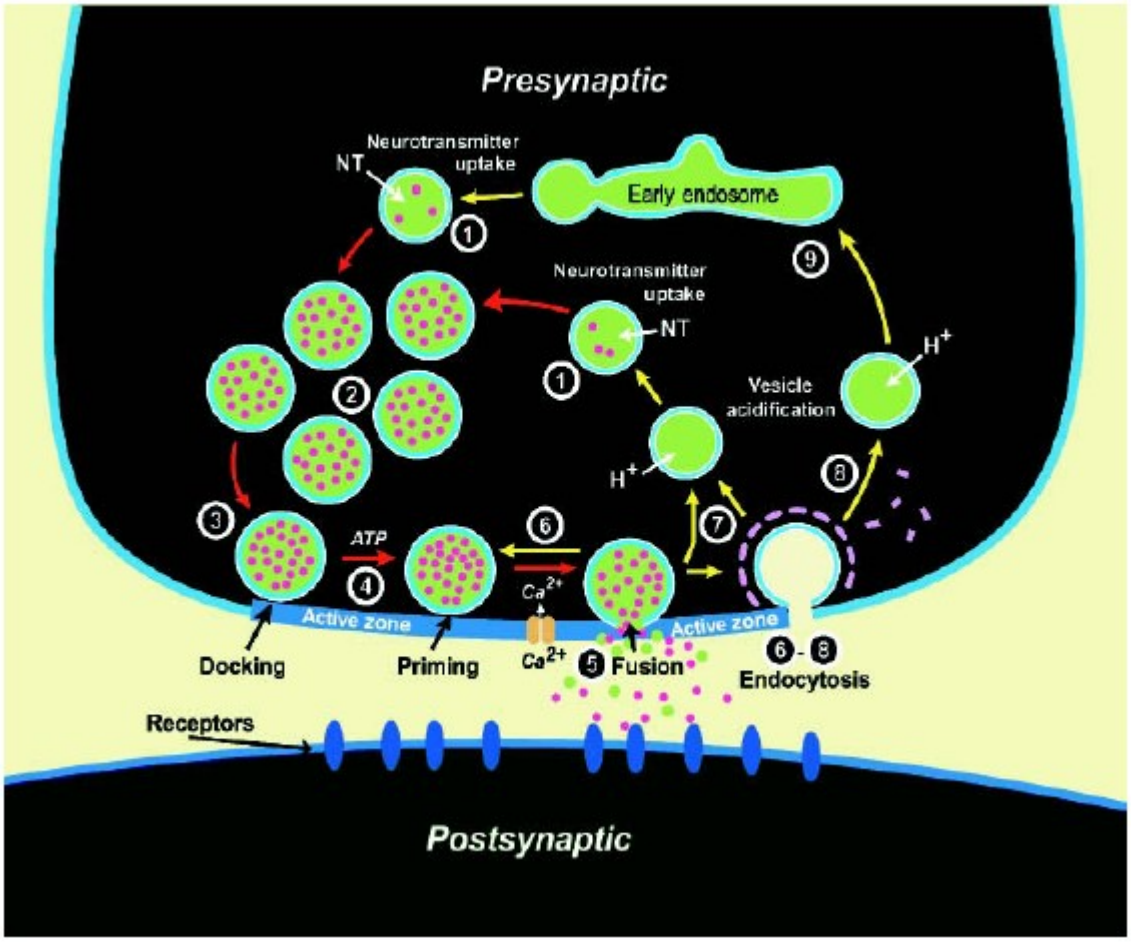

Figure 1.1. The synaptic vesicle cycle. Red arrows indicate steps in exocytosis while yellow arrows are steps in endocytosis. Synaptic vesicles are loaded with neurotransmitter via active transport (1). Vesicles are then mobilized into different pools (2), and eventually docked at the plasma membrane (3). Following the priming step in the active zone (4), the fusion pore is formed and the contents released into the extracellular space upon activation by intacellular Ca^{2+} (5). Vesicles can be recycled in a number of ways including local reuse (6), fast recycling without an endosomal intermediate (7), and clathrin mediated endocytosis with or without an endosomal intermediate (8-9) (Sudhof, 2004).

which are docked near the cell membrane, or, the unprimed pool which is near the cell membrane but has yet to be docked, and the depot (or reserve) pool which is not near the cell membrane and where the vesicles are loaded with neurotransmitter (Becherer and Rettig, 2006). Through a series of ATP-dependent active processes involving many different proteins located on both the vesicle's membrane as well as the cell membrane, the vesicle is recruited, tethered, and docked in the active zone near the presynaptic membrane (Sudhof, 2004). After a final priming step, the vesicle is then ready for a calcium dependent fusion with the cell membrane. As the cell membrane depolarizes, voltage gated calcium channels (VGCCs) open allowing calcium to rush into the cell along its electrochemical gradient. There are many different kinds of VGCCs, and the type and distribution of VGCCs a cell contains varies from cell type to cell type. The P/Q type calcium channels, however, have been shown to be functionally coupled to exocytosis (Alvarez et al., 2008). The calcium entering the cell can bind proteins including synaptotagmin, the main calcium sensor on the vesicular membrane (Xu et al., 2007). The coupling of the vesicle to the cell membrane causes a fusion pore to be formed, and the contents of the vesicle are secreted into the extracellular space. After fusion, the vesicle can then be recycled if the vesicle was not fully incorporated with the cell membrane. Otherwise, a new vesicle must be formed from the cell membrane via a process known as endocytosis.

Non-Classical Transmission

While neurotransmitters, whether packaged into vesicles or not, are often produced via an enzymatic process, some chemical messengers are made intracellularly or extracellularly and diffuse to their point of action. One prominent example of this is the neuromodulator nitric oxide. Nitric oxide is a reactive free radical which because of its small size is able to diffuse across cell membranes and is implicated in various functions in the brain including recovery from ischemia, vasodilation, and synaptic plasticity during the

formation of memory (Garthwaite and Boulton, 1995, Beckman et al., 1996). Nitric oxide is produced from arginine in the presence of various nitric oxide synthases (NOS), including endothelial nitric oxide synthase (eNOS), neuronal nitric oxide synthase (nNOS), and inducted nitric oxide synthase (iNOS). The production of nitric oxide takes place inside post-synaptic cells during activation of NOS by calcium calmodulin after influx of calcium through VGCCs (Ledo et al., 2004). Typically, depolarization of the cell is achieved when glutamate binds to NMDA or AMPA receptors, or acetylcholine binds to nicotinic acetylcholine receptors (Garthwaite and Boulton, 1995, Smith et al., 1998).

Another example of a chemical messenger which is produced via an enzymatic process is the nucleoside adenosine. Ectonucleotidases are enzymes which hydrolyze the nucleotides adenosine triphosphase (ATP), adenosine diphosphate (ADP), and adenosine monophosphate (AMP), and are found throughout the nervous system (Langer et al., 2008, Zimmermann, 2008). There are numerous different isoforms of ectonucleotidases which are present both extracellularly and intracellularly which hydrolyze the nucleotides. The enzymes prostatic acid phosphatase (PAP) and ecto-5'-nucleotidase (CD73, NT5E) are membrane-bound enzymes which hydrolyze AMP to adenosine in the extracellular space (Zylka et al., 2008, Sowa et al., 2010, Zylka, 2011). This is of special importance in lamina II of the spinal cord, where inputs from dorsal root ganglia (DRG) neurons transmit nociceptive information through purinergic signaling. It has been shown that the hydrolysis of AMP into adenosine by PAP and NT5E has strong antinociceptive effects by binding to the adenosine A1 receptor, a G_i coupled receptor, counteracting the signaling produced by ATP (Zylka et al., 2008, Sowa et al., 2010). ATP can be released vesicularly (Pankratov et al., 2006, Sawada et al., 2008), from voltage-activated anion channels (Fields and Ni, 2010), or from hemichannels (Kang et al., 2008). It remains to be seen whether adenosine can be packaged into vesicles or released from other membrane bound transporters (Latini and Pedata, 2001), and this gives an example of where neuromodulators are produced in the

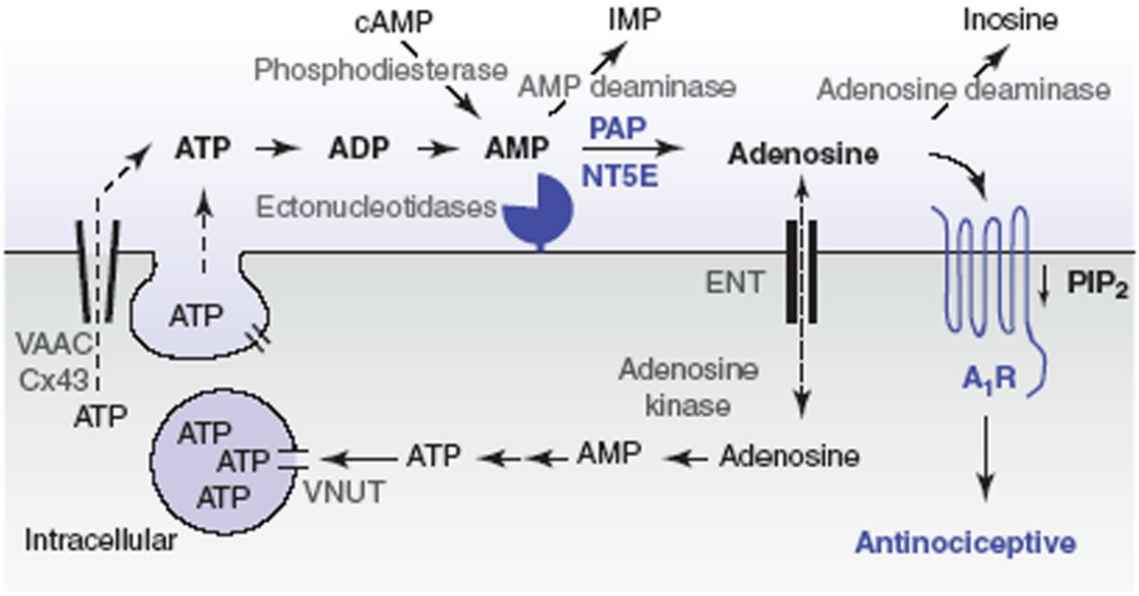

Figure 1.2. Ectonucleotidase function in spinal nociceptive circuits. ATP can be released from neurons or glia via exocytosis, through volume activated anion channels (VAACs), or through hemichannels. ATP is then hydrolyzed by various ectonucleotidases to AMP which can be further hydrolyzed to AMP by prostatic acid phosphatase (PAP) and ecto-5'-ectonucleotidase (CD73, NT5E). Adenosine then binds downstream to A1 receptors and propagates the antinociceptive signal (Zylka, 2011).

extracellular space and subsequently bind to their post-synaptic receptors. Figure 1.2 shows the production of adenosine from ectonucleotidases in spinal nociceptive circuits.

Tissue Slices for Studying Chemical Messengers

There are a number of different tissues which can be isolated from the rest of the body and sliced into thin sections for experiments involving the electrochemical study of the release of neurotransmitters. The first and most obvious example is the brain. Brain slices are a robust and simple preparation for studying various compartments of the brain with either electrochemistry or electrophysiology (Kelly and Wightman, 1987, Stefani et al., 1995). Using a reference atlas such as the Allen Brain Atlas, the sensor can be placed into a specific region of interest in a slice taken sagittally (from the side), coronally (from rostral to caudal), or horizontally (from dorsal to ventral) (Science, 2009). The type of slice taken can be dictated by the desired experiment. If an intact pathway is needed, then a horizontal or sagittal slice can be taken (in some cases), while coronal slices are ideal for studying the terminal region of a pathway in regions such as the striatum. Upon removal from the rest of the brain, the slice can be maintained under physiological conditions by perfusing the slice with a buffer containing all the extracellular ions and glucose necessary for normal cellular function. Figure 1.3A shows a coronal brain slice of the striatum where electrochemical recording of dopaminergic terminals can be performed in the dorsolateral striatum and nucleus accumbens. In order to achieve neurotransmitter release as measured by electrochemistry, electrical stimulation between the two prongs of a bipolar stimulating electrode is performed. Different properties of the stimulation can be fine-tuned for the region of interest including the intensity of the stimulation, the duration of the stimulation, the number of pulses applied, and the frequency of the stimulation.

More recently, a preparation for the slicing of murine (mouse and rat) adrenal glands has been developed for the study of the chromaffin cells located in the adrenal medulla

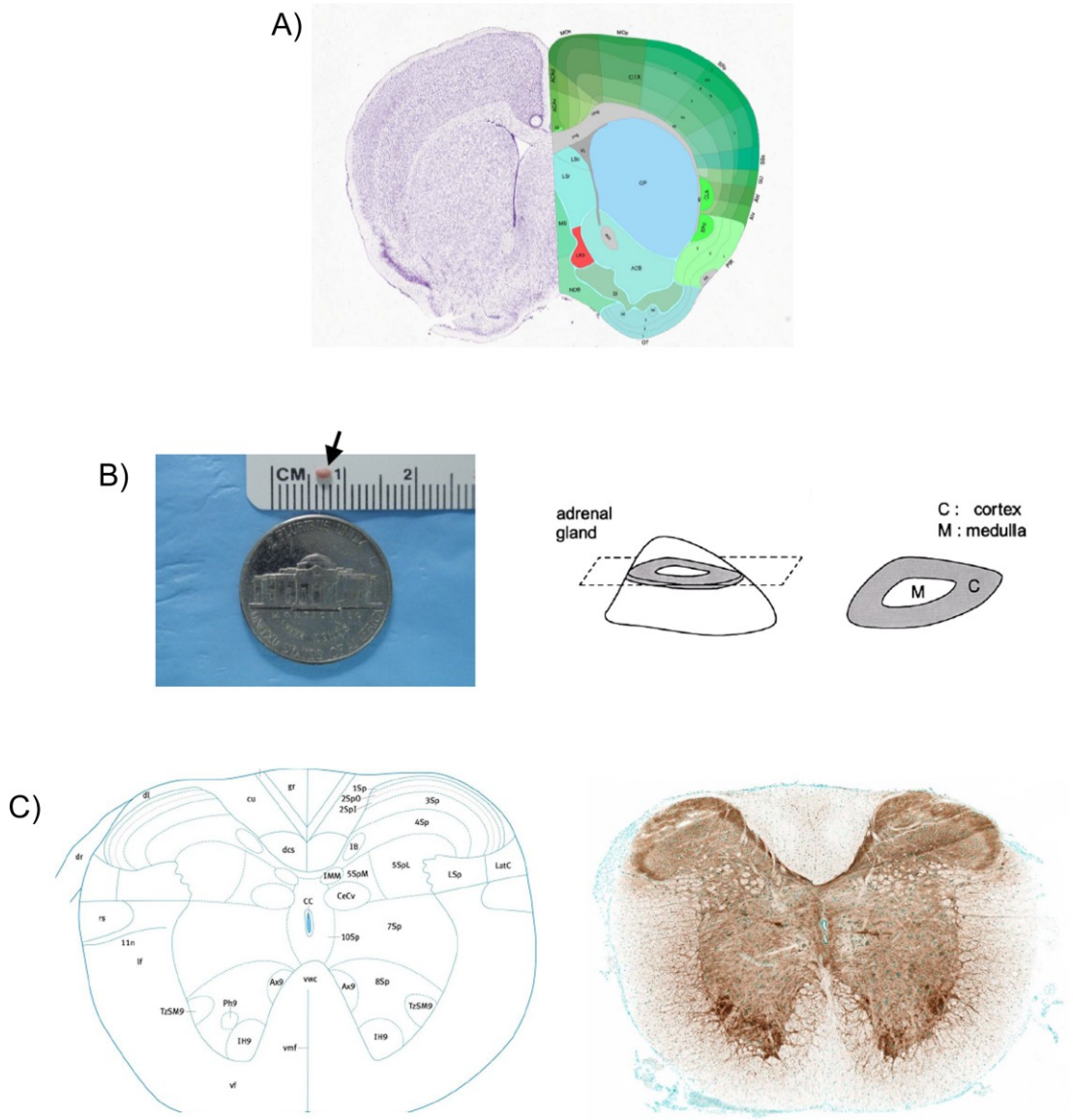

Figure 1.3. Tissue slices for the measurement of chemical messengers with electrochemistry. (A) A coronal brain slice showing the striatum containing dopaminergic terminals (CP, caudate putamen, or dorsolateral striatum; ACB, nucleus accumbens) (Science, 2009). (B) A mouse adrenal gland is shown in the left panel (arrow) with a nickel for scale. The slicing of the adrenal gland shown in the right panel reveals the outer cortex and the inner medulla, where the chromaffin cells which release epinephrine and norepinephrine are contained (Barbara et al., 1998). (C) A coronal slice of the spinal cord with a map shown in the left panel and a spinal slice in the right panel. The dorsal horn contains lamina, labeled 1Sp through 4Sp. The dorsal root (dr) innervates the dorsal horn with signals from afferent neurons (Science, 2009).

(Barbara et al., 1998). Electrophysiological recordings from the chromaffin cells which release the hormones epinephrine and norepinephrine have been conducted in these slice preparations for the study of exocytosis of these chemical messengers (Moser and Neher, 1997, Voets et al., 1999). While brain slice preparations allow for the simplification of experiments by severing the inputs and outputs of the region of interest, adrenal slice preparations create a more physiologically relevant measurement of the physiology of the chromaffin cells to be performed compared to isolated chromaffin cells (Neher and Marty, 1982). Slices maintain the splanchnic nerves which innervate the gland and form synapses onto the chromaffin cells as well as the vasculature to which the released hormones epinephrine and norepinephrine can migrate (Kikuta and Murakami, 1984, Kobayashi and Coupland, 1993). Figure 1.3B shows a picture of a mouse adrenal gland as well as a cartoon showing the methods by which the adrenal gland is sliced, and a diagram outlining the inner medulla containing the chromaffin cells and the outer cortex. Due to the small size of the adrenal gland, slicing is aided by placing the gland inside agarose to hold it in place before orienting it beneath the slicing blade (Barbara et al., 1998).

The spinal cord is also an integral part of the central nervous system which sends signals between the brain and the peripheral nervous system through the dorsal root ganglia which input into the dorsal horn of the spinal cord. Both serotonin and adenosine are known electroactive neurotransmitters released and produced in the spinal cord (Rivot et al., 1995, Zylka, 2011). Just like the brain, the spinal cord can be slices in various orientations. The most common orientation is a coronal slice. Figure 1.3C shows a map of a coronal cross section of the spinal cord as well as a picture of a coronal slice of the spinal cord including the dorsal root.

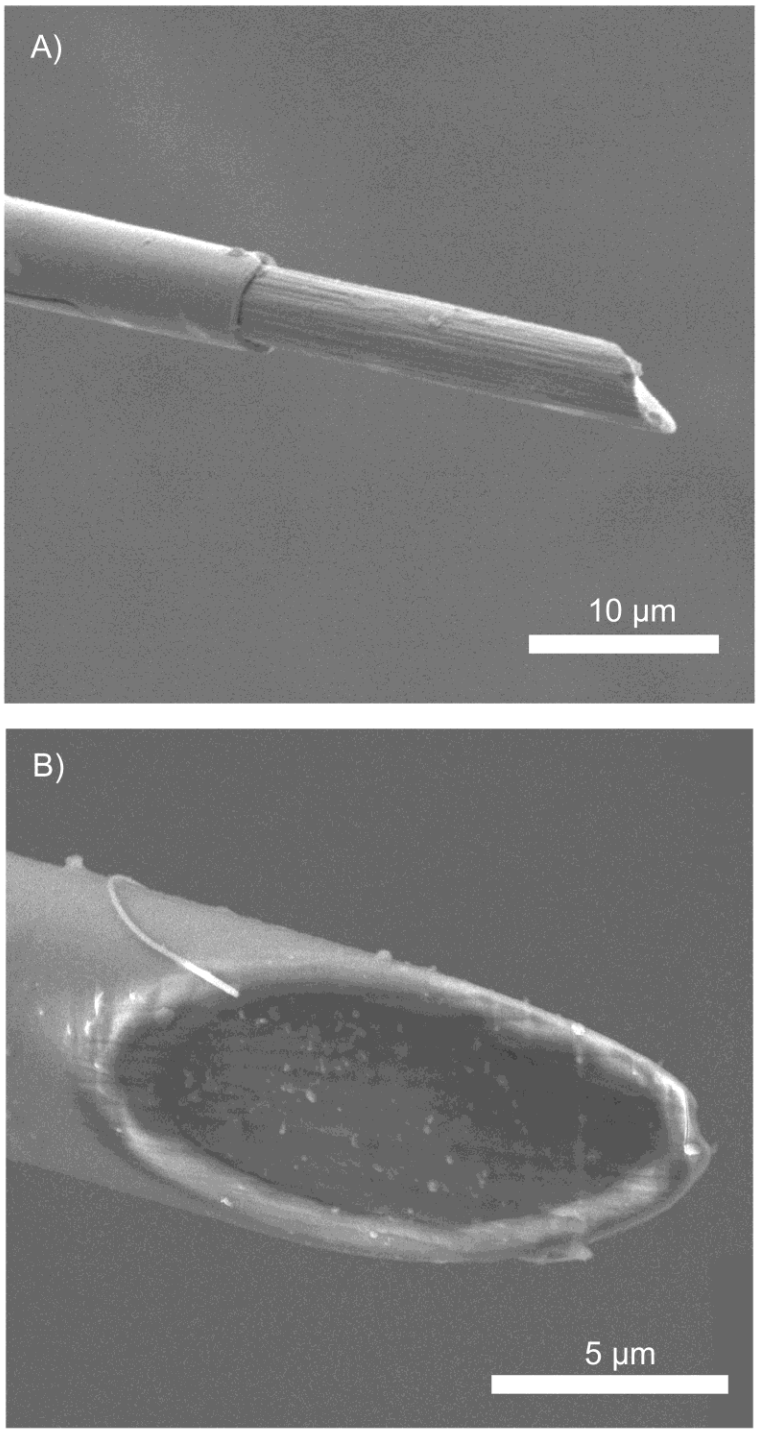

Figure 1.4. SEM images of carbon-fiber microelectrodes. A) Cylindrical T-650 carbon-fiber microelectrode ~25 µm long. B) Disk T-650 carbon-fiber microelectrode beveled at 30°.

Electrochemical Methods for Measuring Chemical Messengers

The carbon-fiber microelectrode is widely accepted as the sensor with the best spatial resolution for probing small brain regions in which neurotransmitters detected electrochemically are released. Fabrication of these electrodes has been previously described (Cahill et al., 1996). Carbon-fiber electrodes can be used in two basic geometries. Cylindrical electrodes typically have higher sensitivity to detected neurotransmitters because of their larger surface area as the carbon-fiber protrudes from the glass seal 25-150 μm depending on the application. For slices, lengths of 25-50 μm are typically used. Polished disk electrodes which have a flat carbon surface exposed at the tip of the glass seal are typically used in single cell experiments, or in slices where the electrode can sit flush on top of cell which release chemical messengers, such as the adrenal gland (Arroyo et al., 2006). Figure 1.4 shows SEM images of the two kinds of carbon-fiber microelectrodes. There are numerous chemical and physical modifications which can be used to increase the sensitivity or selectivity of the electrode. One of the most common modifications performed on carbon- fiber microelectrodes is the coating of Nafion, a cation exchange polymer, onto the surface. Nafion allows for the preconcentration of cationic analytes such as dopamine, norepinephrine and serotonin, while excluding negatively charged interfering species such as ascorbic acid, uric acid, and the dopamine metabolite 3,4-dihydroxyphenylacetic acid (DOPAC) (Brazell et al., 1987). One disadvantage of chemical and physical manipulations of carbon-fiber microelectrodes such as coating the electrode with Nafion is the increase in the time response of the electrode from the partition of species into the film and the diffusion of the species through the film to the electrode.

Constant Potential Amperometry

One of the instrumentally simple electrochemical methods for detecting released neurotransmitters in tissue slices is constant potential amperometry. During recordings, the electrode is held at a constant potential sufficient to completely oxidize the neurotransmitter when it comes into contact with the electrode, typically 650-750 mV for biogenic amines. The main disadvantage of using this method is the lack of chemical resolution. Any species which can be oxidized at the applied potential will cause the flow of current. Therefore, there is no way to tell exactly which neurotransmitter is causing the observed signal. While exogenous neurotransmitter can be injected into tissue to circumvent this issue (Gerhardt et al., 1999), less information can be obtained from these measurements because the concentration of neurotransmitter achieved during ejection are non-physiological, and the data is difficult to interpret due to the long time course of the measurements made.

Increasing chemical resolution during amperometric detection is obtainable through the chemical modifications discussed above. As an example, nitric oxide is a highly reactive gaseous free radical neuromodulator which plays a key role in many brain functions including recovery during brain ischemia as well as learning and memory in the hippocampus (Gally et al., 1990, Garthwaite and Boulton, 1995, Bishop and Anderson, 2005). Carbon-fiber microelectrodes have been modified using a Nafion coating to prevent interference from species like ascorbic acid, and an electropolymerized layer of *o*-phenylenediamine, making them less sensitive to catecholamines while still allowing the smaller gaseous species to diffuse to the electrode (Friedemann et al., 1996). These electrodes have limits of detection in the nanomolar range for nitric oxide, and have been used to detect nitric oxide production in hippocampal brain slices upon stimulation with exogenous stimulants including N-methyl-D-aspartic acid (NMDA) receptor agonist such as

glutamate and NMDA, or cholinergic receptor agonists such as nicotine (Smith et al., 1998, Ferreira et al., 2005).

Although amperometric detection is not always ideal because specific chemical identification is not possible in tissue slices, there are times when amperometry can be used to study release events that occur on very fast time scales. Exocytotic release occurs on the order of millisecond time scales, and constant potential amperometry at carbon-fiber microelectrodes has been shown to be an excellent way of studying the temporal dynamics of the various stages of exocytosis at single cells by directly oxidizing the contents of vesicles as they are released from the cell through the fusion pore (Wightman et al., 1991, Jankowski et al., 1992, Travis and Wightman, 1998, Wightman and Haynes, 2004). When making these measurements, there are a number of different properties of the amperometric spikes which can be analyzed and give information about the neurotransmitter being released. These properties include the total number of spikes observed upon stimulation, the interspike interval, the width at half height of the spike, and the total charge underneath the spike which is related to the number of moles released by Faraday's Law (Bard and Faulkner, 2001):

$$Q=nFm$$

where Q is the total charge (in coulombs), n is the number of electrons transferred during the oxidation, F is Faraday's constant (96,500 coulombs/mole), and m is the number of moles. Additionally, pre-spike features of the exocytotic event can be observed including the presence of a pre-spike foot. Pre-spike feet are present on a fraction of the events observed and are attributed to the leak of transmitter through the fusion pore intermediate before full fusion (Chow et al., 1992).

More recently, constant potential amperometry has been used to study exocytosis from chromaffin cells in intact adrenal slice preparations. Figure 1.5 shows an example of amperometric spikes detected in an adrenal slice upon electrical stimulation as well as an

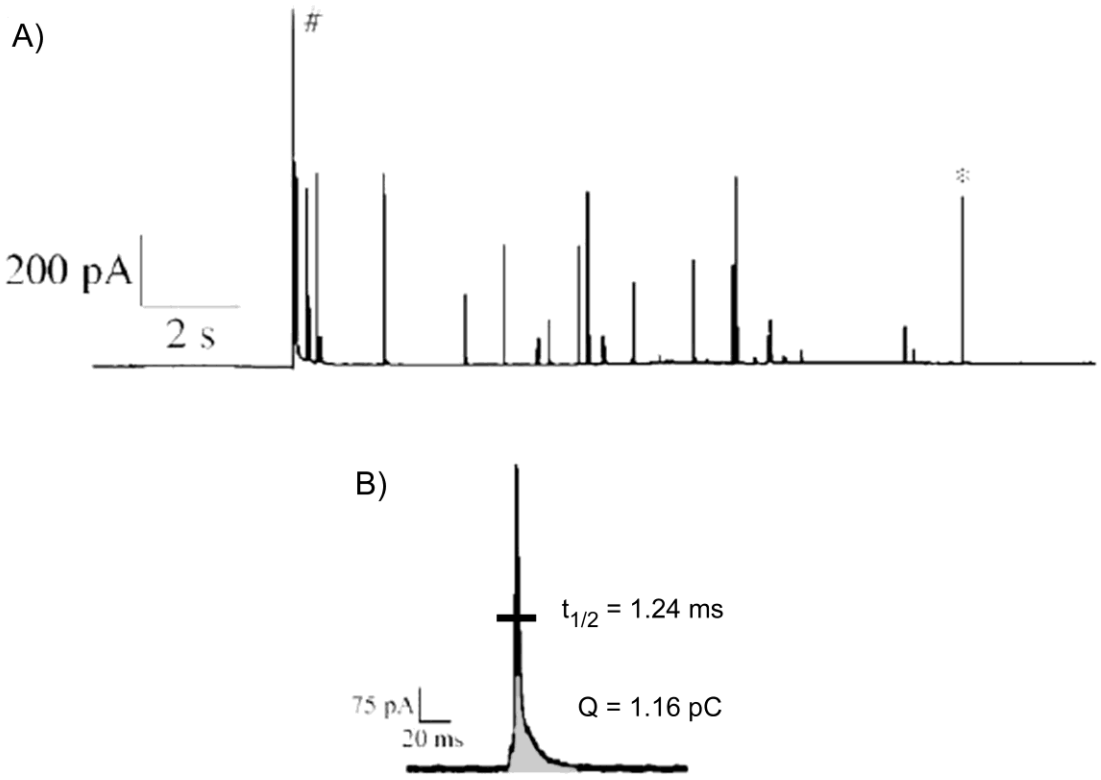

Figure 1.5. Amperometric detection of exocytosis from an adrenal slice. A) Representative amperometric spikes after an electrical pulse (the artifact from the pulse denoted by #). B) A single amperometric spike from (A) (denoted by the asterisk) showing the spike characteristics of width at half height (horizontal bar, $t_{1/2}$) and the charge underneath the spike (shaded gray, Q). Figure modified from Arroyo *et al* (Arroyo et al., 2006).

individual spike showing the characteristics described above. Remarkably, using this technique, the spike features for the exocytosis of epinephrine and norepinephrine including quantal size (charge) and number of spikes upon exposure to a high K^+ solution, were statistically similar between the intact slice preparation and cultured chromaffin cells while others parameters such as the spike half width were statistically different (Arroyo et al., 2006). These differences could be due to the location of the electrode and whether or not it is able to sit flush with the cell surface in the slice preparation. Even small distances can greatly affect this measured value (Wightman et al., 1995). Moving this detection scheme into slices allowed for the detection of quantal release from chromaffin cells by not only application of secretagogues such as a high potassium solution or acetylcholine, but also the use of electrical stimulation to excite the cholinergic splanchnic nerves which innervate the adrenal gland (Douglas and Rubin, 1961b).

Fast-Scan Cyclic Voltammetry

Fast-scan cyclic voltammetry (FSCV) at carbon-fiber microelectrodes has become an excellent alternative to constant potential methods due to its higher chemical resolution when compared to constant potential methods. Although traditionally some temporal resolution is lost (see Chapter 2), the utilization of faster scan rates still allows for sub-second measurements of neurotransmitter concentration to be made within tissue. In FSCV, the potential is scanned at high rates allowing for the oxidation and/or reduction of the species present at the electrode surface. This high scan rate causes a large background current from the charging of the double-layer. The background current is stable, however, allowing for it to be digitally subtracted from a signal when the electrode is in the presence of an analyte. This background subtraction leads to the characteristic cyclic voltammogram (CV) for the analyte of interest. The peak current for the oxidation of the analyte is proportional to the concentration of the analyte according to the equation for

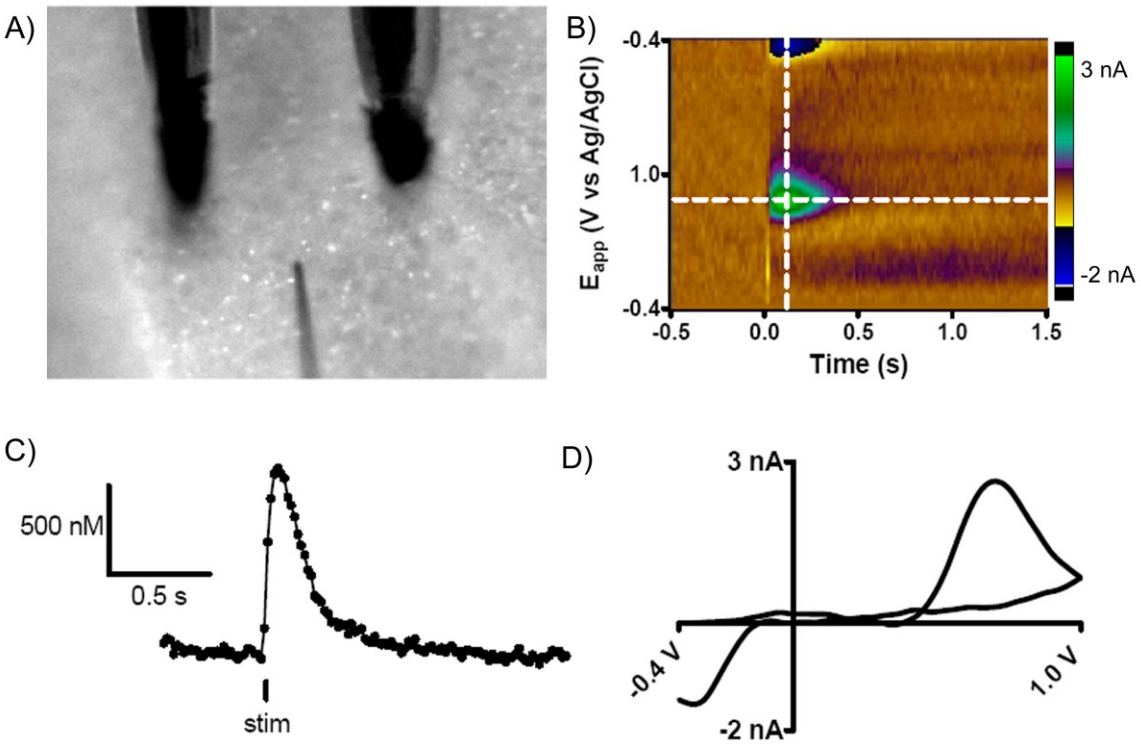

Figure 1.6. Fast-scan cyclic voltammetry data from a brain slice. (A) Brightfield image of a coronal brain slice in the dorsolateral striatum with the bipolar tungsten stimulating electrode on top of the slice above and the carbon fiber microelectrode inserted into the slice below. (B) Color plot of stimulated dopamine release (350 μA, biphasic, 1 pulse), showing time on the abscissa, potential on the ordinate, and current shown in false color with green being oxidative currents, and blue and black being reductive currents. (C) A concentration versus time plot extracted from the horizontal white line in (B). (D) The cyclic voltammogram extracted from the vertical line shown in (B) showing the characteristic shape for dopamine.

adsorbed species and the current change over time can be converted to the change in concentration of the neurotransmitter with time from a post-calibration of the electrode. In order to visualize all three of the variables which take place during FSCV measurements (potential, time and current), experiments use color plots which show time on the abscissa, potential on the ordinate unfolded so for a traditional triangle waveform, the switching potential is in the middle, and current shown in false color, where traditionally oxidation currents are shown in green and reduction currents are shown in blue and black (Michael et al., 1998). Figure 1.6 shows an example of FSCV data collected in the dorsal striatum of a brain slice showing all of the various ways that FSCV data can be displayed with a color plot, concentration versus time with the aide of calibration of the electrode *in vitro*, and the cyclic voltammogram for dopamine.

The main benefit of FSCV is the chemical resolution that it provides compared to amperometry (Robinson et al., 2008). This allows for the specific identification of the neurotransmitter being studied based upon its cyclic voltammogram given the potential limits of the waveform being used. In many cases, the initial potential or the upper limit of the waveform is varied to either promote the adsorption of positively charged biogenic amines to the surface of the electrode in order to increase the sensitivity of the electrode to the analyte (Heien et al., 2003). While some very similar biogenic amines such as dopamine and norepinephrine (which differ solely due to the addition of a hydroxide group on the beta carbon) cannot be differentiated using voltammetry, there are a number of neurotransmitters that can be distinguished. Figure 1.7 shows examples of different waveforms which can be used to detect various neurotransmitters in tissue samples including dopamine or norepinephrine in the striatum or bed nucleus of the stria terminalis (BNST) (Kennedy et al., 1992a, Miles et al., 2002), norepinephrine and epinephrine in adrenal tissue slices (Petrovic et al., 2010), 5-hydroxytryptamine (5-HT, serotonin) in the dorsal raphe nucleus (DRN), the substantia nigra reticulata (SNr) (Bunin and Wightman, 1998) or the dorsal horn of the spinal

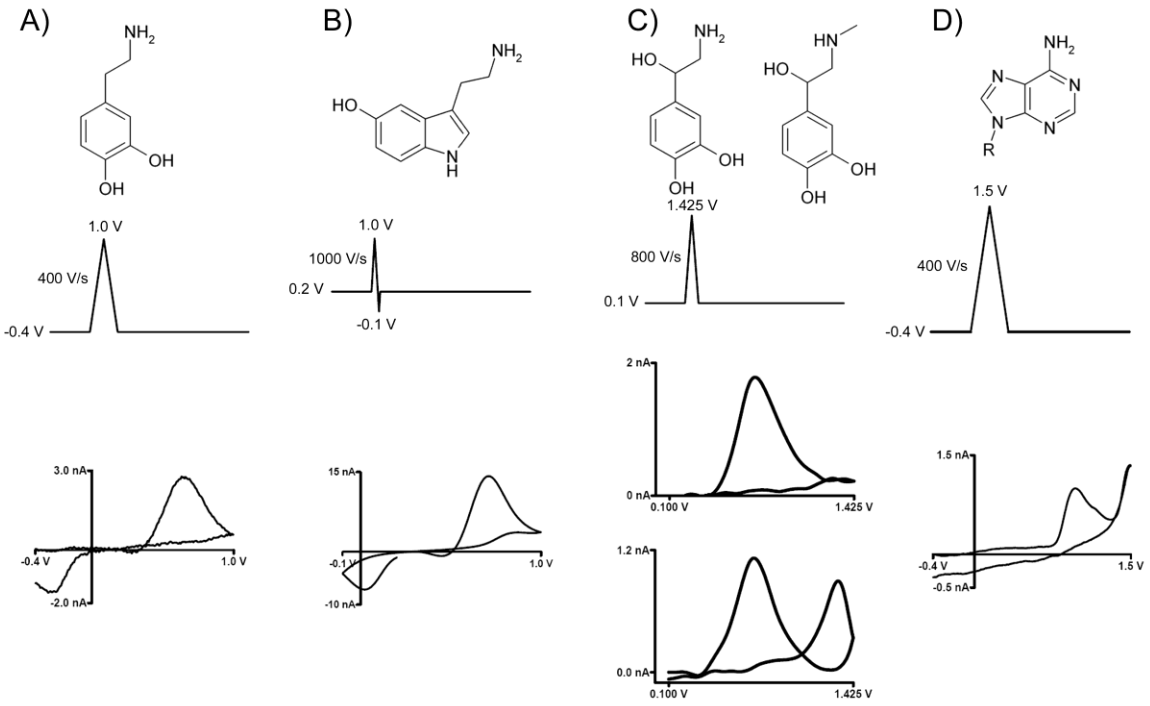

Figure 1.7. Voltammetric waveforms used to detect different neurotransmitters. Top panel: chemical structures of neurotransmitters, middle panel: voltammetric waveforms with starting potential, high potential, low potential, and scan rate labeled, bottom panel: representative cyclic voltammograms. (A) dopamine waveform, (B) serotonin waveform, (C) adrenergic waveform for norepinephreine (left, top), epinephrine (right, bottom), (D) adenosine waveform.

cord (Rivot et al., 1995), and adenosine in the striatum (Pajski and Venton, 2010). Even in areas of the brain where FSCV cannot distinguish two similar catecholamines (dopamine and norepinephrine) that are released such as the bed nucleus of the stria terminalis (BNST) (Miles et al., 2002), coupling FSCV with precise anatomical targeting and pharmacological methods can be used in order to determine which of the two catecholamines is being detected during the experiment (Park et al., 2009).

FSCV has even been used to detect gaseous species such as oxygen. In order to accomplish this, the electrode is scanned to very negative potentials, allowing for oxygen to be reduced to hydrogen peroxide (Zimmerman and Wightman, 1991). This was accomplished in tissue slices in order to study the use of oxygen by tissue (Kennedy et al., 1992b). As the electrode was placed into the tissue, upon electrical stimulation and release of dopamine, more oxygen was used. This response was found to be both calcium and action potential dependent, as removal of extracellular Ca^{2+} from the buffer or addition of tetrodotoxin (TTX) to the perfusion buffer significantly decreased the observed oxygen signal (Kennedy et al., 1992b). This provides yet another example of how FSCV can be utilized to detect a myriad of different analytes and probe the numerous events which must occur in order for synaptic transmission.

Examining Synaptic Mechanisms with Electrochemistry

Pharmacology

Using electrochemistry in brain slices is an excellent method for studying the pharmacological manipulation of receptors, transporters and channels because of the high spatial resolution and the isolation of the tissue from peripheral inputs. Since FSCV measures the release which occurs from the presynaptic terminals, pharmacological manipulations of the region of interest focus on the presynaptic receptors, transporters and channels. Dopaminergic terminals have been thoroughly studied through pharmacology of

both the dopamine transporter using DAT blockers such as cocaine and nomifensine as well as the dopamine D2 autoreceptor using antagonists such as sulpiride and agonists such as quinpirole (Kennedy et al., 1992a, Jones et al., 1995b). Slices are an excellent tool for the study of the pharmacology of these targets because the concentration and timing of the application of drugs can be controlled by perfusion of the drug in the physiological buffer or localized pressure ejection from a micropipette.

One example of the use of pharmacology in brain slices of the striatum is measuring the uptake of dopamine in both the dorsal striatum as well as the nucleus accumbens (Jones et al., 1995b). In these studies, multiple concentrations of cocaine and nomifensine can be applied to the same slice taking measurements of dopamine release and uptake as each concentration is applied to the slice. Using modeling of the profile for the release and uptake, using a Michaelis-Menten model, the amount of transporter near the electrode can be determined (V_{max}), and as the cocaine is applied, the apparent K_m can be determined and when plotted against the concentration of the inhibitor applied, the inhibition constant, K_i can be calculated. It was shown in this study that the K_i for cocaine was not significantly different between the two brain regions, but interestingly the K_i for nomifensine was higher in the dorsal striatum than it was in the nucleus accumbens.

In adrenal slices, the pharmacology of both the splanchnic nerve as well as the chromaffin cells themselves can be exploited, both by local application of secretagogues, as well as the bath application of drugs which block the receptors located on the chromaffin cells which bind to the acetylcholine released by the splanchnic nerve (Douglas and Rubin, 1961a, Arroyo et al., 2006). In these experiments, upon electrical stimulation, which was believed to excite the splanchnic nerve, hexamethonium, a nicotinic acetylcholine receptor blocker (Wakade and Wakade, 1983) was bath applied for a brief time and showed a dramatic decrease in the number of spikes observed while hexamethonium was present. These studies showed that the electrical stimulation applied during these measurements

was indeed stimulating the splanchnic nerve and not the chromaffin cells and the role that the acetylcholine released by the splanchnic nerve plays in the vesicular secretion of epinephrine and norepinephrine by chromaffin cells in the adrenal medulla.

Transgenic Mouse Models

Over the last two decades, transgenic manipulations in mice have become an unprecedented advancement in the field of genetics (Deursen and Hofker, 2003). Specifically, the removal of individual genes, making genetic knockout animals, has allowed for the understanding of the roles that single genes can play in cellular functions. Knockout animals have found a place in research as disease-state models showing that the removal or mutation of a gene can lead to a disease (Kola and Tymms, 2001). While it is not the purpose of this review to discuss the methods used in making these transgenic mouse models, the subsequent analysis of the presynaptic function and neurotransmitter release in tissue slices of these animals is paramount in understanding the depth and breadth that using electrochemistry allows for determining the function of various genes studied and how electrochemical methods can be used to study innumerable synaptic mechanisms.

One of the first studies using electrochemistry to determine the effect of the deletion of a gene on the electrochemical signal observed in brain slices was that of the dopamine transporter (DAT) knockout animal. DAT functions to re-uptake the excess dopamine released into the synapse. Earlier, it had been shown how FSCV can be used in brain slices in order to model the uptake of dopamine by DAT using Michaelis-Menten kinetics allowing for the determination of the amount of DAT near the electrode (V_{max}) as well as the affinity of dopamine for DAT (K_m), and how that affinity changes as drugs which block DAT such as cocaine are applied ($K_{m,app}$) (Jones et al., 1995a). FSCV was used to monitor the release and uptake of dopamine in slices from animals with all copies of the DAT gene ($DAT^{+/+}$), heterozygous animals ($DAT^{+/-}$), and homologous knockouts of the DAT gene (DAT^{-}

$^{-/-}$) (Giros et al., 1996). Differences in uptake were observed between all three genotypes with the slices from the *DAT*$^{-/-}$ animals having the slowest uptake rate. Furthermore, bath application of the drug of abuse amphetamine showed that in animals lacking DAT, tonic extracellular concentrations of dopamine did not increase. These observations coupled with behavioral observations indicated the critical role DAT plays in the molecular function of amphetamine on synapses in the mesolimbic and nigrostriatal pathways. Without the temporal and spatial resolution that FSCV allows, the function of DAT on the synapse and how it relates to the functions of drugs of abuse could not be elucidated.

Another early example of the use of electrochemistry in tissue slices from a disease state animal model is the measurement of dopamine in the dorsal striatum of the R6/2 transgenic mouse model of Huntington's disease (Johnson et al., 2006). Huntington's disease is a neurodegenerative, fatal, genetic disorder in which there is an expansive CAG repeat in the gene which encodes for the gene huntingtin causing an abnormally long polyglutamine segment near the N-terminus (Johnson et al., 2007). The R6/2 transgenic mouse model is one of the models which has been used extensively in the research of this disease (Levine et al., 2004). The release of dopamine in the dorsal striatum is an obvious candidate for being affected due to the symptoms of the disease which include motor and cognitive defects, as well as degeneration of medium spiny neurons in the striatum (Bates et al., 2002). In these studies, it was observed that there is a decrease in the amount of dopamine release in the R6/2 animals at various ages (6-14 weeks old) compared to wild-type (WT) animals. Furthermore, decreases observed in cocaine-induced locomotion were due to this decrease in dopamine release, because the calculated inhibition constants for both cocaine and methamphetamine in these slices at various ages were not significantly different between WT and R6/2 animals.

In subsequent studies, it was determine that this is not limited to dopamine release in the striatum as individual chromaffin cells from these mice showed a decrease in the total

quantal content released by individual vesicular events measured with constant potential amperometry (Johnson et al., 2007). More recently, experiments involving the use of methamphetamine to release intracellular dopamine to be measured by FSCV in the striatum of slices showed that there is a significant decrease in the total amount of dopamine stored vesicularly in R6/2 Huntington's mice (Ortiz et al., 2011a). These experiments show a fundamental difference in the catecholamine release characteristics of animals with a transgenic model of Huntington's disease. Again, the temporal and spatial resolution of FSCV and constant potential amperometry at carbon-fiber microelectrodes allowed for these otherwise unknown characteristics of the disease to be discovered.

One final example of the use of a knockout mouse in order to study the mechanisms by which a specific gene affects synaptic transmission of an electroactive neurotransmitter is the knockout of the synapsin genes. There are three mammalian synapsin genes (synapsin I, II, and III) which are phosphoproteins located on the surface of synaptic vesicles. They are thought to play a role in keeping vesicles in the reserve pool and away from the active zone of the nerve ending where exocytosis occurs (Greengard et al., 1993). In this study, Kile *et al* used mice lacking all three synapsin genes, or a triple knockout animal (TKO), to study the release of two neurotransmitters which are electrochemically active, dopamine and serotonin (5-HT) (Kile et al., 2010). It was found that mice lacking the synapsin genes showed significantly more release of dopamine while 5-HT release was no different between the two genotypes. Total content of both dopamine and 5-HT were the same between the genotypes, pointing to the role that the Synapsin proteins play in exocytotic release of dopamine. Further study of the synapsin III knockout animal showed similar results to the TKO indicating that in the dopamine terminals in the dorsal striatum, the synapsin III gene plays the largest role. This was not unexpected since the synapsin genes are differentially expressed throughout the brain while synapsin III is restricted to regions such as the dentate gyrus of the hippocampus and the caudate putamen (Pieribone et al., 2002). The

differential release was also found to be highly dependent on the concentration of the extracellular calcium indicating the role the protein plays in the exocytotic mechanism. This example once again shows the versatility of FSCV, allowing for differences in the release of two different neurotransmitters, dopamine and 5-HT, in mice lacking proteins which play an important role in vesicular trafficking to be elucidated. This could not be accomplished with another electrochemical technique which does not have the chemical resolution that FSCV has.

The above examples of the use of transgenic mice for the study of synaptic mechanisms with electrochemistry in disease-state animals are just a few selected studies from a myriad of ongoing research in a number of different areas. Some other examples include R6/1 Huntington's disease state mice (Ortiz et al., 2011a), Fragile X retardation syndrome (Annangudi et al., 2010, Fulks et al., 2010), transgenic mice with extra copies of the dopamine transporter gene (Salahpour et al., 2008), Parkinson's disease (Zhang et al., 2011, Littrell et al., 2012), mice lacking MsrA (Oien et al., 2008), mice lacking sulfoxide reductase A (Ortiz et al., 2011b).

Summary

The work reviewed herein shows the ability of electrochemical methods used in tissue slices in order to study the mechanism of neurotransmitter release and uptake at the synaptic level. Using a slice preparation has many advantages over using whole animal experiments including knowing the exact location of where the sensor is placed as well as the ability for local stimulation and the probing of the biological processes in play at the synapse without interference from other systems in the brain. Electrochemistry at carbon fiber microelectrodes has the spatial and temporal resolution other methods do not possess. With the use of FSCV, chemical resolution can also be obtained and allow for the measurement of many different electroactive neurotransmitters. Pharmacological and

transgenic methods have allowed researchers to probe mechanisms at the synaptic level for many different proteins implicated in important diseases including Huntington's and Parkinson's disease. One can imagine that there are a number of different proteins which play key roles in synaptic transmission which have yet to be studied using these methods. With the advancements which have been made in the production of transgenic and genetic knockout animals, the limit of the use of electrochemistry to study synaptic transmission in animals lacking or having excess various genes is only limited by the genome itself and the viability of the animals produced.

Dissertation Overview

In the work presented herein, electrochemistry at carbon-fiber microelectrodes is used in both adrenal as well as spinal cord tissue slices for the evaluation of chemical messenger release. Specifically, CPA and FSCV were used in mouse adrenal slices for the evaluation of biogenic amine release from chromaffin cells. Pharmacological methods were used to study both electrically stimulated as well as spontaneous exocytotic release. A modified waveform was also used to determine the chemical messenger being released from individual chromaffin cell clusters. These techniques were then used to characterize the stimulation methods for eliciting catecholamine release from adrenal slices and the implications of the use of high intensity electrical stimulations in tissue slices. Furthermore, in collaboration with Mark Zylka in the Department of Cell and Molecular Physiology, FSCV was utilized to address the function of ectonucleotidases for the production of adenosine in spinal nociceptive circuits. Furthermore, a possible source of adenosine tone in the spinal cord was discovered. Finally, with the use of high-performance liquid chromatography with electrochemical detection (HPLC-ECD), total tissue and metabolite content was determined in various brain regions of biogenic amines in animal models of disease-states to determine differences. As a whole, these studies help to contribute to solving long-standing

methodological and physiological questions in the fields of analytical chemistry and neuroscience.

References

Alvarez YD, Ibanez LI, Uchitel OD, Marengo FD (2008) P/Q Ca^{2+} channels are functionally coupled to exocytosis of the immediately releasable pool in mouse chromaffin cells. Cell Calcium 43:155-164.

Annangudi SP, Luszpak AE, Kim SH, Ren S, Hatcher NG, Weiler IJ, Thornley KT, Kile BM, Wightman RM, Greenough WT, Sweedler JV (2010) Neuropeptide Release is Impaired in a Mouse Model of Fragile X Mental Retardation Syndrome. ACS Chem Neurosci 1:306-314.

Arroyo G, Fuentealba J, Sevane-Fernandez N, Aldea M, Garcia AG, Albillos A (2006) Amperometric study of the kinetics of exocytosis in mouse adrenal slice chromaffin cells: physiological and methodological insights. J Neurophysiol 96:1196-1202.

Barbara JG, Poncer JC, McKinney RA, Takeda K (1998) An adrenal slice preparation for the study of chromaffin cells and their cholinergic innervation. J Neurosci Methods 80:181-189.

Bard AJ, Faulkner LR (eds.) (2001) Electrochemical Methods: Fundamentals and Applications. New York: John Wiley & Sons, Inc.

Bates G, Harper PS, Jones L (2002) Huntington's disease. Oxford; New York: Oxford University Press.

Becherer U, Rettig J (2006) Vesicle pools, docking, priming, and release. Cell and tissue research 326:393-407.

Beckman JS, Ye YZ, Chen J, Conger KA (1996) The interactions of nitric oxide with oxygen radicals and scavengers in cerebral ischemic injury. Adv Neurol 71:339-350; discussion 350-334.

Bishop A, Anderson JE (2005) NO signaling in the CNS: from the physiological to the pathological. Toxicology 208:193-205.

Brazell MP, Kasser RJ, Renner KJ, Feng J, Moghaddam B, Adams RN (1987) Electrocoating carbon fiber microelectrodes with Nafion improves selectivity for electroactive neurotransmitters. J Neurosci Methods 22:167-172.

Bunin MA, Wightman RM (1998) Quantitative evaluation of 5-hydroxytryptamine (serotonin) neuronal release and uptake: an investigation of extrasynaptic transmission. J Neurosci 18:4854-4860.

Cahill PS, Walker QD, Finnegan JM, Mickelson GE, Travis ER, Wightman RM (1996) Microelectrodes for the measurement of catecholamines in biological systems. Anal Chem 68:3180-3186.

Chaudhry FA, Edwards RH, Fonnum F (2008) Vesicular neurotransmitter transporters as targets for endogenous and exogenous toxic substances. Annu Rev Pharmacol Toxicol 48:277-301.

Chow RH, von Ruden L, Neher E (1992) Delay in vesicle fusion revealed by electrochemical monitoring of single secretory events in adrenal chromaffin cells. Nature 356:60-63.

del Castillo J, Katz B (1954) Quantal components of the end-plate potential. J Physiol 124:560-573.

Deursen Jv, Hofker MH (2003) Transgenic mouse methods and protocols. Totowa, N.J.: Humana Press.

Douglas WW, Rubin RP (1961a) Mechanism of nicotinic action at the adrenal medulla: calcium as a link in stimulus-secretion coupling. Nature 192:1087-1089.

Douglas WW, Rubin RP (1961b) The role of calcium in the secretory response of the adrenal medulla to acetylcholine. J Physiol 159:40-57.

Ferreira NR, Ledo A, Frade JG, Gerhardt GA, Laranjinha J, Barbosa RM (2005) Electrochemical measurement of endogenously produced nitric oxide in brain slices using Nafion/o-phenylenediamine modified carbon fiber microelectrodes. Analytica Chimica Acta 535:1-7.

Fields RD, Ni Y (2010) Nonsynaptic communication through ATP release from volume-activated anion channels in axons. Sci Signal 3:ra73.

Friedemann MN, Robinson SW, Gerhardt GA (1996) o-Phenylenediamine-modified carbon fiber electrodes for the detection of nitric oxide. Anal Chem 68:2621-2628.

Fulks JL, O'Bryhim BE, Wenzel SK, Fowler SC, Vorontsova E, Pinkston JW, Ortiz AN, Johnson MA (2010) Dopamine Release and Uptake Impairments and Behavioral

Alterations Observed in Mice that Model Fragile X Mental Retardation Syndrome. ACS Chem Neurosci 1:679-690.

Gally JA, Montague PR, Reeke GN, Jr., Edelman GM (1990) The NO hypothesis: possible effects of a short-lived, rapidly diffusible signal in the development and function of the nervous system. Proc Natl Acad Sci U S A 87:3547-3551.

Garthwaite J, Boulton CL (1995) Nitric oxide signaling in the central nervous system. Annu Rev Physiol 57:683-706.

Gerhardt GA, Ksir C, Pivik C, Dickinson SD, Sabeti J, Zahniser NR (1999) Methodology for coupling local application of dopamine and other chemicals with rapid in vivo electrochemical recordings in freely-moving rats. J Neurosci Methods 87:67-76.

Giros B, Jaber M, Jones SR, Wightman RM, Caron MG (1996) Hyperlocomotion and indifference to cocaine and amphetamine in mice lacking the dopamine transporter. Nature 379:606-612.

Gonon F, Cespuglio R, Ponchon JL, Buda M, Jouvet M, Adams RN, Pujol JF (1978) In vivo continuous electrochemical determination of dopamine release in rat neostriatum. C R Acad Sci Hebd Seances Acad Sci D 286:1203-1206.

Greengard P, Valtorta F, Czernik AJ, Benfenati F (1993) Synaptic vesicle phosphoproteins and regulation of synaptic function. Science 259:780-785.

Heien ML, Phillips PE, Stuber GD, Seipel AT, Wightman RM (2003) Overoxidation of carbon-fiber microelectrodes enhances dopamine adsorption and increases sensitivity. Analyst 128:1413-1419.

Jankowski JA, Schroeder TJ, Holz RW, Wightman RM (1992) Quantal secretion of catecholamines measured from individual bovine adrenal medullary cells permeabilized with digitonin. J Biol Chem 267:18329-18335.

Jaquins-Gerstl A, Michael AC (2009) Comparison of the brain penetration injury associated with microdialysis and voltammetry. J Neurosci Methods 183:127-135.

Johnson MA, Rajan V, Miller CE, Wightman RM (2006) Dopamine release is severely compromised in the R6/2 mouse model of Huntington's disease. J Neurochem 97:737-746.

Johnson MA, Villanueva M, Haynes CL, Seipel AT, Buhler LA, Wightman RM (2007) Catecholamine exocytosis is diminished in R6/2 Huntington's disease model mice. J Neurochem 103:2102-2110.

Jones SR, Garris PA, Kilts CD, Wightman RM (1995a) Comparison of dopamine uptake in the basolateral amygdaloid nucleus, caudate-putamen, and nucleus accumbens of the rat. J Neurochem 64:2581-2589.

Jones SR, Garris PA, Wightman RM (1995b) Different effects of cocaine and nomifensine on dopamine uptake in the caudate-putamen and nucleus accumbens. J Pharmacol Exp Ther 274:396-403.

Kang J, Kang N, Lovatt D, Torres A, Zhao Z, Lin J, Nedergaard M (2008) Connexin 43 hemichannels are permeable to ATP. The Journal of neuroscience : the official journal of the Society for Neuroscience 28:4702-4711.

Kelly RS, Wightman RM (1987) Detection of dopamine overflow and diffusion with voltammetry in slices of rat brain. Brain Res 423:79-87.

Kennedy RT, Jones SR, Wightman RM (1992a) Dynamic observation of dopamine autoreceptor effects in rat striatal slices. J Neurochem 59:449-455.

Kennedy RT, Jones SR, Wightman RM (1992b) Simultaneous measurement of oxygen and dopamine: coupling of oxygen consumption and neurotransmission. Neuroscience 47:603-612.

Kikuta A, Murakami T (1984) Relationship between chromaffin cells and blood vessels in the rat adrenal medulla: a transmission electron microscopic study combined with blood vessel reconstructions. Am J Anat 170:73-81.

Kile BM, Guillot TS, Venton BJ, Wetsel WC, Augustine GJ, Wightman RM (2010) Synapsins differentially control dopamine and serotonin release. J Neurosci 30:9762-9770.

Kim D, Koseoglu S, Manning BM, Meyer AF, Haynes CL (2011) Electroanalytical Eavesdropping on Single Cell Communication. Anal Chem 83:7242-7249.

Kobayashi S, Coupland RE (1993) Morphological aspects of chromaffin tissue: the differential fixation of adrenaline and noradrenaline. J Anat 183 (Pt 2):223-235.

Kola I, Tymms MJ (2001) Gene knockout protocols. Totowa, NJ: Humana Press.

Langer D, Hammer K, Koszalka P, Schrader J, Robson S, Zimmermann H (2008) Distribution of ectonucleotidases in the rodent brain revisited. Cell Tissue Res 334:199-217.

Latini S, Pedata F (2001) Adenosine in the central nervous system: release mechanisms and extracellular concentrations. J Neurochem 79:463-484.

Ledo A, Frade J, Barbosa RM, Laranjinha J (2004) Nitric oxide in brain: diffusion, targets and concentration dynamics in hippocampal subregions. Mol Aspects Med 25:75-89.

Levine MS, Cepeda C, Hickey MA, Fleming SM, Chesselet MF (2004) Genetic mouse models of Huntington's and Parkinson's diseases: illuminating but imperfect. Trends Neurosci 27:691-697.

Littrell OM, Pomerleau F, Huettl P, Surgener S, McGinty JF, Middaugh LD, Granholm AC, Gerhardt GA, Boger HA (2012) Enhanced dopamine transporter activity in middle-aged Gdnf heterozygous mice. Neurobiology of Aging 33:427 e421-427 e414.

Michael D, Travis ER, Wightman RM (1998) Color images for fast-scan CV measurements in biological systems. Anal Chem 70:586A-592A.

Miles PR, Mundorf ML, Wightman RM (2002) Release and uptake of catecholamines in the bed nucleus of the stria terminalis measured in the mouse brain slice. Synapse 44:188-197.

Moser T, Neher E (1997) Rapid exocytosis in single chromaffin cells recorded from mouse adrenal slices. J Neurosci 17:2314-2323.

Neher E, Marty A (1982) Discrete changes of cell membrane capacitance observed under conditions of enhanced secretion in bovine adrenal chromaffin cells. Proc Natl Acad Sci U S A 79:6712-6716.

Oien DB, Osterhaus GL, Latif SA, Pinkston JW, Fulks J, Johnson M, Fowler SC, Moskovitz J (2008) MsrA knockout mouse exhibits abnormal behavior and brain dopamine levels. Free Radic Biol Med 45:193-200.

Ortiz AN, Kurth BJ, Osterhaus GL, Johnson MA (2011a) Impaired dopamine release and uptake in R6/1 Huntington's disease model mice. Neurosci Lett 492:11-14.

Ortiz AN, Oien DB, Moskovitz J, Johnson MA (2011b) Quantification of reserve pool dopamine in methionine sulfoxide reductase A null mice. Neuroscience 177:223-229.

Pajski ML, Venton BJ (2010) Adenosine Release Evoked by Short Electrical Stimulations in Striatal Brain Slices is Primarily Activity Dependent. ACS Chem Neurosci 1:775-787.

Pankratov Y, Lalo U, Verkhratsky A, North RA (2006) Vesicular release of ATP at central synapses. Pflugers Arch 452:589-597.

Park J, Kile BM, Wightman RM (2009) In vivo voltammetric monitoring of norepinephrine release in the rat ventral bed nucleus of the stria terminalis and anteroventral thalamic nucleus. Eur J Neurosci 30:2121-2133.

Petrovic J, Walsh PL, Thornley KT, Miller CE, Wightman RM (2010) Real-Time Monitoring of Chemical Transmission in Slices of the Murine Adrenal Gland. Endocrinology 151:1773-1783.

Pieribone VA, Porton B, Rendon B, Feng J, Greengard P, Kao HT (2002) Expression of synapsin III in nerve terminals and neurogenic regions of the adult brain. J Comp Neurol 454:105-114.

Rivot JP, Cespuglio R, Puig S, Jouvet M, Besson JM (1995) In vivo electrochemical monitoring of serotonin in spinal dorsal horn with Nafion-coated multi-carbon fiber electrodes. J Neurochem 65:1257-1263.

Robinson DL, Hermans A, Seipel AT, Wightman RM (2008) Monitoring rapid chemical communication in the brain. Chem Rev 108:2554-2584.

Salahpour A, Ramsey AJ, Medvedev IO, Kile B, Sotnikova TD, Holmstrand E, Ghisi V, Nicholls PJ, Wong L, Murphy K, Sesack SR, Wightman RM, Gainetdinov RR, Caron MG (2008) Increased amphetamine-induced hyperactivity and reward in mice overexpressing the dopamine transporter. Proc Natl Acad Sci U S A 105:4405-4410.

Sawada K, Echigo N, Juge N, Miyaji T, Otsuka M, Omote H, Yamamoto A, Moriyama Y (2008) Identification of a vesicular nucleotide transporter. Proc Natl Acad Sci U S A 105:5683-5686.

Science AIfB (2009) Allen Mouse Brain Atlas [Internet]. In: http://mousebrain-maporg(Science, A. I. f. B., ed) Seattle (WA): Allen Institute for Brain Science.

Smith DA, Hoffman AF, David DJ, Adams CE, Gerhardt GA (1998) Nicotine-evoked nitric oxide release in the rat hippocampal slice. Neurosci Lett 255:127-130.

Sowa NA, Taylor-Blake B, Zylka MJ (2010) Ecto-5'-nucleotidase (CD73) inhibits nociception by hydrolyzing AMP to adenosine in nociceptive circuits. The Journal of neuroscience : the official journal of the Society for Neuroscience 30:2235-2244.

Stefani A, De Murtas M, Pisani A, Stratta F, Bonci A, Mercuri NB, Calabresi P (1995) Electrophysiology of dopamine D-1 receptors in the basal ganglia: old facts and new perspectives. Prog Neuropsychopharmacol Biol Psychiatry 19:779-793.

Sudhof TC (2004) The synaptic vesicle cycle. Annu Rev Neurosci 27:509-547.

Travis ER, Wightman RM (1998) Spatio-temporal resolution of exocytosis from individual cells. Annu Rev Biophys Biomol Struct 27:77-103.

Voets T, Neher E, Moser T (1999) Mechanisms underlying phasic and sustained secretion in chromaffin cells from mouse adrenal slices. Neuron 23:607-615.

Wakade AR, Wakade TD (1983) Contribution of nicotinic and muscarinic receptors in the secretion of catecholamines evoked by endogenous and exogenous acetylcholine. Neuroscience 10:973-978.

Wightman RM, Haynes CL (2004) Synaptic vesicles really do kiss and run. Nat Neurosci 7:321-322.

Wightman RM, Jankowski JA, Kennedy RT, Kawagoe KT, Schroeder TJ, Leszczyszyn DJ, Near JA, Diliberto EJ, Jr., Viveros OH (1991) Temporally resolved catecholamine spikes correspond to single vesicle release from individual chromaffin cells. Proc Natl Acad Sci U S A 88:10754-10758.

Wightman RM, Schroeder TJ, Finnegan JM, Ciolkowski EL, Pihel K (1995) Time course of release of catecholamines from individual vesicles during exocytosis at adrenal medullary cells. Biophys J 68:383-390.

Xu J, Mashimo T, Sudhof TC (2007) Synaptotagmin-1, -2, and -9: Ca(2+) sensors for fast release that specify distinct presynaptic properties in subsets of neurons. Neuron 54:567-581.

Zhang L, Le W, Xie W, Dani JA (2011) Age-related changes in dopamine signaling in Nurr1 deficient mice as a model of Parkinson's disease. Neurobiology of Aging.

Zimmerman JB, Wightman RM (1991) Simultaneous electrochemical measurements of oxygen and dopamine in vivo. Anal Chem 63:24-28.

Zimmermann H (2008) Ectonucleotidases in the Nervous System. In: Purinergic Signalling in Neuron–Glia Interactions, pp 113-130: John Wiley & Sons, Ltd.

Zylka MJ (2011) Pain-relieving prospects for adenosine receptors and ectonucleotidases. Trends Mol Med 17:188-196.

Zylka MJ, Sowa NA, Taylor-Blake B, Twomey MA, Herrala A, Voikar V, Vihko P (2008) Prostatic acid phosphatase is an ectonucleotidase and suppresses pain by generating adenosine. Neuron 60:111-122.

Chapter II

Real-Time Chemical Transmission in Mouse Adrenal Slices

Introduction

Electrophysiological and electrochemical measurements at chromaffin cells, homologues of sympathetic ganglion cells, have revealed fundamental mechanisms underlying exocytosis, the secretory process that initiates intercellular signaling (Travis and Wightman, 1998, von Gersdorff and Matthews, 1999, Bader et al., 2002, Borges et al., 2008, Suudhof, 2008). The majority of these studies have been conducted in primary cultures of chromaffin cells where exocytosis was evoked by pressure ejection of secretagogues such as K^+ and Ba^{2+} (Fox, 1996, Montero et al., 2000, Amatore et al., 2005, Amatore et al., 2006, Haynes et al., 2007, Montesinos et al., 2008). *In vivo*, splanchnic innervations consisting of preganglionic cholinergic neurons play a central role in the initiation of catecholamine secretion (Douglas and Rubin, 1961b). They synapse onto chromaffin cells and release acetylcholine that binds to postsynaptic cholinergic nicotinic and muscarinic receptors located on chromaffin cells. Binding of acetylcholine at cholinergic receptors leads to cell depolarization (Wakade and Wakade, 1982, Borges, 1997, Kajiwara et al., 1997, Aunis and Langley, 1999, de Diego et al., 2008). This change in membrane potential triggers the entry of extracellular Ca^{2+} (Brandt et al., 1976, Kidokoro and Ritchie, 1980). A rise in cytosolic Ca^{2+} concentration initiates a series of events culminating in exocytosis of catecholamines.

To evaluate processes that occur after exocytosis, more intact preparations are required. One approach is to perfuse the blood vessels of the intact adrenal gland.

Catecholamines released into the perfusion fluid can then be analyzed by traditional methods (Wakade and Wakade, 1982). While this approach allows triggers of secretion to be identified, it does not have sufficient time resolution to determine fast events. An alternate approach is to use microelectrodes in adrenal slices, thin pieces of tissue that retain many of the features of the intact gland. Using patch-clamp techniques, the capacitance of cells within slices have been investigated (Moser and Neher, 1997, Barbara et al., 1998). However, these electrophysiological signals can be difficult to interpret since they represent a temporal mosaic of both exocytotic and endocytotic events. Recently, Arroyo *et al.* reported on the kinetics of exocytosis in murine adrenal slices employing constant potential amperometry at carbon-fiber microelectrodes (Arroyo et al., 2006). They showed that catecholamine exocytosis from individual chromaffin cells located on a slice's surface could be measured when evoked by electrical field stimulation of the splanchnic nerve innervations.

In this work we describe a real-time study of factors that control the secretion of catecholamines in an *in situ* murine adrenal slice preparation. The spatial and temporal resolution of carbon-fiber microelectrode sensor was exploited to probe the heterogeneity of the preparation. Cyclic voltammetry was used to identify the released substances as catecholamines. Optical imaging techniques, in particular standard light microscopy and confocal laser scanning microscopy, were utilized for identification and visualization of adrenomedullary compartments. Both spontaneous and electrically stimulated release of catecholamines were measured inside clusters of chromaffin cells. Spontaneous events originated from single vesicles whereas electrical stimulation evoked release comprised of multiple vesicles.

Experimental

Animals

Wild-type C57BL/6J female mice 4-8 weeks of age were used in the experiments described herein (stock no. 000664, Jackson Laboratories, Bar Harbor, ME, USA). Mice were housed at the University of North Carolina Husbandry Facility (Kerr Hall – UNC School of Pharmacy) with *ab libitum* access to food and water and under closely controlled environmental conditions (temperature, humidity, and 12-hr light/dark cycles). Live animal handling procedures and experimental protocols have been approved by the University of North Carolina's Institutional Animal Care and Use Committee.

Adrenal Slice Methods

Adrenal gland slicing procedures were as described previously with slight modifications (Moser and Neher, 1997, Barbara et al., 1998). Mice were anesthetized using ethyl ether (Fisher Scientific), decapitated, and subjected to a midline abdominal incision which allowed for access to the adrenal glands. Glands were placed into ice-cold and 95 % O_2 – 5 % CO_2 saturated bicarbonate-buffered saline containing (in mM): 0.1 $CaCl_2$, 125 NaCl, 26 $NaHCO_3$, 2.5 KCl, 1.25 NaH_2PO_4, 3 $MgCl_2$, 10 glucose and 10 HEPES or Tris at pH=7.4. Fat tissue was removed under a dissecting microscope (Leica Wild M3Z) and each gland was placed into 3 % agarose (w / v), (Promega, gelling point of 24-28 °C). Agarose blocks containing a gland were placed on ice in order to complete gel formation (< 3 min), secured onto the Teflon specimen holder, and mounted into a vibroslicer (Campden Instruments, World Precision Instruments, Leics, U.K.) filled with ice-cold buffer. The agarose block was oriented so that the largest base of the gland was parallel to the specimen holder (Barbara et al., 1998). Adrenal glands were cut into slices of ~ 200 μm in thickness.

Slices were immediately placed into a perfusion chamber (open diamond bath heated chamber, RC-22, Warner Instruments, Hamden, CT) and secured with a Lycra® thread anchor (1.5 mm-2.0 mm thread spacing, Warner Instruments, Hamden, CT). The chamber was continually perfused with 95 % O_2 – 5 % CO_2 saturated bicarbonate-buffered saline at a rate of 1-2 mL/min and containing (in mM): 2 $CaCl_2$, 125 NaCl, 26 $NaHCO_3$, 2.5 KCl, 1.25 NaH_2PO_4, 1 $MgCl_2$, 10 glucose and 10 HEPES or Tris at pH=7.4. Osmolarities of all buffers were maintained at ~ 310 mOsM/L by adjusting the concentrations of $MgCl_2$ and $CaCl_2$ accordingly. The temperature of the perfusion chamber was kept at 37 °C using a dual automatic temperature controller (Warner Instruments, LLC). Slices were electrically stimulated via two tungsten microelectrodes glued together and separated by a distance of approximately 150 µm (FHC, Bowdoin, ME). To evoke catecholamine release, trains of biphasic pulses (150 µA, 2 ms each phase, 10 pulse, 10 Hz) were applied to the stimulating electrodes. These stimulation parameters are similar to those used in brain slices (Miles et al., 2002). All of the experiments were completed within a 10-hr *post mortem* period. To avoid recordings from a damaged tissue layer, microelectrodes were lowered to a distance of approximately 30 µm below the slice surface (Kennedy et al., 1992). Slices were equilibrated for ~ 2 hrs prior to data collection. During the equilibration period slices were electrically stimulated every 3-5 min. These data were used to establish a baseline level of catecholamine release.

Immunohistochemistry and Confocal Microscopy

Free-floating 200 µm thick adrenal tissue slices were fixed in 2 % para-formaldehyde solution, made from a 37 % formaldehyde solution in H_2O (Sigma-Aldrich), which was diluted in Sorensen's phosphate buffer (0.15 M K_2HPO_4/NaH_2PO_4, pH=7.4). After a 4 hr fixation period, slices were rinsed with phosphate buffered saline (PBS) at room temperature (6 x 10 min, pH=7.4). Slices were then transferred to blocking solution containing 25 mL of

PBS (pH=7.4), 1 % bovine serum albumin (Sigma-Aldrich), 10 % normal goat serum (Invitrogen) and 0.3 % Triton-X 100 (The Chemistry Store, Pompano Beach, FL) for 2 hrs at room temperature. The blocking solution was then removed and slices were incubated with the primary antibody to tyrosine hydroxylase (1/100, Chemicon-Millipore AB152) at 4 °C for 72 hrs. Slices were rinsed with PBS (6 x 10 min) at room temperature and incubated with the secondary antibody for 48 hours at 4 °C (1/4000, Molecular Probes, A21245). Hoechst 33342 nuclear stain (Invitrogen) was added after 6 x 10 min PBS rinses following secondary antibody incubation for 10 min and was followed by rinsing with PBS (6 x 10 min). The slices were then affixed to microscope slides with ProLong Gold mounting media (Invitrogen). Slides were then coverslipped and the mounting media was allowed to dry for 24 hrs. Adrenal tissue slices were examined with a Leica SP2 laser scanning confocal fluorescence microscope (Michael J. Hooker Microscopy Facility, UNC-CH). A photomultiplier tube was used as a detector. Confocal images were processed in Leica Confocal Software (Leica Microsystems, Germany) and Adobe Photoshop (version 7.0).

Preparation of Isolated Chromaffin Cells

Murine chromaffin cells were prepared as previously described (Kolski-Andreaco et al., 2007) with some modifications. Mice were deeply anesthetized with ether, decapitated, and the adrenal glands rapidly removed into ice-cold, oxygenated Ca^{2+} and Mg^{2+}-free Locke's buffer containing (in mM): 154 NaCl, 3.6 KCl, 5.6 $NaHCO_3$, 5.6 glucose, and 10 HEPES, pH = 7.2. The medullae were isolated via gentle removal of cortical tissue and digested for 20 min at 37 ^{o}C in Dulbecco's Modified Eagle's Medium/Nutrient Mixture F-12 Ham (DMEM/F12) with 25 U/mL papain. The digestion media was replaced with a fresh aliquot, followed by a second 20 min digestion period. Digested tissue was washed and triturated with pipette tips of decreasing bore size in 500 µL DMEM/F12 with 10 % fetal bovine serum and 2 % horse serum. The resulting cell suspension was distributed evenly to

3 poly-L-lysine-coated (0.1 mg/mL) 25 mm round glass coverslips. After 15 min attachment, plates were fed with 2 mL DMEM/F12 containing 100 U/mL penicillin, 0.1 mg/mL streptomycin, 50 U/mL nystatin, and 40 µg/mL gentamicin. Plates were maintained in a humidified, 5 % CO_2 atmosphere at 37 ^oC for at least 24 hrs prior to experimentation.

Fabrication of the Microelectrode

Carbon-fiber elliptical microelectrodes were fabricated as previously described (Kawagoe et al., 1993, Cahill et al., 1996). A single T-650 or P-55 carbon fiber (Thornel, Amoco Corp., Greenville, SC) was aspirated into a glass capillary (1.2 mm x 0.68 mm x 4," A-M Systems, Sequim, WA) and gravity pulled with a vertical pipette puller (model PE-21, Narishige Group, Japan). The glass seal was cut with a surgical blade, sealed with epoxy as previously described (Kawagoe et al., 1993), and polished at 45^o on a fine diamond abrasive plate mounted onto a microelectrode beveler (BV-10, Sutter Instruments). Prior to use, carbon-fiber microelectrodes were soaked in activated carbon / 2-propanol mixture for a minimum of 30 min. Microelectrodes were backfilled with 4 M CH_3COOK/0.15 M NaCl and mounted onto a potentiostat headstage using stainless steel wire to make an electrical contact.

Fast-Scan Cyclic Voltammetry

In FSCV studies, a triangular waveform was applied to the carbon-fiber microelectrode with an Axopatch 200B patch-clamp amplifier in voltage clamp mode and β=0.1 configuration (Axon Instruments, Molecular Devices, Union City, CA). The potential was swept at 600 V/s from - 400 mV to + 1000 mV and back to - 400 mV at a frequency of 10 Hz. Under these conditions the catecholamines are oxidized at + 600 mV and reduced at - 200 mV versus Ag/AgCl reference electrode. In between scans, the electrode potential

was held at - 400 mV allowing for catecholamine adsorption onto the carbon fiber surface. The signal was filtered with a built-in analog low-pass Bessel filter (80 dB/decade) at 5 kHz.

To distinguish between epinephrine and norepinephrine an extended waveform was used as previously described (Pihel et al., 1994). Briefly, the working electrode was held at + 100 mV and scanned from + 100 mV to + 1425 mV at 800 V/s at a frequency of 10 Hz. Due to the Axopatch 200B being unable to perform potential scans beyond 1000 mV, a custom made Universal Electrochemistry Instrument (UEI, UNC Electronics Design Facility) was used. This instrument is a two-electrode system optimized for FSCV. While this waveform eliminates catecholamine reduction, it forces epinephrine to undergo a secondary amine oxidation reaction resulting in a second oxidation peak at near + 1400 mV. Norepinephrine does not undergo this second oxidation since it is a primary amine.

Both potentiostats as well as the stimulation parameters were controlled via locally written LABVIEW software, TarHeel CV (ESA, Chelmsford, MA). Stimulations were applied in between each voltammetric scan while the working electrode was held at - 400 mV so electrochemical recordings were not stopped during the electrical stimulation. Measured currents were digitized using a National Instruments PCI-MIO-16XE-10 card and monitored as a function of the applied potential.

Voltammetric Data Analysis

Voltammetric data analysis was performed with the locally written LABVIEW software TarHeel CV data analysis (ESA, Chelmsford, MA). The voltammograms were background subtracted using files obtained before stimulation. Sets of background-subtracted cyclic voltammograms were displayed as color plots (Michael et al., 1998) in which the cyclic voltammograms are sequentially stacked together in time (abscissa) and plotted against the applied potential (ordinate). The measured currents are shown in false color. The current that flows at + 600 mV is due to catecholamine oxidation, and it was calibrated in

concentration units by measurement of authentic standards in a flow injection analysis system. Since the electrochemical signals recorded in the adrenal medulla consist of both epinephrine and norepinephrine, calibration factors in this work were derived using solutions of 1-10 μM epinephrine, norepinephrine, or mixtures. Data obtained during administration of pharmacological agents are reported as current values normalized to currents recorded under control (pre-drug) conditions.

Constant-Potential Amperometry

The potential applied to the carbon-fiber microelectrode was + 700 mV to assure complete electrolysis of released catecholamines. Amperometric data was obtained at a collection frequency of 20-50 kHz, and recorded amperometric traces were analog filtered at 5 kHz with an internal low-pass Bessel filter (Digidata 1320A controlled by P-Clamp software, Molecular Devices). The data were then digitally filtered at 300 Hz with a Butterworth filter in locally written LABVIEW program (Tar Heel Amperometry) (Haynes et al., 2007). Exocytosis was monitored either in the absence or presence of electrical or chemical stimulation. Acetylcholine (1 mM) was pressure ejected at 2-5 psi for 50-100 ms using a Picospritzer (Parker Instruments, Pine Brook, NJ) from capillaries with a 0.68 mm inner diameter (AM Systems, Sequim, WA) that were pulled on a Sachs-Flaming Micropipette Puller Model PC-84 (Sutter Instruments, Novato, CA) and adjusted to a final inner diameter of 10-15 μm at the tip.

Amperometric Data Analysis

Amperometric traces were analyzed with MiniAnalysis software (version 6.0.3, Synaptosoft, Inc., Decatur, GA). Events were classified as an exocytotic event if they were five times greater than the root mean square of noise. Amperometric spike parameters quantified were the area under the spike (Q) and the spike's width at half height ($t_{1/2}$).

Examination of $t_{1/2}$ allowed for kinetics and underlying physiological mechanisms of catecholamine release to be studied.

Pharmacology

Pharmacological agents employed in studies include tetrodotoxin (TTX), hexamethonium (HEX), atropine (ATR), 4-Diphenylacetoxy-N-(2-chloroethyl)piperidine hydrochloride (4-DAMP), and carbenoxolone (COX). Drugs were dissolved in recording buffer and superfused through the slice chamber at a rate of ~ 2 mL/min. All of the drugs were obtained from Sigma-Aldrich (St. Louis, MO, USA) and used as received.

Statistical Analysis

Statistical analysis was performed in GraphPad Prism (GraphPad Software, Inc., San Diego, CA, USA). Data are reported as means ± SEM. Student's *t*-test (paired) was used to test for significant differences between data sets. Data were considered significant at the 95 % confidence level and are reported as the mean ± SEM. The number of slices is indicated by n, unless noted otherwise.

Results

Brightfield and Immunofluorescent Assessment of Murine Adrenal Slices

Rat chromaffin cells within the adrenal medulla are organized into clusters containing ~ 20 cells with each cell receiving one to four synaptic boutons (splanchnic nerve innervations) (Kajiwara et al., 1997). Brightfield imaging of murine tissue slices revealed similar clusters. In addition to chromaffin cell clusters, the pericellular space (space between two neighboring clusters), and the vasculature (in particular the central vein) were

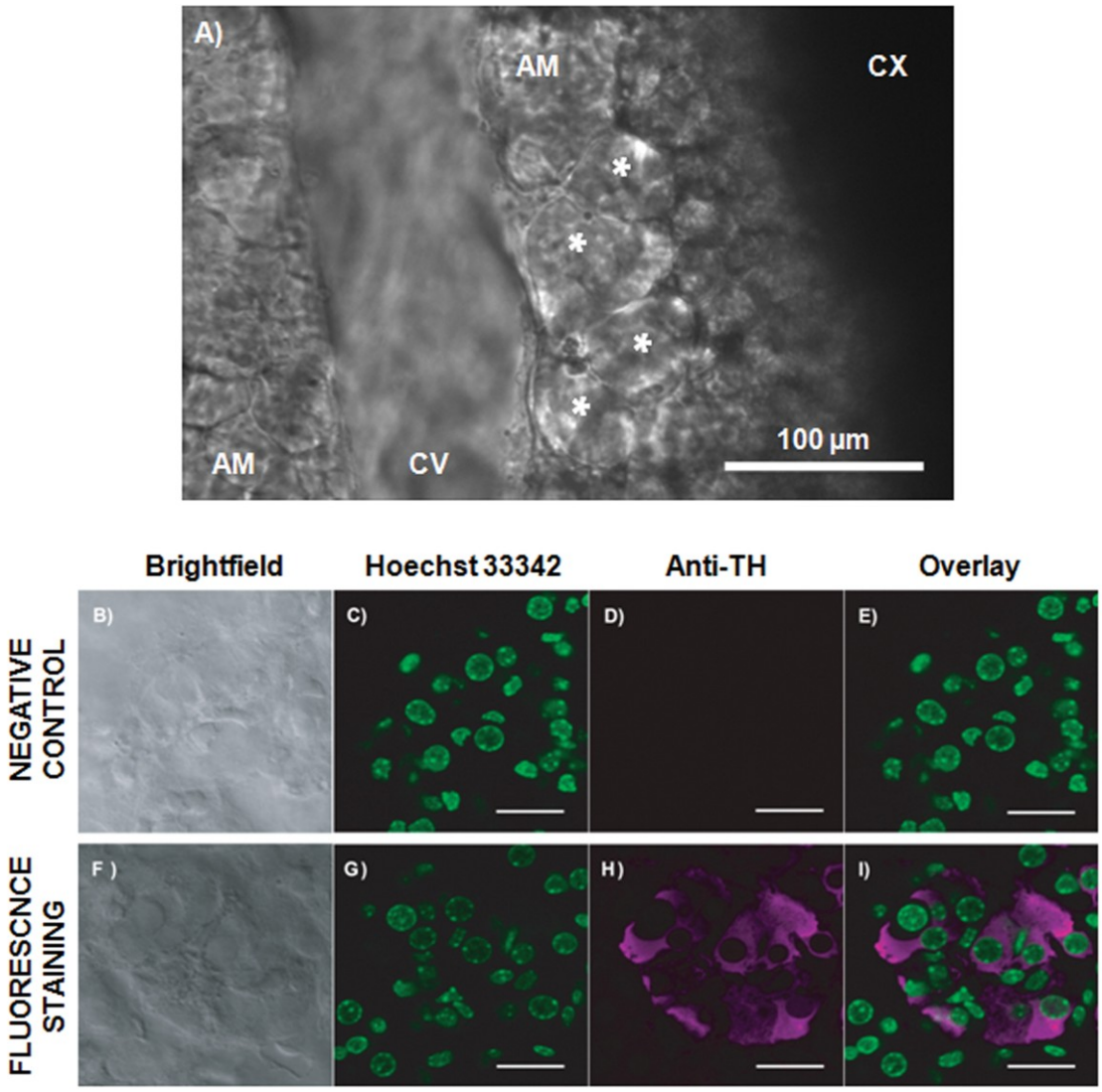

Figure 2.1. Adrenomedullary microenvironments. (A) Representative brightfield image of adrenomedullary microenvironments: AM – adrenal medulla, CV – central vein, CX – adrenal cortex. Asterisks mark four chromaffin cell clusters. Brightfield images (B) and (F) show two adrenomedullary microenvironments identified as chromaffin cell clusters. Fluorescent images (C – E) show a negative control experiment where the primary antibody to TH was omitted from the immunohistochemical protocol. Images (G – I) show the localization of the TH immunofluorescence to cytoplasm of chromaffin cells contained within a cluster. In both experiments, the nuclei were stained with Hoechst 33342 (C) and (G). In H, TH antibody conjugated to Alexa Fluor® 647 labels chromaffin cells contained within a cluster. (E) and (I) show C / D and G / H overlays respectively. Scale bar: 25 µm.

also apparent (Figure 2.1A). The murine chromaffin cell clusters were on average 60-80 μm in diameter and contained ~ 15 chromaffin cells.

Brightfield images of clusters are shown in Figure 2.1, B and F. These slices were labeled to allow confocal microscopy of nuclei and tyrosine hydroxylase (TH). To visualize cell nuclei, tissue slices were incubated with Hoechst 33342, and, as expected, labeling was found in all cells (Figure 2.1, C and G). To visualize TH containing cells, an indirect immunofluorescence method was employed. A secondary antibody conjugated to Alexa Fluor® 647 fluorochrome was used to react with the primary antibody to TH (Pickel et al., 1975) (Figure 2.1H). In a negative control experiment the primary antibody to TH was omitted from the immunohistochemical protocol and no labeling was present (Figure 2.1D). The overlay reveals tight packaging of chromaffin cells within a cluster (Figure 2.1, E and I) that is apparent even with brightfield illumination. These experiments make clear that chromaffin cells exist in clustered arrangements in murine adrenal glands, and the clusters can be visualized by brightfield microscopy.

Cyclic Voltammetric Recording of Electrically Evoked Release

Clusters were chosen for the measurement of electrically evoked catecholamine release. A carbon-fiber microelectrode was positioned within a cluster, approximately 30 μm below the slice surface, with the stimulating electrodes on either side of the working electrode (Figure 2.2). The color plot (lower part of Figure 2.3) reveals the cyclic voltammetric changes in electrochemically active species that occur over a 55 s interval. At t = 0 in Figure 2.3, an electrical stimulation (1-s train of biphasic pulses, 10 Hz) was initiated. Catecholamines are oxidized at + 600 mV under these voltammetric conditions, and the current at this potential is plotted above the color plot in Figure 2.3. Fluctuations in catecholamine concentrations are apparent before and after the stimulation, and this was the case in 90 % of adrenal tissue preparations (14 out of 16 slices). Typically, the rapid

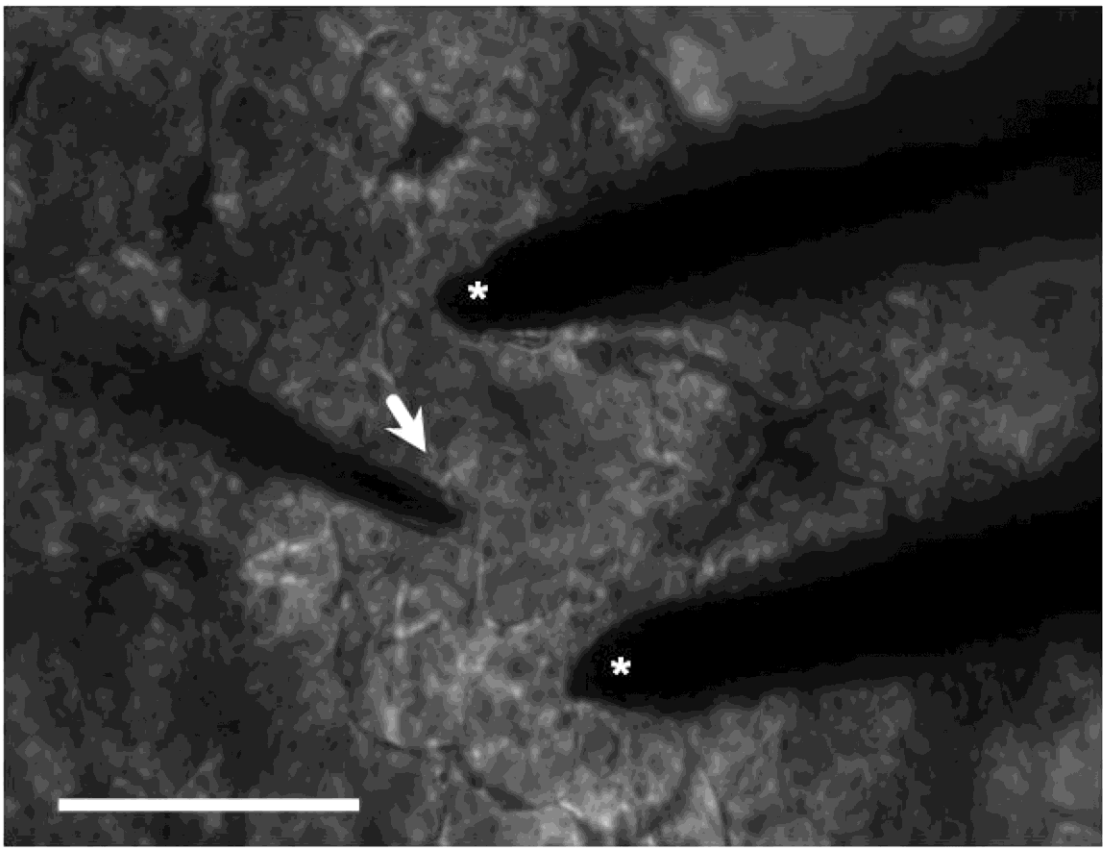

Figure 2.2. Brightfield micrograph of an electrochemical recording setup. Carbon-fiber microelectrode (arrow points to the microelectrode tip) is positioned within a chromaffin cell cluster; the stimulating electrode consisting of two tungsten electrodes (tip of each is marked with an asterisk) is placed on top a slice straddling the electrochemical sensor. Scale bar: 100 μm.

spontaneous events occurred near the natural basal firing frequency of chromaffin cells, 0.5 Hz (Chan and Smith, 2003). The electrical stimulation evokes a large, immediate increase in catecholamine concentration, and the increase continues for ~ 2 s after the end of the stimulation. The concentration then returns to baseline within 10-15 s where the spontaneous release events are apparent. The cyclic voltammograms for both the electrically evoked release and the spontaneous events (Figure 2.3, *inset*) were identical to those of norepinephrine and epinephrine.

Modulation of Electrically Evoked Release by Ions

Exocytotic release of catecholamines is Ca^{2+} dependent at isolated bovine chromaffin cells (von Ruden and Neher, 1993). To verify that this is the case in chromaffin cells of murine adrenal slices, tissue was superfused with low Ca^{2+} buffer (0.1 mM). Electrically evoked release was completely eliminated (Figure 2.4A, upper panel) at a location where spontaneous events were not evident. Cumulative results are summarized in Figure 2.4A, lower panel (n = 3 slices). Reintroduction of 2.0 mM Ca^{2+} restored the electrically stimulated release (97 ± 4 % of control, $p > 0.05$).

To confirm that release in murine adrenal slices requires electrical excitability, slices were superfused with physiological buffer containing 1 μM tetrodotoxin, TTX, a Na^{+} channel blocker (Fuhrman, 1986). With a superfusion rate of 2 mL/min, it took 5 minutes for TTX to abolish catecholamine release (Figure 2.4A, lower panel, n = 4 slices). Evoked release returned to pre-drug levels 20 min after its washout (95 ± 2 % of control, $p > 0.05$).

Role of Cholinergic Neurotransmission and Gap Junctions During Electrically Evoked Catecholamine Release

Chromaffin cells have nicotinic and muscarinic receptors that are activated by acetylcholine release from the splanchnic nerve (Douglas and Rubin, 1961a, Douglas and Poisner, 1965).

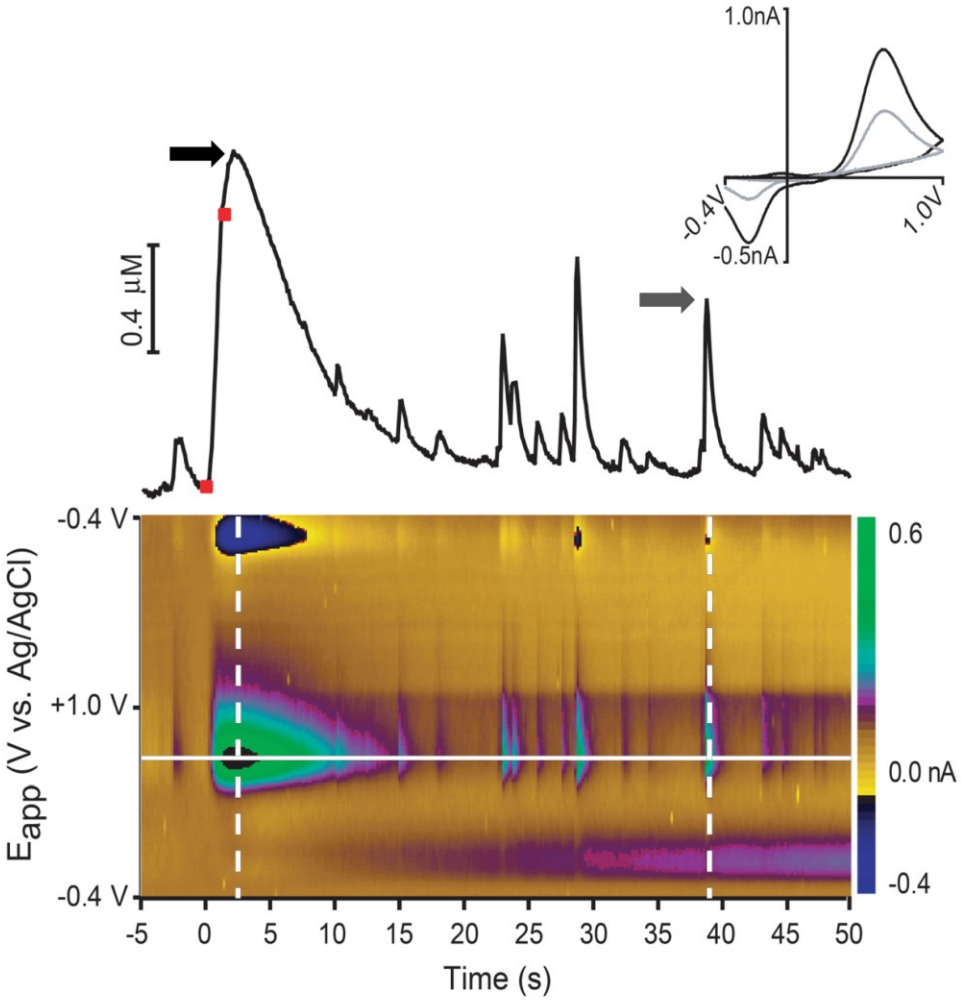

Figure 2.3. Representative electrically evoked catecholamine release event in a chromaffin cell cluster. The color plot shows current changes observed prior to (-5 s to 0 s), during (0 s to 1 s), and following (1 s to 50 s) the delivery of an electrical stimulus. Catecholamines are oxidized at + 600 mV vs. Ag/AgCl (green) and the resultant *o*-quinone is reduced at – 200 mV (dark blue). The trace above the color plot shows the changes in catecholamine concentrations that occur as a result of the electrical stimulation (extracted at + 600 mV, solid horizontal line). The delivery of electrical stimulation at time 0 s is indicated by a red bar; the second red bar at time 1 s marks the end of stimulation. Cyclic voltammograms (inset) that confirms signal's catecholaminergic chemical identity were extracted from the color plot at the time of the maximum concentration change (striped vertical lines). The black arrow points to the maximum concentration change for electrically stimulated release and it corresponds to the cyclic voltammogram plotted in black; the gray arrow points to the maximum concentration change for spontaneous catecholamine release event and it corresponds to the gray cyclic voltammogram.

To establish whether elements of the splanchnic nerve are depolarized by the stimulation, two pharmacological agents were used. The cholinergic nicotinic receptor (nAChR) antagonist, hexamethonium (HEX, 100 μM) was perfused through the slice. Following 20 min of superfusion with HEX, electrically evoked catecholamine release was inhibited (representative example in Figure 2.4B, upper panel, cumulative results in Figure 2.4B, lower panel, $n = 5$ slices, $p < 0.001$). Release returned to its original levels 20 min after removal of HEX. In contrast, 25 min exposure of slices to the muscarinic receptor (mAChR) antagonists, atropine (ATR, 0.5 μM), competitive and nonselective antagonist at mAChR's (Zwart and Vijverberg, 1997) or 4-DAMP (1 μM), an irreversible antagonist at M_1, M_3, M_4 and M_5 mAChR subtypes (Moriya et al., 1999), did not significantly affect the released catecholamine concentrations (Figure 2.4B, lower panel, $n = 3$ and $p > 0.05$ for both drugs).

We also examined whether gap junctions (electrical synapses) were involved in the electrically evoked release in slices (Moser, 1998, Martin et al., 2001). Superfusion of murine adrenal slices with the uncoupling agent and gap junction blocker carbenoxolone (COX, 100 μM) did not alter electrically evoked catecholamine release (Figure 2.4B, lower panel, $n = 3$, $p > 0.05$). Thus, chromaffin cell junctional coupling does not contribute to catecholamine secretion evoked by electrical stimulation.

Spontaneous Catecholamine Secretion

Spontaneous events closely resemble the exocytotic release events recorded at individual cultured chromaffin cells (Troyer and Wightman, 2002). The spiking activity was confined to cell clusters and it was entirely absent in the pericellular microdomain and vascular recordings (data not shown). We used FSCV to find sites that exhibited spontaneous catecholamine release, and the recording mode was then switched to amperometry to determine coulometrically the amount released (representative example in Figure 2.5A). When the electrode potential was held at 0.0 V instead of + 700 mV,

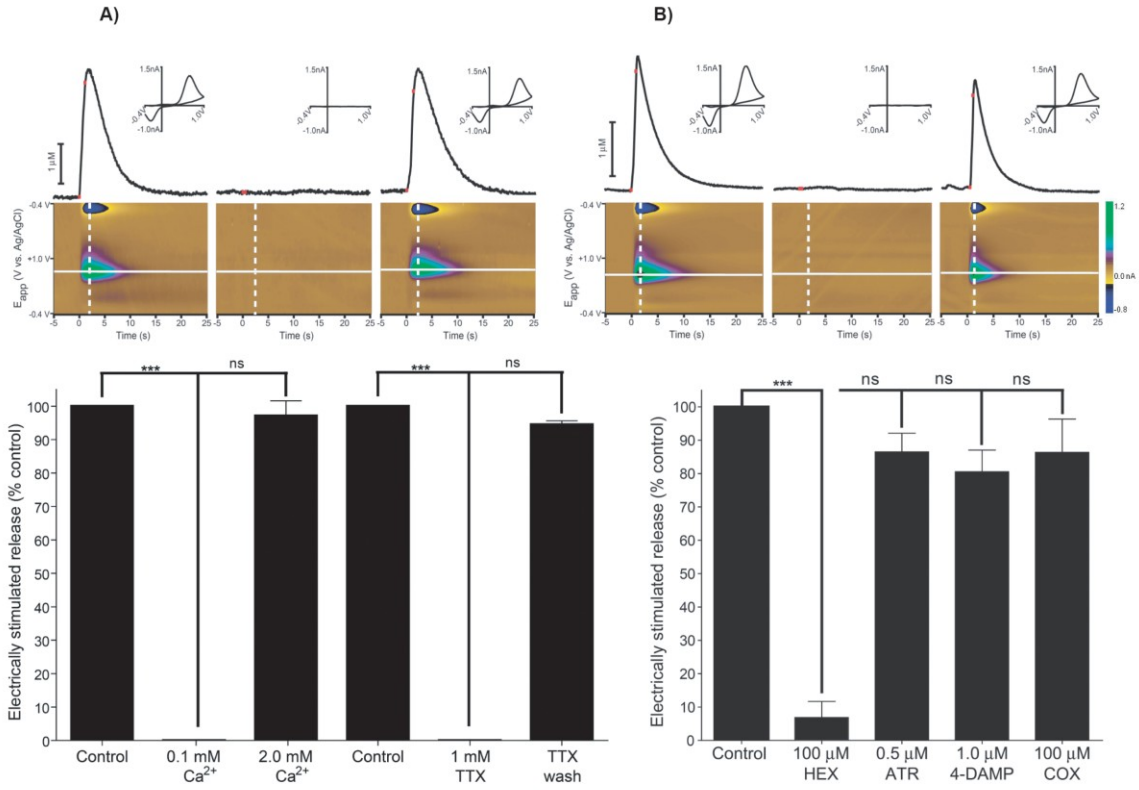

Figure 2.4. Modulation of electrically stimulated catecholamine release. (A) Transmural electrical stimulation of tissue slices during perfusion of low Ca^{2+} buffer (0.1 mM) results in the absence of catecholamine release. Top panel shows representative catecholamine concentration vs. time traces and their corresponding color plots before (left), during (middle), and after (right) low Ca^{2+} buffer perfusion. The inset cyclic voltammograms confirm catecholaminergic nature of the detected signal. Lower panel shows a summary of the modulation of catecholamine release by low Ca^{2+} buffer and tetrodotoxin. (B) Slice perfusion with HEX abolishes electrically stimulated release. Similar to (A), top panel of (B) shows representative catecholamine concentration vs. time traces and their corresponding color plots before (left), during (middle), and after (right) 100 µM HEX perfusion. Lower panel summarizes the modulation of release by the nicotinic (HEX) and muscarinic (ATR and 4-DAMP) AChR antagonists as well as the gap junction blocker COX. *** $p < 0.001$

spontaneous activity was not observed (data not shown). Amperometric spikes were recorded at 7 spontaneously active sites, and the area under each spike (Q, fC) and the width at half height ($t_{1/2}$, ms), were quantified. These were compared to the same values measured during exocytosis at 21 isolated murine chromaffin cells stimulated with a high extracellular K^+ solution. In slices the average Q value was 418 ± 37 fC whereas in cells it was 377 ± 43 fC. In slices the average $t_{1/2}$ value was 12.5 ± 1.7 ms whereas it was 8.9 ± 1.5 ms at single cells. The values of Q and $t_{1/2}$ are not statistically different in the two preparations ($p > 0.05$).

To test whether these spontaneous events were triggered by endogenous acetylcholine, 100 μM HEX was perfused through the slice. Twenty minutes after HEX perfusion, the number of spontaneous events was dramatically reduced (Figure 2.5B). While Q and $t_{1/2}$ remained unchanged between the pre-drug recordings and those obtained in the presence of HEX (data not shown), the spiking frequency was found to decrease to 30% of the pre-drug levels (Table 2.1, $p > 0.05$). Therefore, spontaneous catecholaminergic release events are triggered by acetylcholine originating either from leakage or spontaneous activity at the splanchnic nerve terminals. To confirm both the exocytotic origin of the events, low Ca^{2+} (0.1 mM) buffer was perfused through the slice. Twenty minutes after perfusion with low Ca^{2+}, the number of spontaneous events was 10% of pre-drug levels (Table 2.1, Figure 2.5, C and D). After the reintroduction of 2 mM Ca^{2+}, spontaneous exocytotic event frequency remained low (Figure 2.5E, 0.03 ± 0.01 Hz). However, catecholamine secretion events were evoked by pressure ejection of 1 mM acetylcholine (ACh) and returned to a modest frequency of 0.24 ± 0.09 Hz for $t > 1$ min (Figure 2.5F). In this experiment, the concentration of ACh that reaches the secreting cell is not known—it is certainly lower than the applied concentration because the 60 μm distance between the pressure ejection pipette and the secretion site within the slice is much larger than the radius of the ejected droplet (~20 μm).

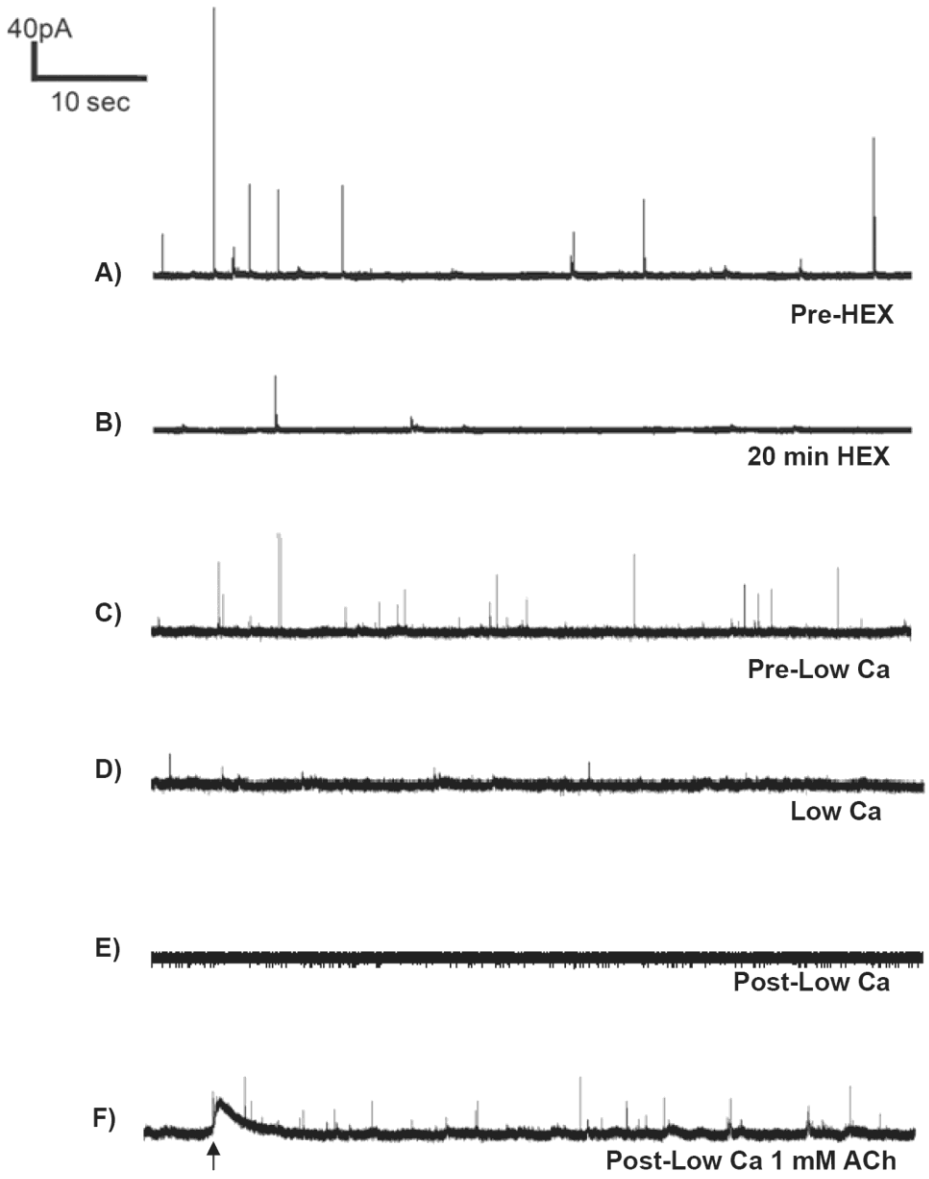

Figure 2.5. Biological origin of spontaneous catecholamine secretion. The representative amperometric recording of spontaneous catecholamine release in (A) was obtained by holding the microelectrode at a DC potential of + 700 mV; in (B), the number of spontaneous release events was reduced by ~ 70 % following a 20 min perfusion of the slice preparation with HEX, a nAChR blocker. A 20 min perfusion with a low Ca^{2+} (0.1 mM) buffer reduced the number of spontaneous events by ~ 90% (C and D) and was recoverable by pressure ejection of 1 mM ACh (E and F).

Table 2.1. Summary of exocytotic spikes measured by amperometry in adrenal slices. Amperometric spike parameter analysis prior to and following inclubation in hexamethonium or low extracellular Ca^{2+} treatment. For hexamethonium, n = 9 slices and for low Ca^{2+}, n = 5 slices.

Trace	f (Hz)	t_{total} (sec)	n_{spikes}
HEX Control	0.27 ± 0.03	540	146
HEX	0.08 ± 0.01	540	44
Ca^{2+} Control	0.33 ± 0.10	300	100
Low Ca^{2+}	0.04 ± 0.01	300	11
Post Low Ca^{2+}	0.03 ± 0.01	300	8
1 mM ACh Pressure Ejection	0.24 ± 0.09	300	73

Chemical Analysis of Spontaneous and Electrically Stimulated Release

Murine adrenal glands contain approximately twice as much epinephrine as norepinephrine and negligible amounts of dopamine (Ally et al., 1986). To reveal the contributions of individual catecholamines to both spontaneous and electrically stimulated release, cyclic voltammetric measurements were made using a waveform that allows the two catecholamines to be distinguished (Pihel et al., 1994). Epinephrine yields a second oxidation wave at + 1300 mV on the reverse scan. Thus, the cyclic voltammogram is due to epinephrine if there is a peak at + 600 mV and + 1300 mV, and it is norepinephrine if it only has a peak at + 600 mV. With the microelectrode in a chromaffin cell cluster, the voltammograms revealed that spontaneous release events were either adrenergic or noradrenergic but not both (representative example in Figure 2.6). Note that the norepinephrine example shown has no peaks at + 1300 mV and the current trace from that potential exhibits no fluctuations. A total of 13 cells were investigated; 8 were adrenergic and 5 were noradrenergic.

Upon electrical stimulation, sites that spontaneously released exclusively epinephrine remained adrenergic (representative example in Figure 2.7, left panel). Post-calibration of the electrode in norepinephrine and epinephrine solutions confirmed that the signal was 95.5 ± 1.3 % epinephrine (n = 8). However, electrically stimulated release in sites where spontaneous release was due to norepinephrine showed a different response. Release at these sites clearly contained an epinephrine component (Figure 2.7, right panel). In this case post-calibration showed that the electrically stimulated release was 43.5 ± 8.1 % epinephrine (n = 5).

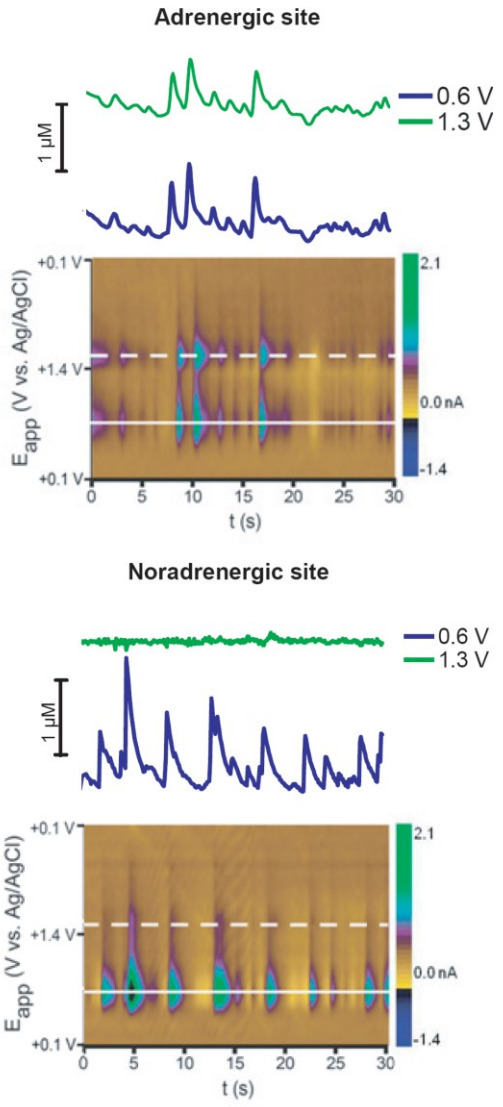

Figure 2.6. Electrochemical analysis of spontaneous catecholamine release. Catecholamine concentration vs. time traces and their corresponding color plots show spontaneous adrenergic (left panel) and noradrenergic (right panel) secretory activity observed within two separate cell clusters. Top (green, extracted at + 1300 mV) and bottom (blue, extracted at + 600 mV) concentration traces reveal chemical identity of the catecholamine released: spontaneous secretion of epinephrine is established by the presence of voltammetric spikes at both + 1300 mV (striped white line in color plot) and + 600 mV (solid white line in color plot) while spontaneous norepinephrine secretion is confirmed by the presence of spikes at + 600 mV but not at + 1300 mV. Catecholamine concentration vs. time traces for + 600 mV and + 1300 mV are offset for clarity.

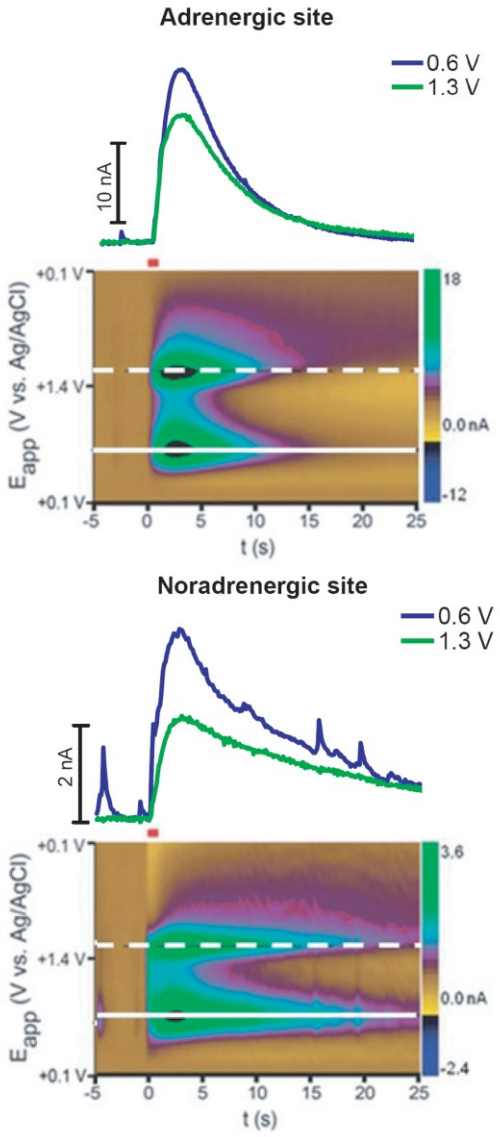

Figure 2.7. Electrochemical analysis of electrically evoked catecholamine release. Catecholamine concentration vs. time traces and their corresponding color plots reveal the chemical identity of electrically evoked release in locations that have been identified based on spontaneous secretory activity as either adrenergic (left) or noradrenergic (right). The site that was previously found to spontaneously release only norepinephrine displays the presence of a second oxidation event as evident from the color plot on the right as well as the concentration vs. time trace at + 1300 mV.

Discussion

This work extends that of Arroyo *et al.* who examined catecholamine release by amperometry at the surface of murine adrenal slices (Arroyo et al., 2006). Here, we have used cyclic voltammetry to identify the released substances as catecholamines. In addition, we measured release from chromaffin cells located deep within tissue slices where they are surrounded by their normal physiological conditions. Consistent with the work of Arroyo *et al.*, we found two patterns of release. Spontaneous release events occurred at a low frequency, were composed of either norepinephrine or epinephrine, and had a duration of a few milliseconds. These events appeared to be triggered by endogenous acetylcholine since they were significantly less frequent in the presence of the nicotinic receptor antagonist, HEX. The amount released during those events was identical to individual exocytotic events at single cultured cells. Local electrical stimulation evoked a massive release that lasted for multiple seconds. Electrically stimulated release was almost completely eliminated by HEX indicating that the secretion was not a direct consequence of depolarization of chromaffin cells. Rather, electrical stimulation appeared to activate the splanchnic nerve, releasing acetylcholine that in turn triggered catecholamine secretion. In contrast to the spontaneous release events, electrically stimulated release at sites that showed noradrenergic release was composed of a mixture of adrenergic and noradrenergic electrochemical signals. This finding supports the concept that electrically evoked release consists of multiple catecholamine quanta originating from several chromaffin cells that release in synchrony.

Although chromaffin cells are electrically excitable (Biales et al., 1976, Kidokoro and Ritchie, 1980), the electrical stimulation used in this work does not directly affect them. Rather, the stimulation appears to be activating the splanchnic nerve, a group of fibers that are not distinguishable by brightfield microscopy (Barbara et al., 1998), because it was virtually abolished by HEX. Electrically stimulated release in murine slices was independent

of ATR and 4-DAMP, the two pharmacological agents that collectively block all five subtypes of muscarinic receptors found in chromaffin cells. Thus, electrically stimulated release is mediated by the evoked release of acetylcholine that activates nicotinic receptors on chromaffin cells. While some literature reports that muscarinic receptor activation can evoke catecholamine release (Nassar-Gentina et al., 1988), we did not find that muscarinic antagonists affected release even with long incubation times. We did not investigate other agents that have been reported to evoke catecholamine release from adrenal cells such as pituitary adenylate cyclase-activating polypeptide (Przywara et al., 1996) or opioids (Malhotra and Wakade, 1987). Electrically evoked catecholamine release in adrenal slices was dependent on extracellular [Ca^{2+}] implying that release arises from exocytosis. Release was also blocked by TTX indicating that functional Na^{+} channels are necessary for release. However, due to the involvement of the splanchnic nerve in electrically stimulated release, the TTX and low Ca^{2+} findings may be due to regulation of acetylcholine release, which in turn regulates catecholamine release. Unlike prior work, we did not find evidence for cell junctional coupling in the slice (Moriya et al., 1999).

Spontaneous catecholamine release events were detected via fast scan cyclic voltammetry and their vesicular nature was confirmed with amperometry. By comparison with results in cultured cells, it is clear that these events are single exocytotic events ongoing within adrenal tissue slices. This finding was unexpected because in brain slices, prepared in an identical fashion, spontaneous release events are not observed with carbon-fiber microelectrodes in regions that are rich in catecholaminergic terminals (Kelly and Wightman, 1987, Jones et al., 1995, Jones et al., 1996, Bunin et al., 1998, Miles et al., 2002, Johnson et al., 2007). However, chemical neurotransmission in the brain is a local process with transporters regulating the long range spread of chemical messengers. In contrast, the adrenal gland architecture is optimized to allow access of catecholamines to the blood stream where they are directed to distant receptors. Similar to electrically evoked

release, the spontaneous events are triggered by endogenous acetylcholine, presumably arising from the splanchnic nerve.

Some spikes may originate from damaged chromaffin cells caused while lowering the microelectrode. However, the approximate 3-fold reduction in the frequency of spontaneous catecholamine secretory events caused by HEX indicates that a significant amount of the release was from intact chromaffin cells. In a survey of 16 tissue slices that exhibited spontaneous release when the electrode was first inserted, only two showed a rundown of secretory events after two hours. Additionally, after perfusion in a low Ca^{2+} buffer, spontaneous release events decreased by 90% and they did not recover when high Ca^{2+} was reintroduced. However, pressure ejection of 1 mM ACh after reintroduction of extracellular Ca^{2+} caused spontaneous catecholamine release events indicating the rundown was in the splanchnic nerve, not in chromaffin cells.

Electrochemical detection of a single exocytotic event requires that it occurs very close (within a few micrometers) to the sensor surface. The approximately 1×10^6 molecules (obtained from the Q values and Faraday's law (Wightman et al., 1991)) in a vesicle are rapidly diluted following release. When this number of molecules is confined to the volume of a chromaffin cell vesicle, the concentration is very high, on the order of 0.5 M (Wightman et al., 1991). However, upon release the concentration rapidly dissipates until it reaches an immeasurable concentration a few micrometers from the cell surface (Wightman et al., 1995, Cragg and Rice, 2004). Thus, the vesicular release site on the cell surface can be viewed as a point source of material that rapidly dilutes into the extracellular space due to the steep concentration gradient. For this reason, the microelectrode has to be directly adjacent to a vesicular release site when fast exocytotic events are observed. This is true even with cyclic voltammetry, an experiment in which the catecholamines are oxidized and then returned to their original, reduced form.

Amperometry can also be used to analyze observed release during electrical stimulation. The average quantal size of spontaneously released catecholamines in slices (~ 418 fC) and electrically stimulated catecholamine release at the same location yields ~ 600,000 fC detected when measured by amperometry. Thus, the minimum number of quantal events that were evoked was 600,000 fC / 418 fC or ~ 1440 exocytotic events (since release is evoked over a larger spatial area than sampled by the electrode, this number is a significant underestimate). If each chromaffin cell contains ~ 140 vesicles in its readily releasable pool (Voets et al., 1999), the measured charge corresponds to the contribution from a minimum of 10 cells. Thus, electrically stimulated catecholamine release is the merger of release from multiple cells.

Immunohistochemical surveys (Kippenberger et al., 1999), and content data (Ally et al., 1986, Ciolkowski et al., 1992) show that the murine adrenal medulla contain fewer noradrenergic than adrenergic sites. Evidence for this has also been shown in levels of the two catecholamines in the blood stream of mice (Forman et al., 1988). Using a voltammetric waveform that allows distinction of norepinephrine and epinephrine, we found that exocytotic spikes were always of the same catecholamine subtype when sampled at the same location. This is because the majority of chromaffin cells contain only one catecholamine, epinephrine or norepinephrine (Ciolkowski et al., 1992), and they secrete what they contain (Pihel et al., 1994). However, in cultured cells a minority (< 20 %) release both catecholamines (Ciolkowski et al., 1992). We found that sites that exhibited adrenergic spontaneous events showed adrenergic release evoked by electrical stimulation. A very different situation was found during electrical stimulation in which sites that were noradrenergic with respect to spontaneous release showed a mixture of catecholamines released with electrical stimulation.

We interpret this as a consequence of forcing multiple cells to fire in synchrony. With synchronous firing from multiple sites, the extracellular concentrations merge. This makes

the concentration gradient less steep and decreases the tendency to dilute. Thus, appreciable concentrations accumulate around the sensor and it takes longer for their dilution (Garris et al., 1994). At adrenergic sites, the probability is that it is surrounded by other adrenergic secreting cells because epinephrine is the major catecholamine. Indeed, labeling for phenylethanolamine N-methyltransferase (PNMT), the enzyme that methylates norepinephrine into epinephrine, provides evidence that clusters are either adrenergic or noradrenergic (Kippenberger et al., 1999, Phillips et al., 2001). In contrast, noradrenergic sites are more likely to have adrenergic neighbors. Thus, consistent with the experimental findings, contributions from both catecholamines become evident during electrically stimulated release.

Conclusion

Prior to the present work, only individual exocytotic events from cells on the surface of adrenal slices had been investigated using constant potential amperometry. Here, carbon-fiber microelectrodes were inserted beneath the surface of mouse adrenal slices in order to look at spontaneous exocytotic and electrically evoked release using both constant potential amperometry and fast-scan cyclic voltammetry. Pharmacological manipulation of the observed signals showed that both electrically stimulated release as well as spontaneous release occurs from acetylcholine released from the splanchnic nerve binding to nAChR on the chromaffin cells, and is exocytotic in nature. An FSCV waveform which can distinguish between epinephrine and norepinephrine was utilized for the first time in slices and data collected agreed with previous findings which show that individual clusters of chromaffin cells release either epinephrine or norepinephrine, but not both. The work presented here is a major step forward in advancing the methodologies used to study the adrenal gland as well as the knowledge of the release of the major hormones released into the bloodstream by the adrenal gland.

Dr. Jelena Petrovic is gratefully acknowledged for her contributions for the early study of electrically stimulated and spontaneous catecholamine release.

References

Ally AI, Vieira L, Reuhl KR (1986) Trimethyltin as a selective adrenal chemosympatholytic agent in vivo: effect precedes both clinical and histopathological evidence of toxicity. Toxicology 40:215-229.

Amatore C, Arbault S, Bonifas I, Bouret Y, Erard M, Ewing AG, Sombers LA (2005) Correlation between vesicle quantal size and fusion pore release in chromaffin cell exocytosis. Biophys J 88:4411-4420.

Amatore C, Arbault S, Bouret Y, Guille M, Lemaitre F, Verchier Y (2006) Regulation of exocytosis in chromaffin cells by trans-insertion of lysophosphatidylcholine and arachidonic acid into the outer leaflet of the cell membrane. Chembiochem 7:1998-2003.

Arroyo G, Fuentealba J, Sevane-Fernandez N, Aldea M, Garcia AG, Albillos A (2006) Amperometric study of the kinetics of exocytosis in mouse adrenal slice chromaffin cells: physiological and methodological insights. J Neurophysiol 96:1196-1202.

Aunis D, Langley K (1999) Physiological aspects of exocytosis in chromaffin cells of the adrenal medulla. Acta Physiol Scand 167:89-97.

Bader MF, Holz RW, Kumakura K, Vitale N (2002) Exocytosis: the chromaffin cell as a model system. Ann N Y Acad Sci 971:178-183.

Barbara JG, Poncer JC, McKinney RA, Takeda K (1998) An adrenal slice preparation for the study of chromaffin cells and their cholinergic innervation. J Neurosci Methods 80:181-189.

Biales B, Dichter M, Tischler A (1976) Electrical excitability of cultured adrenal chromaffin cells. J Physiol 262:743-753.

Borges R (1997) The rat adrenal gland in the study of the control of catecholamine secretion. Semin Cell Dev Biol 8:113-120.

Borges R, Camacho M, Gillis KD (2008) Measuring secretion in chromaffin cells using electrophysiological and electrochemical methods. Acta Physiol (Oxf) 192:173-184.

Brandt BL, Hagiwara S, Kidokoro Y, Miyazaki S (1976) Action potentials in the rat chromaffin cell and effects of acetylcholine. J Physiol 263:417-439.

Bunin MA, Prioleau C, Mailman RB, Wightman RM (1998) Release and uptake rates of 5-hydroxytryptamine in the dorsal raphe and substantia nigra reticulata of the rat brain. J Neurochem 70:1077-1087.

Cahill PS, Walker QD, Finnegan JM, Mickelson GE, Travis ER, Wightman RM (1996) Microelectrodes for the measurement of catecholamines in biological systems. Anal Chem 68:3180-3186.

Chan SA, Smith C (2003) Low frequency stimulation of mouse adrenal slices reveals a clathrin-independent, protein kinase C-mediated endocytic mechanism. J Physiol 553:707-717.

Ciolkowski EL, Cooper BR, Jankowski JA, Jorgenson JW, Wightman RM (1992) Direct observation of epinephrine and norepinephrine co- secretion from individual adrenal medullary chromaffin cells. J Am Chem Soc 114:2815-2821.

Cragg SJ, Rice ME (2004) DAncing past the DAT at a DA synapse. Trends Neurosci 27:270-277.

de Diego AMG, Gandia L, Garcia AG (2008) A physiological view of the central and peripheral mechanisms that regulate the release of catecholamines at the adrenal medulla. Acta Physiologica 192:287-301.

Douglas WW, Poisner AM (1965) Preferential release of adrenaline from the adrenal medulla by muscarine and pilocarpine. Nature 208:1102-1103.

Douglas WW, Rubin RP (1961a) Mechanism of nicotinic action at the adrenal medulla: calcium as a link in stimulus-secretion coupling. Nature 192:1087-1089.

Douglas WW, Rubin RP (1961b) The role of calcium in the secretory response of the adrenal medulla to acetylcholine. J Physiol 159:40-57.

Forman DT, Bradford BU, Handler JA, Glassman EB, Thurman RG (1988) Involvement of hormones in the swift increase in alcohol metabolism. Ann Clin Lab Sci 18:318-325.

Fox GQ (1996) A morphometric analysis of exocytosis in KCl-stimulated bovine chromaffin cells. Cell Tissue Res 284:303-316.

Fuhrman FA (1986) Tetrodotoxin, tarichatoxin, and chiriquitoxin: historical perspectives. Ann N Y Acad Sci 479:1-14.

Garris PA, Ciolkowski EL, Pastore P, Wightman RM (1994) Efflux of dopamine from the synaptic cleft in the nucleus accumbens of the rat brain. J Neurosci 14:6084-6093.

Haynes CL, Siff LN, Wightman RM (2007) Temperature-dependent differences between readily releasable and reserve pool vesicles in chromaffin cells. Biochim Biophys Acta 1773:728-735.

Johnson MA, Villanueva M, Haynes CL, Seipel AT, Buhler LA, Wightman RM (2007) Catecholamine exocytosis is diminished in R6/2 Huntington's disease model mice. J Neurochem 103:2102-2110.

Jones SR, Garris PA, Wightman RM (1995) Different effects of cocaine and nomifensine on dopamine uptake in the caudate-putamen and nucleus accumbens. J Pharmacol Exp Ther 274:396-403.

Jones SR, Lee TH, Wightman RM, Ellinwood EH (1996) Effects of intermittent and continuous cocaine administration on dopamine release and uptake regulation in the striatum: in vitro voltammetric assessment. Psychopharmacology (Berl) 126:331-338.

Kajiwara R, Sand O, Kidokoro Y, Barish ME, Iijima T (1997) Functional organization of chromaffin cells and cholinergic synaptic transmission in rat adrenal medulla. Jpn J Physiol 47:449-464.

Kawagoe KT, Zimmerman JB, Wightman RM (1993) Principles of voltammetry and microelectrode surface states. J Neurosci Methods 48:225-240.

Kelly RS, Wightman RM (1987) Detection of dopamine overflow and diffusion with voltammetry in slices of rat brain. Brain Res 423:79-87.

Kennedy RT, Jones SR, Wightman RM (1992) Simultaneous measurement of oxygen and dopamine: coupling of oxygen consumption and neurotransmission. Neuroscience 47:603-612.

Kidokoro Y, Ritchie AK (1980) Chromaffin cell action potentials and their possible role in adrenaline secretion from rat adrenal medulla. J Physiol 307:199-216.

Kippenberger AG, Palmer DJ, Comer AM, Lipski J, Burton LD, Christie DL (1999) Localization of the noradrenaline transporter in rat adrenal medulla and PC12 cells: evidence for its association with secretory granules in PC12 cells. J Neurochem 73:1024-1032.

Kolski-Andreaco A, Cai H, Currle DS, Chandy KG, Chow RH (2007) Mouse adrenal chromaffin cell isolation. J Vis Exp 129.

Malhotra RK, Wakade AR (1987) Non-cholinergic component of rat splanchnic nerves predominates at low neuronal activity and is eliminated by naloxone. J Physiol 383:639-652.

Martin AO, Mathieu MN, Chevillard C, Guerineau NC (2001) Gap junctions mediate electrical signaling and ensuing cytosolic Ca^{2+} increases between chromaffin cells in adrenal slices: A role in catecholamine release. J Neurosci 21:5397-5405.

Michael D, Travis ER, Wightman RM (1998) Color images for fast-scan CV measurements in biological systems. Anal Chem 70:586A-592A.

Miles PR, Mundorf ML, Wightman RM (2002) Release and uptake of catecholamines in the bed nucleus of the stria terminalis measured in the mouse brain slice. Synapse 44:188-197.

Montero M, Alonso MT, Carnicero E, Cuchillo-Ibanez I, Albillos A, Garcia AG, Garcia-Sancho J, Alvarez J (2000) Chromaffin-cell stimulation triggers fast millimolar mitochondrial Ca2+ transients that modulate secretion. Nat Cell Biol 2:57-61.

Montesinos MS, Machado JD, Camacho M, Diaz J, Morales YG, Alvarez de la Rosa D, Carmona E, Castaneyra A, Viveros OH, O'Connor DT, Mahata SK, Borges R (2008) The crucial role of chromogranins in storage and exocytosis revealed using chromaffin cells from chromogranin A null mouse. J Neurosci 28:3350-3358.

Moriya H, Takagi Y, Nakanishi T, Hayashi M, Tani T, Hirotsu I (1999) Affinity profiles of various muscarinic antagonists for cloned human muscarinic acetylcholine receptor (mAChR) subtypes and mAChRs in rat heart and submandibular gland. Life Sci 64:2351-2358.

Moser T (1998) Low-conductance intercellular coupling between mouse chromaffin cells in situ. J Physiol 506 (Pt 1):195-205.

Moser T, Neher E (1997) Rapid exocytosis in single chromaffin cells recorded from mouse adrenal slices. J Neurosci 17:2314-2323.

Nassar-Gentina V, Pollard HB, Rojas E (1988) Electrical activity in chromaffin cells of intact mouse adrenal gland. Am J Physiol 254:C675-683.

Phillips JK, Dubey R, Sesiashvilvi E, Takeda M, Christie DL, Lipski J (2001) Differential expression of the noradrenaline transporter in adrenergic chromaffin cells, ganglion cells and nerve fibres of the rat adrenal medulla. J Chem Neuroanat 21:95-104.

Pickel VM, Joh TH, Field PM, Becker CG, Reis DJ (1975) Cellular localization of tyrosine hydroxylase by immunohistochemistry. J Histochem Cytochem 23:1-12.

Pihel K, Schroeder TJ, Wightman RM (1994) Rapid and Selective Cyclic Voltammetric Measurements of Epinephrine and Norepinephrine as a method to Measure Secretion from Single Bovine Adrenal Medullary Cells. Anal Chem 66:4532-4537.

Przywara DA, Guo X, Angelilli ML, Wakade TD, Wakade AR (1996) A non-cholinergic transmitter, pituitary adenylate cyclase-activating polypeptide, utilizes a novel mechanism to evoke catecholamine secretion in rat adrenal chromaffin cells. J Biol Chem 271:10545-10550.

Suudhof TC (2008) Neurotransmitter release. Handb Exp Pharmacol 1-21.

Travis ER, Wightman RM (1998) Spatio-temporal resolution of exocytosis from individual cells. Annu Rev Biophys Biomol Struct 27:77-103.

Troyer KP, Wightman RM (2002) Temporal separation of vesicle release from vesicle fusion during exocytosis. J Biol Chem 277:29101-29107.

Voets T, Neher E, Moser T (1999) Mechanisms underlying phasic and sustained secretion in chromaffin cells from mouse adrenal slices. Neuron 23:607-615.

von Gersdorff H, Matthews G (1999) Electrophysiology of synaptic vesicle cycling. Annu Rev Physiol 61:725-752.

von Ruden L, Neher E (1993) A Ca-dependent early step in the release of catecholamines from adrenal chromaffin cells. Science 262:1061-1065.

Wakade AR, Wakade TD (1982) Secretion of catecholamines from adrenal gland by a single electrical shock: electronic depolarization of medullary cell membrane. Proc Natl Acad Sci U S A 79:3071-3074.

Wightman RM, Jankowski JA, Kennedy RT, Kawagoe KT, Schroeder TJ, Leszczyszyn DJ, Near JA, Diliberto EJ, Jr., Viveros OH (1991) Temporally resolved catecholamine spikes correspond to single vesicle release from individual chromaffin cells. Proc Natl Acad Sci U S A 88:10754-10758.

Wightman RM, Schroeder TJ, Finnegan JM, Ciolkowski EL, Pihel K (1995) Time course of release of catecholamines from individual vesicles during exocytosis at adrenal medullary cells. Biophys J 68:383-390.

Zwart R, Vijverberg HP (1997) Potentiation and inhibition of neuronal nicotinic receptors by atropine: competitive and noncompetitive effects. Mol Pharmacol 52:886-895.

Chapter III

Distinguishing Splanchnic Nerve and Chromaffin Cell Stimulation

Introduction

Electrical stimulation is frequently used to excite neuronal tissue and evoke exocytosis. However, selectivity is always a concern because the stimulus can cause exocytosis from afferent terminals within the tissue as well as depolarizing cell bodies within the tissue (Merrill et al., 2005). An example that was characterized several years ago is the electrical stimulation of the intact adrenal gland. Wakade and Wakade showed that an electrical stimulation could evoke catecholamine release both by directly depolarizing the chromaffin cells as well as by depolarizing the splanchnic nerve that causes acetylcholine release that in turn triggers catecholamine exocytosis from chromaffin cells (Wakade and Wakade, 1982). These investigators were able to distinguish these two contributions by the select use of pharmacological agents and well as by adjusting the stimulation parameters.

Release of catecholamines from isolated chromaffin cells has been extensively investigated in recent years by electrochemical and patch-clamp techniques. Electrochemistry with carbon-fiber microelectrodes can resolve each exocytotic event by oxidizing the packet of released catecholamines. Patch clamp probes exocytosis by measuring capacitance changes as the area of the cell membrane is increased by exocytotic events (Neher and Marty, 1982, Wightman et al., 1991, Travis and Wightman, 1998, Troyer and Wightman, 2002). More recently, these techniques have been used in slices of the adrenal gland to understand the processes that occur in a more intact

preparation (Moser and Neher, 1997, Voets et al., 1999). Arroyo *et al.* showed that amperometric recordings in adrenal slices can resolve exocytotic events that are identical to those measured at the single cell level (Arroyo et al., 2006). Petrovic *et al.* used both amperometry and cyclic voltammetry to probe the pharmacology of catecholamine release within adrenal slices (Petrovic et al., 2010). Cyclic voltammetry is an electrochemical method that allows the identification of the species detected, allowing norepinephrine and epinephrine to be distinguished. Both electrochemical studies in intact slices demonstrated that electrically evoked release was caused by activation of the splanchnic nerve because hexamethonium, a nicotinic receptor antagonist, blocked the evoked release.

In this work, we reinvestigate the dual release pathway identified many years ago by Wakade and Wakade. Patch clamp recordings have shown that chromaffin cells become permeable to Ca^{2+} when their membranes are depolarized and that Ca^{2+} plays an integral role in the process of exocytosis (Augustine and Neher, 1992, Neher and Augustine, 1992, Neher, 1998, Smith et al., 1998). In addition, chromaffin cells are capable of firing action potentials that can be decreased in frequency by tetrodotoxin (TTX), a Na^{+} channel blocker, and that is dependent on K^{+} channels for repolarization (Kidokoro and Ritchie, 1980, Nassar-Gentina et al., 1988). Here, we use a method with high special and temporal resolution, fast-scan cyclic voltammetry (FSCV), as well as more modern pharmacology probing the roles of specific Ca^{2+} channels to resolve the originally claimed dual mechanism of electrically evoked catecholamine release with contribution both from splanchnic nerve stimulation and direct chromaffin cell depolarization. These studies reveal that the chromaffin cell is more difficult to depolarize than the splanchnic nerve.

Experimental

Animals

Wild-type C57BL/6J female mice, 4-8 weeks old, were used in this work (stock no. 000664, Jackson Laboratories, Bar Harbor, ME, USA). Upon receipt, mice were housed at the University of North Carolina Husbandry Facility with *ab libitum* access to food and water and under closely controlled environmental conditions (temperature, humidity, and 12-hr light/dark cycles). Live animal handling procedures and experimental protocols were approved by the University of North Carolina's Institutional Animal Care and Use Committee.

Adrenal Slice Methods

Adrenal gland slicing procedures were adapted from literature descriptions with slight modification (Moser and Neher, 1997, Barbara et al., 1998, Petrovic et al., 2010). Mice were anesthetized under anhydrous ethyl ether (Fisher Scientific) and decapitated. A midline abdominal incision allowed for access to the adrenal glands. Glands were placed into ice-cold and 95 % O_2 – 5 % CO_2 saturated low Ca^{2+} bicarbonate-buffered saline (BBS), containing (in mM): 0.1 $CaCl_2$, 125 NaCl, 26 $NaHCO_3$, 2.5 KCl, 1.25 NaH_2PO_4, 3 $MgCl_2$, 10 glucose, and 10 HEPES, and its pH was adjusted to 7.4. Excess fat was removed from the glands, and the glands were embedded in a 3% agarose (w/v) in low Ca^{2+} BBS (Promega). Once cooled, agarose blocks containing the glands were secured onto a Teflon specimen holder that was used to orient the largest base of the gland parallel to the slicing blade. The glands were cut into slices of ~200 μm in thickness using a vibratome slicer filled with low Ca^{2+} BBS (Campden Instruments, World Precision Instruments, Leics, U.K.).

Slices were immediately placed into a perfusion chamber (open diamond bath heated chamber, RC-22, Warner Instruments, Hamden, CT) and secured with a stainless steel Lycra® thread anchor (1.5 mm-2.0 mm thread spacing, Warner Instruments, Hamden,

CT). The chamber was continually perfused with 95 % O_2 – 5 % CO_2 saturated BBS, at a rate of 1-2 mL/min with the same composition as the low Ca^{2+} BBS, except with 2 mM $CaCl_2$ and 1 mM $MgCl_2$ at pH 7.4. To ensure physiological conditions and to minimize slice perturbations, the temperature of the perfusion chamber was kept at 37 °C using an automatic temperature controller (Warner Instruments, LLC). All of the experiments were completed within a 10-hr *post mortem* period.

Fast-Scan Cyclic Voltammetry

Carbon-fiber elliptical microelectrodes were fabricated as previously described (Kawagoe et al., 1993, Cahill et al., 1996). Prior to use, carbon-fiber microelectrodes were soaked in an activated carbon / 2-propanol mixture for a minimum of 30 min to remove surface debris (Ranganathan et al., 1999). Microelectrodes were then backfilled with 4 M CH_3COOK / 0.15 M NaCl and mounted onto a potentiostat headstage. A stainless-steel wire was inserted into the microelectrode to make electrical contact. Experiments were conducted inside a grounded Faraday's cage. Catecholamine release was monitored with an Axopatch 200B patch-clamp amplifier in voltage clamp mode and β=0.1 configuration (Axon Instruments, Molecular Devices, Union City, CA). The signal was filtered with a built-in analog low-pass Bessel filter (80 dB/decade) at 5 kHz. The potentiostat was controlled via LABVIEW software, TarHeel CV (ESA, Chelmsford, MA). Measured currents were digitized using a National Instruments PCI-MIO-16XE-10 card and monitored as a function of the applied potential. The waveform for cyclic voltammetry was a potential sweep from -400 mV to +1000 mV and back to -400 mV at a scan rate of 600 V/s applied at a 10 Hz repetition rate. In between scans, the electrode potential was held at -400 mV allowing for catecholamine adsorption onto a carbon fiber surface, a procedure that increases the sensitivity to catecholamines (Heien et al., 2003).

Electrical stimulation of slices employed two tungsten microelectrodes glued together with their tips separated by approximately 250 μm (FHC, Bowdoin, ME). The stimulating electrode was positioned on the slice surface under a 40X water immersion objective Fluor WD 2.0 on an upright microscope (Nikon Eclipse E600FN, Lewisville, TX). Microelectrodes were positioned with a multi-manipulator controller (1 μm display resolution, MPC-200-ROE, Sutter Instruments). To avoid recordings from a damaged tissue layer, microelectrodes were lowered approximately 30 μm below the slice surface (Kennedy et al., 1992, Petrovic et al., 2010). To evoke catecholamine release, trains of initially positive biphasic pulses (10 pulse, 10 Hz) were applied to the stimulating electrodes between scans using a National Instruments PCI-6711 card, controlled by Tar Heel CV to ensure no overlap between CV scans for data collection and stimulation pulses. Slices were equilibrated for ~ 2 hrs prior to data collection. During the equilibration period slices were electrically stimulated every 3-5 min. These data were used to establish a baseline level of catecholamine release.

Voltammetric data analysis employed the TarHeel CV data analysis package (ESA, Chelmsford, MA). Digital background subtraction was used to remove the background current to reveal the cyclic voltammogram of the species detected. Sets of cyclic voltammograms were displayed as color plots (Michael et al., 1998). Each color plot displays a set of cyclic voltammograms that were sequentially acquired in time (abscissa) while the applied potential is shown as the ordinate. The currents are shown in color. To follow the time course of concentration changes, the current at +600 mV (the peak current for catecholamine oxidation) was extracted from the color plots. Since the electrochemical signals recorded in the adrenal gland are a mixture of epinephrine, and norepinephrine (Petrovic et al., 2010), electrodes were post calibrated in a flow injection system with 5 μM epinephrine, norepinephrine, and a 50:50 mixture of 2.5 μM of each catecholamine. Concentrations measured during application of pharmacological agents are reported as values normalized to currents recorded before drug application.

Pharmacology

Pharmacological agents employed herein include thapsigargin (THG), tetrodotoxin (TTX), hexamethonium (HEX), 4-DAMP, ethylene glycol tetraacetic acid (EGTA), and nifedipine, were all from Sigma-Aldrich (St. Louis, MO, USA) and used as received. Drugs were dissolved in low Ca^{2+} or recording BBS and superfused through a slice chamber at a rate of ~ 2 mL/min.

Statistical Analysis

Statistical analysis was done in GraphPad Prism (GraphPad Software, Inc., San Diego, CA, USA). Student's *t*-test (unpaired) was used to test for significant differences between data sets. Data were considered significantly different at the 95 % confidence level. n = number of slices, unless noted otherwise.

Results

Characteristics of Evoked Catecholamine Release

In prior work we showed that local electrical stimulation of adrenal medullary slices with stimulus trains consisting of 10 biphasic pulses, 1 ms/phase, 150 μA at 10 Hz results in catecholamine release that increases during the stimulation and then decreases 1-2 s after the stimulation is terminated (Petrovic et al., 2010). Furthermore, we showed that the pharmacological manipulation during such stimulations were consistent with activation of the splanchnic nerve causing release of acetylcholine. We refer to this as the fast phase of catecholamine release. However, quite different results were obtained with an identical stimulation except with a greater amplitude (n = 3, Figure 3.1A). With stimulus amplitude of 450 μA, catecholamine release is still evoked, but it lasts over a longer time frame. A maximum corresponding to the fast phase is observed shortly (1-2 s) after the stimulation is terminated and it is followed by a broad, larger increase that maximizes ~ 8 -10 s after the

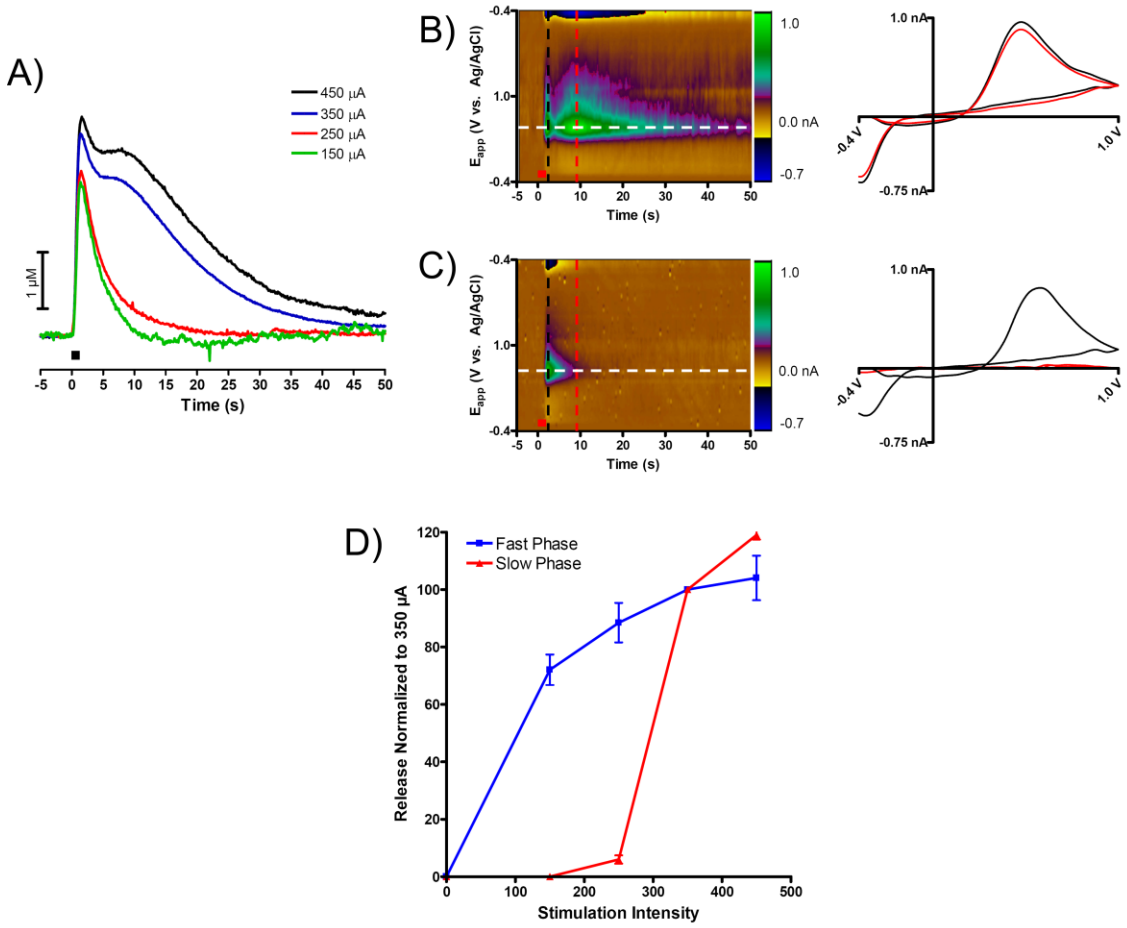

Figure 3.1. Effect of stimulation intensity on biphasic release. (A) Representative electrically stimulated catecholamine release with decreasing intensity (350 – 150 µA) with 2.0 ms/phase pulse width. (B) Color plot of catecholamine release from a 450 µA stimulation. Cyclic voltammograms at 2 (black, fast phase) and 9 (red, slow phase) seconds are shown on the right as indicated by the dashed lines. (C) Color plot of catecholamine release from a 150 µA stimulation. Cyclic voltammograms at 2 (black, fast phase) and 9 (red, slow phase) seconds are shown on the right as indicated by the dashed lines. (D) Stimulation intensity data were summarized for the fast and slow phase as the amount of release relative to that collected with a 350 µA stimulation (n = 3).

stimulation. We refer to this second feature as the slow phase of release. As the stimulus amplitude was diminished, the slow phase diminished more rapidly than the fast phase. Similar behavior was seen within chromaffin-cell clusters throughout the adrenal medulla. In some instances, the slow phase was larger in amplitude than the fast phase and overwhelmed it. The cyclic voltammograms (Figure 3.1B and C, encoded as color plots) show that catecholamine release is the primary contributor to both phases. The maximum amplitude of each phase as a function of stimulus intensity is shown in Figure 3.1D.

To probe further the effects of electrical stimulation parameters on catecholamine release, various stimulation pulse widths were applied to the slice using a 350 μA stimulation amplitude. Stimulating pulse widths (per phase) of 2.0 ms, 1.5 ms, 1.0 ms, and 0.5 ms were employed (pulse widths were delivered in random order). The slow phase was not present with stimulation widths of ≤ 1 ms per phase (n = 5, Figure 3.2). The remaining experiments described here were designed to probe the origin of the slow release phase and used relatively large stimulations (350 μA and 2.0 ms/phase width).

Modulation of Catecholamine Release by Ions

We investigated the role of cholinergic receptors on the slow phase of catecholamine release. As previously shown, the fast phase was diminished in the presence of 100 μM HEX, a nicotinic acetylcholine receptor blocker. In contrast, the slow phase was only marginally affected by HEX (representative traces in Figure 3.3A, average maximal amplitudes in Figure 3.3B, n = 5). Previous work has shown that splanchnic nerve dependent catecholamine release measured by FSCV is independent of muscarinic receptors (Petrovic et al., 2010). Perfusion with 1.0 μM 4-DAMP (n = 3, data not shown), a selective muscarinic receptor antagonist also did not affect the slow phase of electrically stimulated release. Further, perfusion with 0.5 μM atropine (n = 3, data not shown), a high affinity muscarinic receptor antagonist had no effect on the biphasic release. The inability of

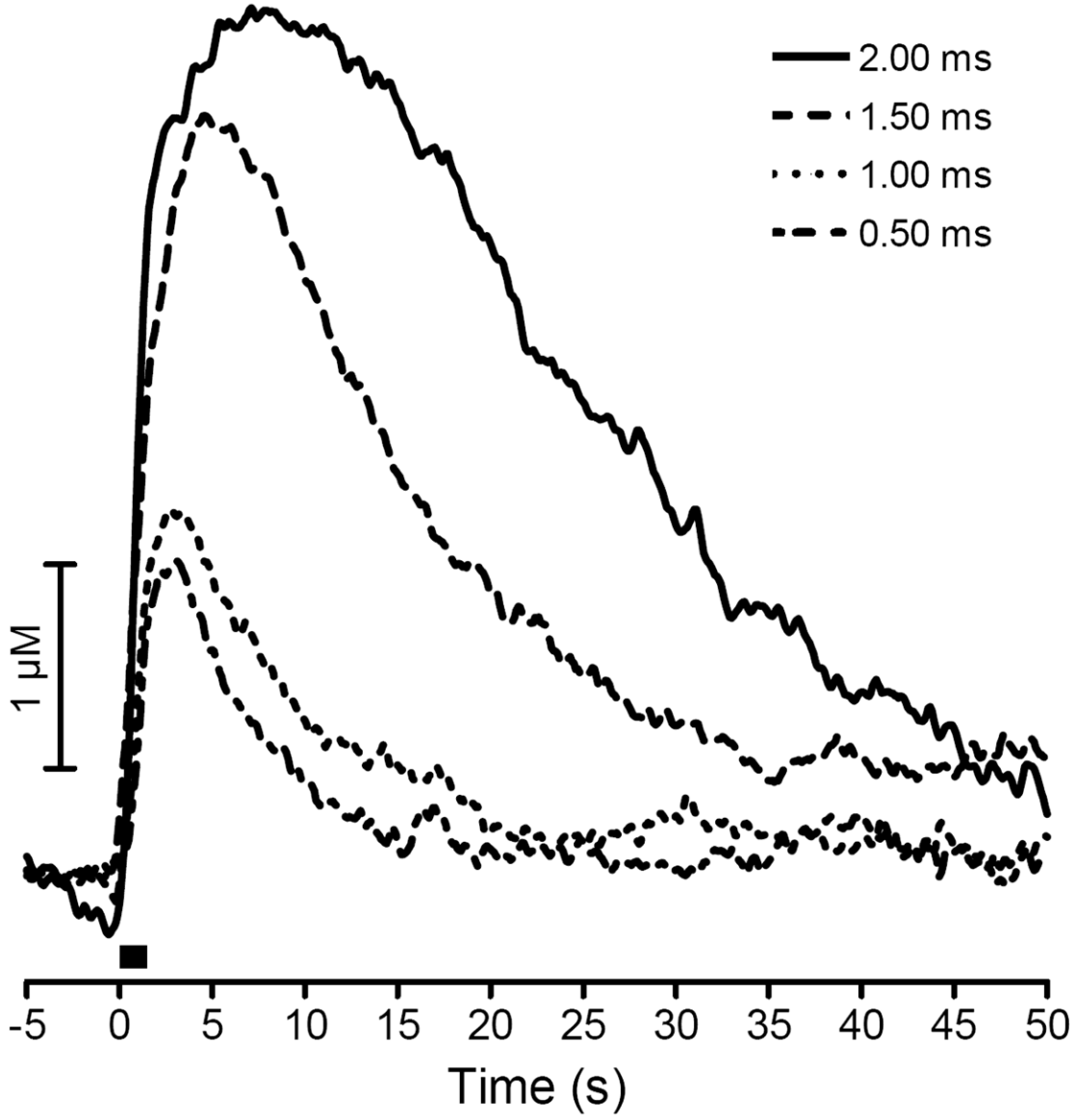

Figure 3.2. Effect of stimulation width on biphasic release. Representative electrically stimulated catecholamine release at an intensity of 350 µA with decreasing pulse width (2.0 – 0.5 ms/phase).

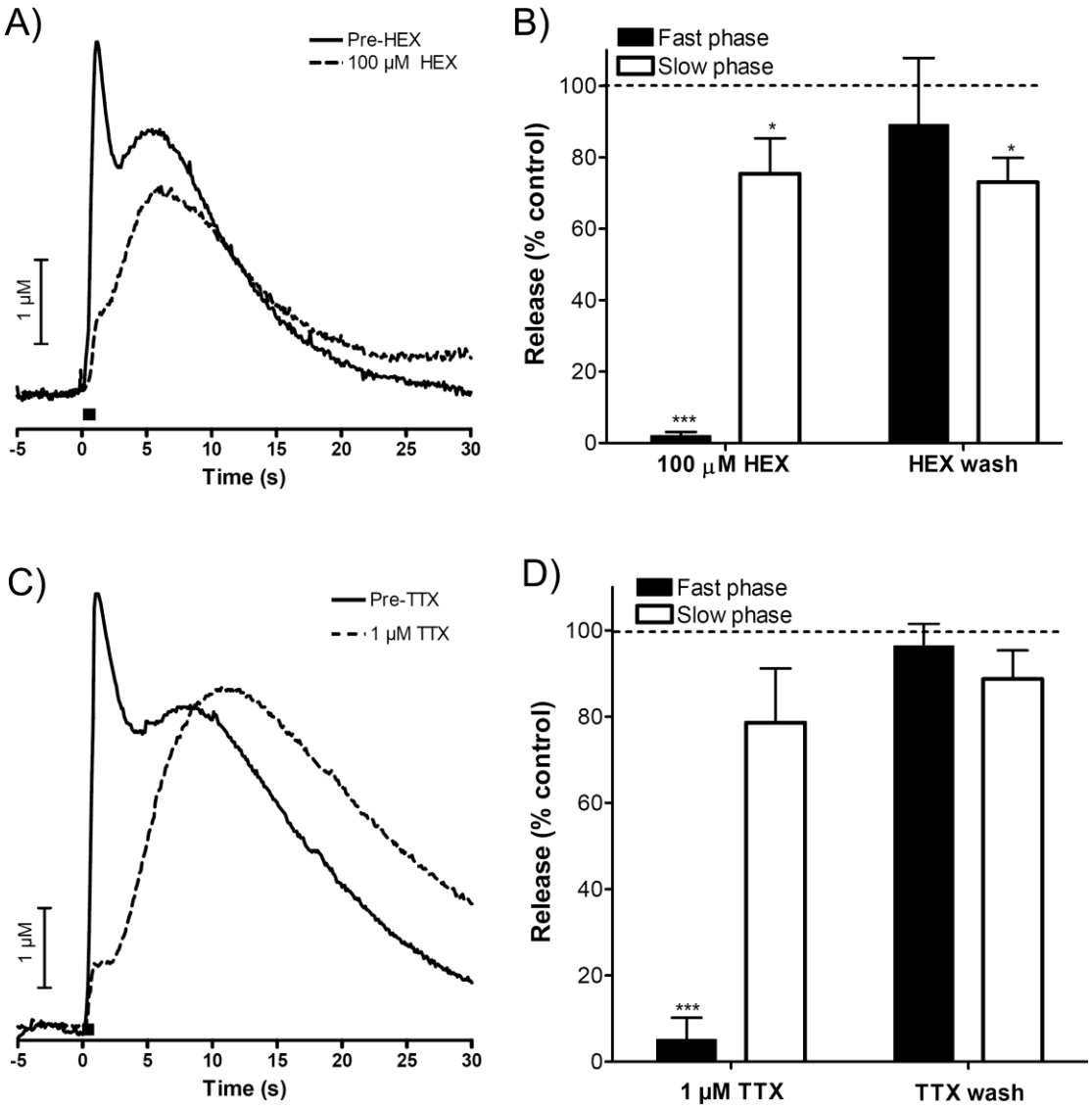

Figure 3.3. Modulation of catecholamine release by ions. (A) Representative trace for the perfusion of 100 µM HEX before and after the application of drug. (B) Summary of effects of HEX on fast and slow catecholamine release (n = 5). (C) Representative trace for the perfusion of 1 µM TTX before and after the application of drug. (D) Summary of effects of TTX on fast and slow catecholamine release (n = 5). *, $p<0.05$, ***, $p<0.001$.

cholinergic antagonists to affect the slow phase of catecholamine release indicates that acetylcholine released from the splanchnic nerve is unnecessary for this type of release.

To evaluate the involvement of Na^+-dependent action potentials in slow phase catecholamine release, 1 μM TTX, an inhibitor of voltage-gated Na^+ channels (Catterall, 1980), was perfused through the slice. The slow phase of the electrically stimulated release was found to be much less sensitive to TTX than the fast phase, which was abolished almost immediately upon perfusion as previously reported (representative example m Figure 3.3C). A summary of the effects of TTX on the maximum amplitude of the two phases is shown in Figure 3.3D (n = 5).

Biphasic Signal Dependence on Intra- and Extracellular [Ca^{2+}]

To explore the [Ca^{2+}] dependence of the slow phase of electrically stimulated release, the slices were perfused with BBS containing 0.1 mM Ca^{2+}. In this media, the fast phase release component was eliminated while the slow phase remained intact (representative example shown in Figure 3.4A). Data from multiple trials are summarized in Figure 3.4B (n = 3). When the slice was perfused with BBS containing 0 mM Ca^{2+} and 1 mM EGTA, both the fast and slow release was abolished within 15 minutes (representative example in Figure 3.4C). Both phases partially recovered when extracellular Ca^{2+} levels were returned to their normal level (2 mM). These data are summarized in Figure 3.4D (n = 5). Thus, while the slow phase does not require concentrations of physiological levels of extracellular Ca^{2+}, it does require some Ca^{2+} for release to occur.

To test the possibility that the slow phase requires release of cytoplasmic Ca^{2+} levels from intracellular stores such as endoplasmic reticulum, the slices were perfused with thapsigargin (THG). THG is a pharmacological agent that increases cytosolic Ca^{2+} levels by binding to SERCA enzymes and preventing Ca^{2+} from being pumped into the sarcoplasmic and endoplasmic reticula (Miranda-Ferreira et al., 2009). Perfusion of 1 μM

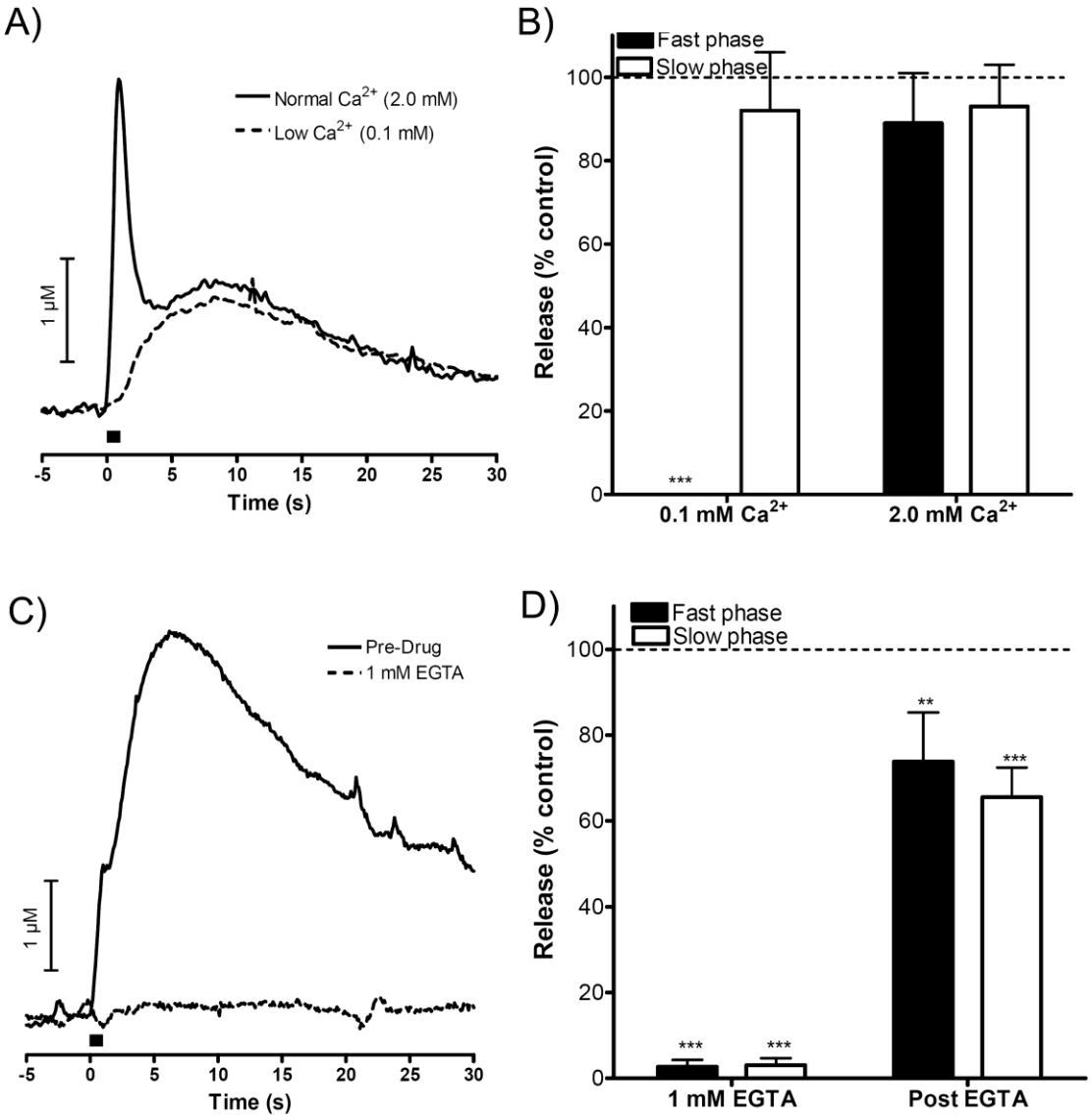

Figure 3.4. Biphasic signal dependence on extracellular Ca^{2+}. (A) Representative experiment for perfusion with a low extracellular calcium (0.1 mM) buffer before and after application of low Ca^{2+} buffer. (B) Summary of effects of perfusion of low calcium buffer on fast and slow catecholamine release (n = 3). (C) Representative experiment where extracellular calcium was completely removed from the perfusion buffer using 1 mM EGTA before and after application of drug. (D) Summary of effects of EGTA on fast and slow catecholamine release (n = 5). **, $p<0.01$, ***, $p<0.001$.

THG dissolved in low [Ca^{2+}] BBS buffer for 1 hour did not have an effect on either the fast or the slow components of electrically stimulated release (n = 4, data not shown).

Effect of L-type Ca^{2+} Channel Blocker on Slow Release

It has been shown that L-type voltage gated Ca^{2+} channels (VGCCs) are located on chromaffin cells but not on the splanchnic nerve and that they play a key role in the homeostatic mechanism of catecholamine release (Shukla and Wakade, 1991, Akiyama et al., 2004, Marcantoni et al., 2008). To evaluate the role of these channels in the different phases of release, we perfused 10 μM nifedipine, an L-type Ca^{2+} channel blocker, through the slice. The maximal amplitude of the slow phase was decreased to 29% of its original value by this perfusion while 74% of the fast phase remained. Figure 3.5A shows biphasic release before nifedipine is put onboard, while 5B is the observed release 10 minutes after nifedipine application, and finally Figure 3.5C shows that the slow phase was completely abolished by nifedipine 20 minutes after nifedipine had been put on board. A summary of the effects of nifedipine on the biphasic response is shown in Figure 3.5D (n = 5).

Biphasic Signal Dependence on the Distance between Working and Stimulating Electrodes

To probe the effect of the location of the stimulating electrode relative to the carbon fiber microelectrode, the stimulating electrode was moved away from the working electrode in 50 μm increments and release was evoked (Figure 3.6). At increasing distances, both the fast and slow phases decrease in intensity. The slow phase is diminished to a greater degree, however, allowing the fast phase to predominate at greater separations of the stimulating electrode and the carbon-fiber microelectrode. At the greatest distances between the electrodes, where only the fast phase was present (200 μm), perfusion with 100 μM HEX (Figure 3.7A), or 1 μM TTX (Figure 3.7B) reversibly eliminated the stimulated release. These data are summarized in Figure 3.7C (n = 3, $p<0.001$ for each drug).

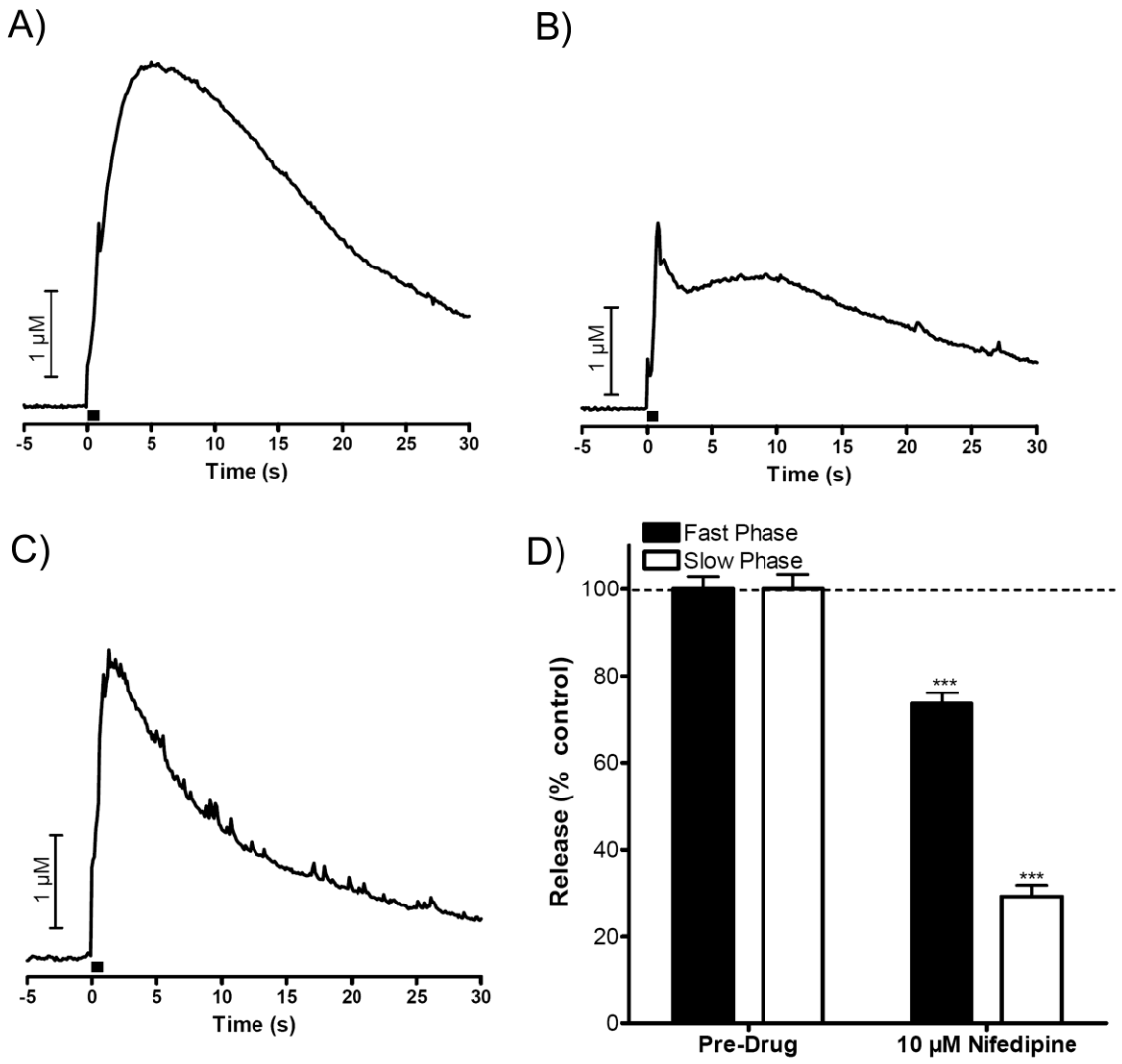

Figure 3.5. Role of L-type Ca^{2+} channels on biphasic release. (A) Biphasic release before the application of drug. (B) Release 10 min into perfusion with 10 µM nifedipine. (C) Release 20 min into perfusion with 10 µM nifedipine. (D) Summary of effects of nifedipine on fast and slow catecholamine release after at least 15 minutes of incubation (n = 5). ***,$p<0.001$.

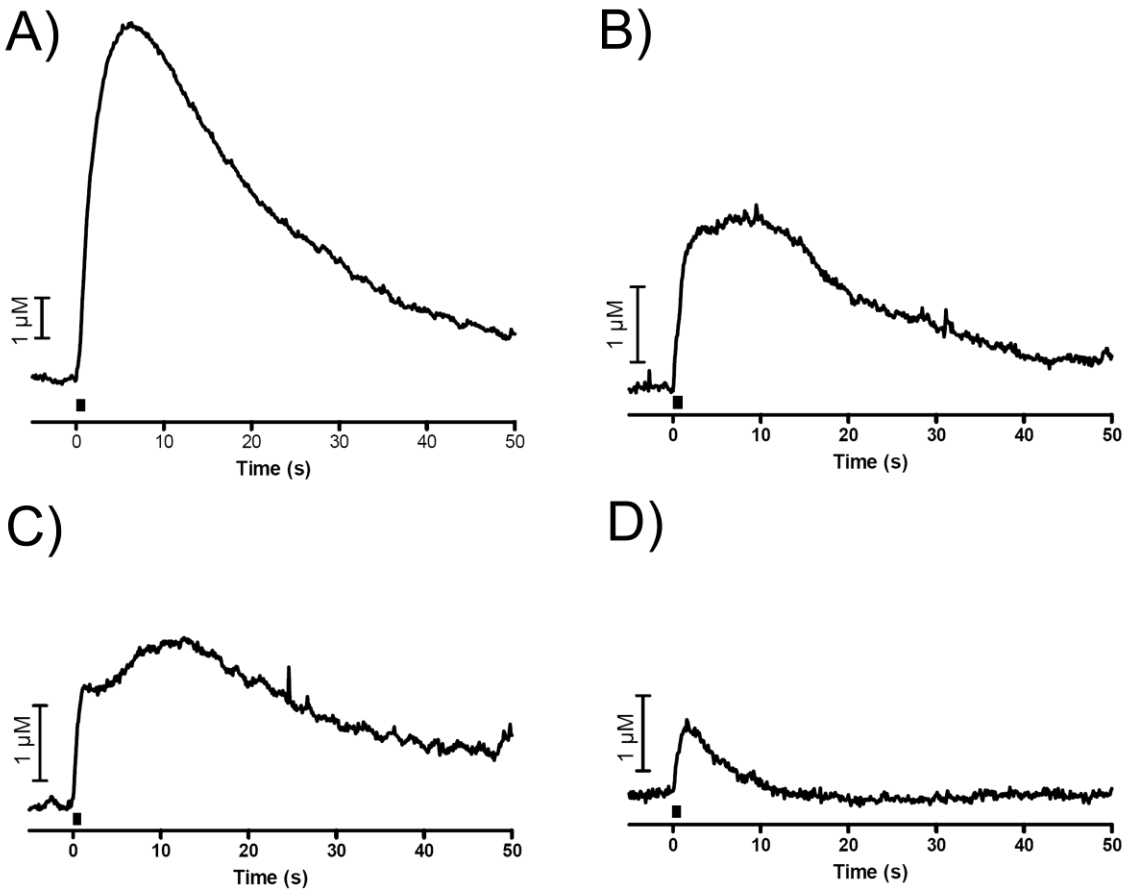

Figure 3.6. Biphasic signal dependence on the distance between the working and stimulating electrodes. Using a 350 µA, 1 ms/phase stimulation (10 Hz, 10 pulses), the stimulating electrode was placed (A) 0 µm, (B) 50 µm, (C) 100 µm, (D) 200 µm away from the working electrode.

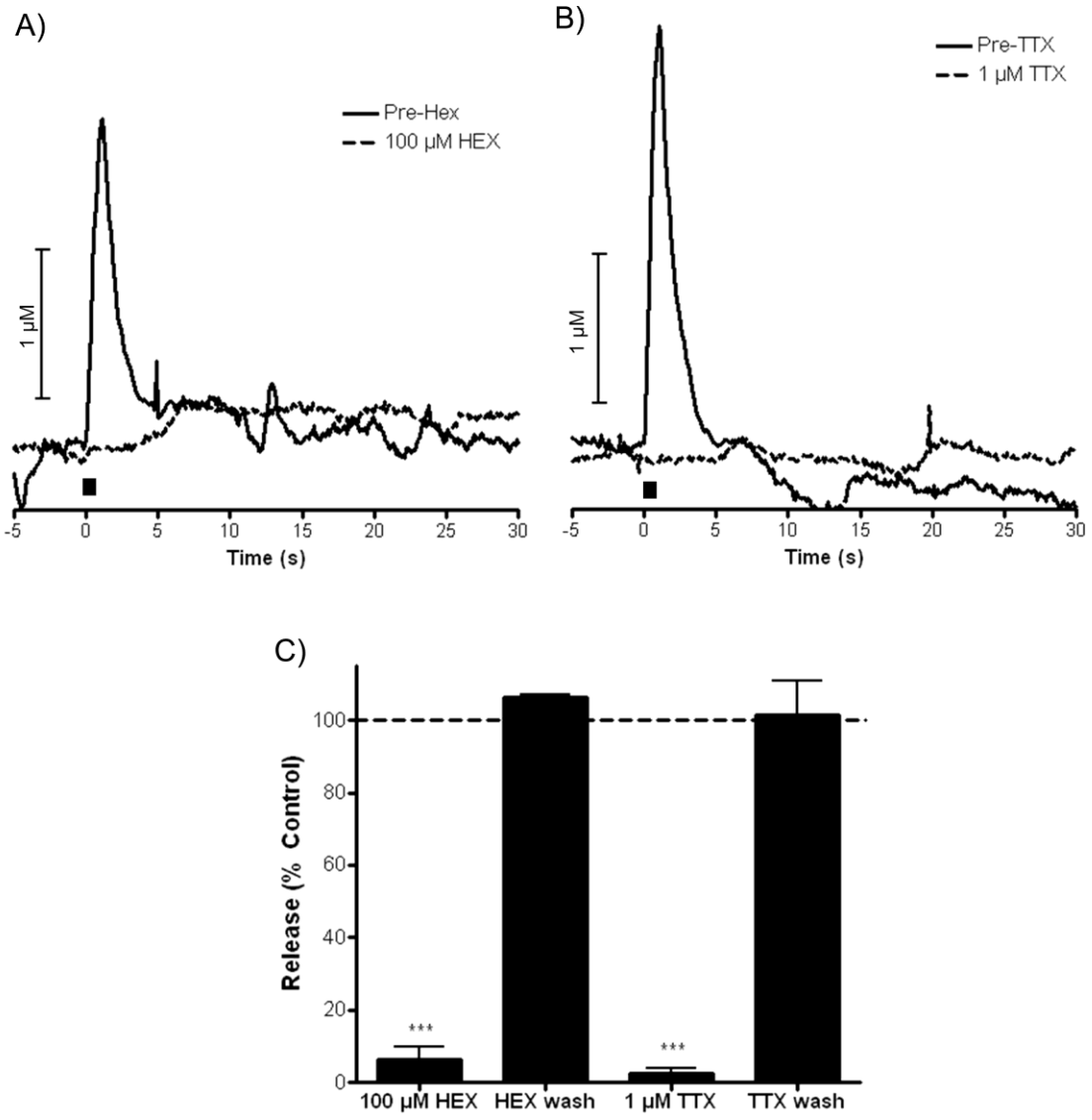

Figure 3.7. Modulation of remotely stimulated release by ions. (A) Representative experiment showing the effect of 100 µM HEX with 200 µm between the stimulating and working electrode. (B) Representative experiment showing the effect of 1 µM TTX with 200 µm between the stimulating and working electrode. (C) Summary of effects of perfusion of HEX (n = 3) and TTX (n = 3) as well as the recovery of fast release when the stimulating electrode is 200 µm from the working electrode. ***, $p<0.001$.

Discussion

Prior work in the perfused adrenal gland demonstrated that electrical stimulation could evoke catecholamine release by two mechanisms: indirectly by depolarization of the splanchnic nerve or directly by depolarization of the chromaffin cells themselves (Wakade, 1981, Wakade and Wakade, 1982). Catecholamine release arising from splanchnic nerve stimulation occurs because released acetylcholine from the splanchnic nerve activates nicotinic receptors on chromaffin cells. The prior work demonstrated that direct depolarization of chromaffin cells required higher stimulation intensity than were required to activate the splanchnic nerve. The present work in which release is detected with a microsensor inserted directly into slices containing the adrenal medulla supports the prior findings, and provides additional information concerning the temporal and spatial dependence of the two mechanisms that cause catecholamine release. The fast phase of release clearly originates from splanchnic nerve stimulation because it is blocked by a nicotinic antagonist. The slow phase of release is unaffected by nicotinic antagonists, but it is inhibited by an L-type calcium channel antagonist. This demonstrates that the slow phase of release originates from direct depolarization of chromaffin cells because acetylcholine release from the splanchnic nerve is known to be unaffected by L-type calcium channel antagonists whereas their presence inhibits catecholamine release from electrically excited adrenal glands (Akiyama et al., 2004).

Evidence that the splanchnic nerve is not involved in the slow phase of catecholamine release also comes from the experiments with TTX incubation. Consistent with our prior work, TTX blocked the splanchnic-nerve dependent component of release of catecholamines, demonstrating the need for action potential propagation supported by voltage-dependent Na^+ channels (Kao and Fuhrman, 1963, Watanabe et al., 1967). Chromaffin cells are drastically different, however, because they do not require the opening

of Na^+ for catecholamine release. Rather, direct depolarization of the chromaffin cell can cause release due to opening of VGCCs (Sontag et al., 1990, Gerber et al., 1995). This is an important distinction as it illustrates the different mechanisms in play during high intensity electrical stimulation and the resulting biphasic release.

The splanchnic nerve consists of fine fibers closely associated with Schwann cells that innervate the chromaffin cells (Tomlinson and Coupland, 1990, de Diego, 2010). As such, they would be expected to be depolarized by milder electrical stimulations than the chromaffin cells themselves. The splanchnic nerve can be depolarized over large distances (over 200 μm) due to the morphology of its innervation throughout the gland (Tomlinson and Coupland, 1990, Kajiwara et al., 1997, de Diego, 2010). This propagation of the stimulation through the splanchnic nerve network allows release to be evoked from chromaffin cells throughout the tissue including those directly adjacent to the microelectrode. Release adjacent to the microelectrode would appear rapidly leading to the fast appearance of released catecholamines. While chromaffin cells themselves are electrically excitable (Kidokoro and Ritchie, 1980), their lack of myelination and their larger size requires that they receive a greater stimulus intensity to cause exocytosis (Millar et al., 1985). Thus, the chromaffin cells most likely to be directly depolarized by the stimulation are those that are closest to the stimulating electrode. For detection, the released catecholamines from direct chromaffin cell stimulation must diffuse to the detecting microelectrode, a time-dependent process. Consistent with this interpretation, the amplitude of the slow phase diminished more rapidly than the fast phase when the stimulating electrode was moved further away from the carbon-fiber microelectrode.

We also considered other mechanisms that could be the origin of the slow phase of release. One is the interplay of intracellular [Ca^{2+}] and muscarinic cholinergic receptors. At isolated chromaffin cells muscarinic receptor activation has been shown to cause release of Ca^{2+} from intracellular stores (Role and Perlman, 1983, Wakade and Wakade, 1983, Cheek

et al., 1989). Exocytosis, when evoked by mobilization of intracellular Ca^{2+} stores, is temporally delayed in comparison to endogenous acetylcholine induced response (Misbahuddin et al., 1985). However, the slow phase did not display any dependence on THG, a pharmacological agent that causes release of Ca^{2+} from intracellular stores. Furthermore, the slow phase was insensitive to both ATR and 4-DAMP, a group of highly selective muscarinic receptor blockers. Taken together, the negative findings indicate that the slow phase of catecholamine release does not originate from mobilization of intracellular Ca^{2+} via activation of muscarinic receptors. Electroporation was also considered as a mechanism contributing to the slow phase of release. High electric fields are known to cause transient pores in cell membranes (Ryttsen et al., 2000, Gehl, 2003, Olofsson et al., 2003). Electroporation was achieved at single cells stimulated with microelectrodes as evidenced by entry of fluorescent dye (Figure 3.8A-D) (Ryttsen et al., 2000). However, no evidence for electroporation was detected within slices using the tungsten stimulating electrodes with the stimulation parameters used to observe the slow (or fast) phases of catecholamine release (Figure 3.8E-F). It requires very large electric fields to cause electroporation of cells (at least 1 kV/cm). Given the intensity of the stimulation (2.45 V to achieve 350 μA) as well as the distance between the stimulating electrodes (100 μm), electric fields no larger than 250 V/cm were exposed to chromaffin cells within a slice. Furthermore, when electric fields close to 1 kV/cm were applied to the tungsten stimulating electrodes, bubbles were observed at the electrode surface indicating that electroporation using electrodes with a tungsten surface is not feasible because the electric fields required to cause electroporation also cause the breakdown of water at the electrode.

Due to the crucial contribution of Ca^{2+} signaling in the secretion of catecholamines (Burgoyne, 1991, Burgoyne et al., 1993, Garcia et al., 2006), it is important to pay close attention to the types of VGCCs that are present on the cell being studied, as well as the different roles each plays in the multi-step process of release. It has been shown that while

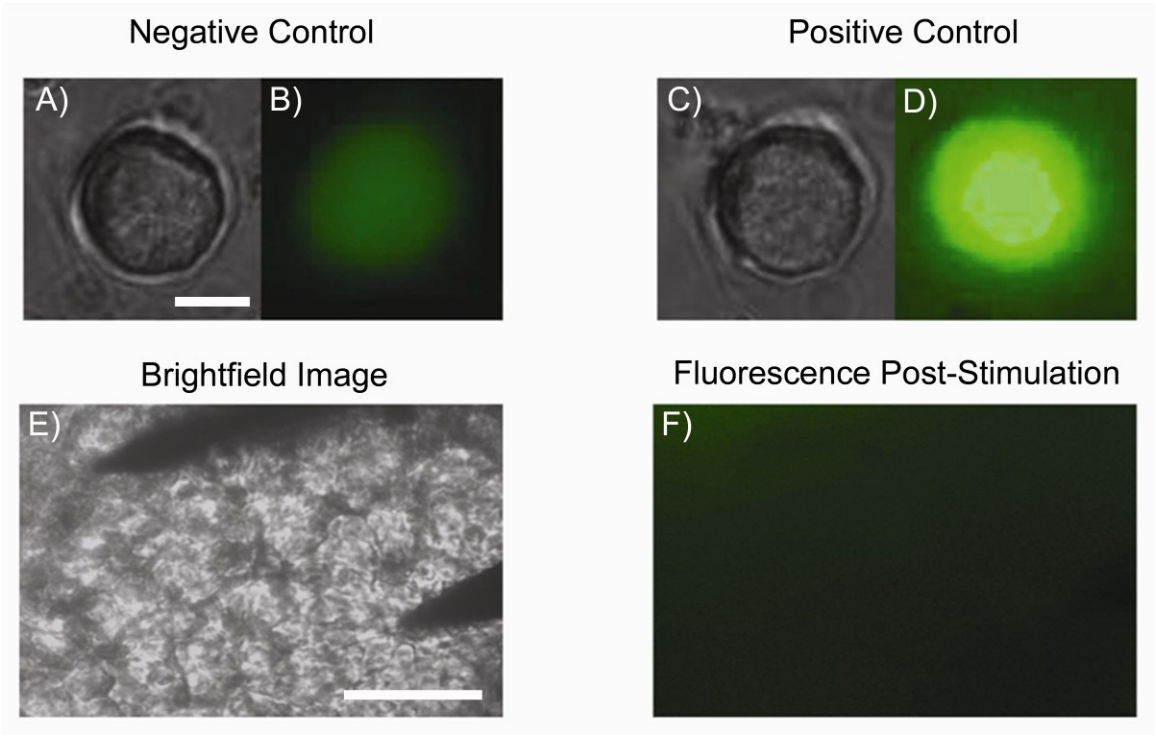

Figure 3.8. Analysis of electroporation at single cells and in slices. (A) and (C) Brightfield images of single chromaffin cells. (B) Fluorescence of the same cell as in (A) after incubation with 10 μM fluorescein but not exposed to an electric field. (D) Fluorescence of the same cell as in (C) after incubation with 10 μM fluorescein and electroporated with a 1.5 kV/cm electric field between two plastic insulated carbon-fiber microelectrodes. (E) Brightfield image of an adrenal slice with the tungsten stimulating electrodes placed on the surface. (F) Fluorescence image of the slice shown in (E) after incubation with 10 μM fluorescein and applied stimulation between the bipolar tungsten electrode (350 μA, biphasic, 10 Hz, 10 pulses). Scale bar A-D, 5 μm. Scale bar E-F, 50 μm.

N and P/Q VGCCs are functionally coupled with exocytosis on chromaffin cells and are believed to be spatially related to one another (Alvarez et al., 2008, Fox et al., 2008), while L-type VGCCs, which take a longer time than P/Q and N VGCCs to inactivate, are known to regulate the autorhythmicity of chromaffin cell action potentials and could play a key role in the homeostatic mechanism of catecholamine release (Marcantoni et al., 2008). However, L-type VGCCs are not present on splanchnic nerves (Akiyama et al., 2004). These properties of L-type VGCCs support the data observed here where the slow phase, not observed in stimulations exciting only the splanchnic nerve, is slower in onset and due to chromaffin cell excitation near the stimulating electrodes. Similar to results previously observed, the nicotinic acetylcholine receptor mediated release decreased approximately 25% in the presence of nifedipine, while the slow phase was no longer distinguishable, leaving only the signal due to the decay of the fast phase (Akiyama et al., 2004). Similar to earlier work, the fast phase was highly dependent on extracellular calcium, further corroborating the splanchnic origin of this signal. As shown by Wakade and Wakade, completely depleting the extracellular buffer of calcium using EGTA abolishes catecholamine release elicited by direct depolarization of the chromaffin cells (Wakade and Wakade, 1982).

In this study, the high temporal and spatial resolution of FSCV at carbon fiber microelectrodes allowed us to distinguish between direct depolarization of chromaffin cells in murine adrenal slices and depolarization of splanchnic nerves that innervate them. While whole gland stimulations (Wakade, 1981, Wakade and Wakade, 1982, Malhotra and Wakade, 1987) established this difference, in this work we were able to temporally and spatially resolve the two components. It is well known in the literature that care must be taken to select appropriate parameters for electrical stimulation of living tissue to study mechanisms of release (Merrill et al., 2005). The present work shows that lower currents and smaller stimulation pulse widths are the proper choice when studying secretion from

murine adrenal slices since they trigger the physiological mechanisms which lead to catecholamine release.

Conclusions

The present work uses an electrochemical technique in order to monitor the direct release of the hormones epinephrine and norepinephrine directly in mouse adrenal slices to determine the effects of varying the stimulating current used to elicit the exocytotic events. Prior to these studies being performed, the only direct chemical analysis of the catecholamines released was performed by analyzing the perfusate of whole glands by HPLC upon stimulation, and subsequent application of pharmacological agents, experiments which are inherently lacking in temporal resolution. By employing FSCV, a technique with a sub-second temporal resolution, the stimulation of the splanchnic nerve and chromaffin cells were distinguished and examined pharmacologically. Given the results of these experiments, prior experimentation on adrenal glands, or adrenal slices where large stimulation intensities and durations must be taken with a grain of salt given that both the splanchnic nerve and the chromaffin cells could have been depolarized by these stimulations. Furthermore, future studies should use smaller intensity electrical stimulations since they elicit release from the physiologically relevant mechanism.

Dr. Jelena Petrovic is gratefully acknowledged for her contributions to the early pharmacological studies on biphasic release.

References

Akiyama T, Yamazaki T, Mori H, Sunagawa K (2004) Effects of Ca^{2+} channel antagonists on acetylcholine and catecholamine releases in the in vivo rat adrenal medulla. Am J Physiol Regul Integr Comp Physiol 287:R161-166.

Alvarez YD, Ibanez LI, Uchitel OD, Marengo FD (2008) P/Q Ca^{2+} channels are functionally coupled to exocytosis of the immediately releasable pool in mouse chromaffin cells. Cell Calcium 43:155-164.

Arroyo G, Fuentealba J, Sevane-Fernandez N, Aldea M, Garcia AG, Albillos A (2006) Amperometric study of the kinetics of exocytosis in mouse adrenal slice chromaffin cells: physiological and methodological insights. J Neurophysiol 96:1196-1202.

Augustine GJ, Neher E (1992) Calcium requirements for secretion in bovine chromaffin cells. J Physiol 450:247-271.

Barbara JG, Poncer JC, McKinney RA, Takeda K (1998) An adrenal slice preparation for the study of chromaffin cells and their cholinergic innervation. J Neurosci Methods 80:181-189.

Burgoyne RD (1991) Control of exocytosis in adrenal chromaffin cells. Biochim Biophys Acta 1071:174-202.

Burgoyne RD, Morgan A, Robinson I, Pender N, Cheek TR (1993) Exocytosis in adrenal chromaffin cells. J Anat 183 (Pt 2):309-314.

Cahill PS, Walker QD, Finnegan JM, Mickelson GE, Travis ER, Wightman RM (1996) Microelectrodes for the measurement of catecholamines in biological systems. Anal Chem 68:3180-3186.

Catterall WA (1980) Neurotoxins that act on voltage-sensitive sodium channels in excitable membranes. Annu Rev Pharmacol Toxicol 20:15-43.

Cheek TR, O'Sullivan AJ, Moreton RB, Berridge MJ, Burgoyne RD (1989) Spatial localization of the stimulus-induced rise in cytosolic Ca^{2+} in bovine adrenal chromaffin cells. Distinct nicotinic and muscarinic patterns. FEBS Lett 247:429-434.

de Diego AM (2010) Electrophysiological and morphological features underlying neurotransmission efficacy at the splanchnic nerve-chromaffin cell synapse of bovine adrenal medulla. Am J Physiol Cell Physiol 298:C397-405.

Fox AP, Cahill AL, Currie KP, Grabner C, Harkins AB, Herring B, Hurley JH, Xie Z (2008) N- and P/Q-type Ca^{2+} channels in adrenal chromaffin cells. Acta Physiol (Oxf) 192:247-261.

Garcia AG, Garcia-De-Diego AM, Gandia L, Borges R, Garcia-Sancho J (2006) Calcium signaling and exocytosis in adrenal chromaffin cells. Physiol Rev 86:1093-1131.

Gehl J (2003) Electroporation: theory and methods, perspectives for drug delivery, gene therapy and research. Acta Physiol Scand 177:437-447.

Gerber SH, Haunstetter A, Kruger C, Kaufmann A, Nobiling R, Haass M (1995) Role of $[Na^{+}]_i$ and $[Ca^{2+}]_i$ in nicotine-induced norepinephrine release from bovine adrenal chromaffin cells. Am J Physiol 269:C572-581.

Heien ML, Phillips PE, Stuber GD, Seipel AT, Wightman RM (2003) Overoxidation of carbon-fiber microelectrodes enhances dopamine adsorption and increases sensitivity. Analyst 128:1413-1419.

Kajiwara R, Sand O, Kidokoro Y, Barish ME, Iijima T (1997) Functional organization of chromaffin cells and cholinergic synaptic transmission in rat adrenal medulla. Jpn J Physiol 47:449-464.

Kao CY, Fuhrman FA (1963) Pharmacological studies on tarichatoxin, a potent neurotoxin. J Pharmacol Exp Ther 140:31-40.

Kawagoe KT, Zimmerman JB, Wightman RM (1993) Principles of voltammetry and microelectrode surface states. J Neurosci Methods 48:225-240.

Kennedy RT, Jones SR, Wightman RM (1992) Simultaneous measurement of oxygen and dopamine: coupling of oxygen consumption and neurotransmission. Neuroscience 47:603-612.

Kidokoro Y, Ritchie AK (1980) Chromaffin cell action potentials and their possible role in adrenaline secretion from rat adrenal medulla. J Physiol 307:199-216.

Malhotra RK, Wakade AR (1987) Non-cholinergic component of rat splanchnic nerves predominates at low neuronal activity and is eliminated by naloxone. J Physiol 383:639-652.

Marcantoni A, Carabelli V, Comunanza V, Hoddah H, Carbone E (2008) Calcium channels in chromaffin cells: focus on L and T types. Acta Physiol (Oxf) 192:233-246.

Merrill DR, Bikson M, Jefferys JG (2005) Electrical stimulation of excitable tissue: design of efficacious and safe protocols. J Neurosci Methods 141:171-198.

Michael D, Travis ER, Wightman RM (1998) Color images for fast-scan CV measurements in biological systems. Anal Chem 70:586A-592A.

Millar J, Stamford JA, Kruk ZL, Wightman RM (1985) Electrochemical, pharmacological and electrophysiological evidence of rapid dopamine release and removal in the rat caudate nucleus following electrical stimulation of the median forebrain bundle. Eur J Pharmacol 109:341-348.

Miranda-Ferreira R, de Pascual R, Caricati-Neto A, Gandia L, Jurkiewicz A, Garcia AG (2009) Role of the endoplasmic reticulum and mitochondria on quantal catecholamine release from chromaffin cells of control and hypertensive rats. J Pharmacol Exp Ther 329:231-240.

Misbahuddin M, Isosaki M, Houchi H, Oka M (1985) Muscarinic receptor-mediated increase in cytoplasmic free Ca^{2+} in isolated bovine adrenal medullary cells. Effects of TMB-8 and phorbol ester TPA. FEBS Lett 190:25-28.

Moser T, Neher E (1997) Rapid exocytosis in single chromaffin cells recorded from mouse adrenal slices. J Neurosci 17:2314-2323.

Nassar-Gentina V, Pollard HB, Rojas E (1988) Electrical activity in chromaffin cells of intact mouse adrenal gland. Am J Physiol 254:C675-683.

Neher E (1998) Vesicle pools and Ca^{2+} microdomains: new tools for understanding their roles in neurotransmitter release. Neuron 20:389-399.

Neher E, Augustine GJ (1992) Calcium gradients and buffers in bovine chromaffin cells. J Physiol 450:273-301.

Neher E, Marty A (1982) Discrete changes of cell membrane capacitance observed under conditions of enhanced secretion in bovine adrenal chromaffin cells. Proc Natl Acad Sci U S A 79:6712-6716.

Olofsson J, Nolkrantz K, Ryttsen F, Lambie BA, Weber SG, Orwar O (2003) Single-cell electroporation. Curr Opin Biotechnol 14:29-34.

Petrovic J, Walsh PL, Thornley KT, Miller CE, Wightman RM (2010) Real-Time Monitoring of Chemical Transmission in Slices of the Murine Adrenal Gland. Endocrinology 151:1773-1783.

Ranganathan S, Kuo T-C, McCreery RL (1999) Facile Preparation of Active Glassy Carbon Electrodes with Activated Carbon and Organic Solvents. Anal Chem 71:3574-3580.

Role LW, Perlman RL (1983) Both nicotinic and muscarinic receptors mediate catecholamine secretion by isolated guinea-pig chromaffin cells. Neuroscience 10:979-985.

Ryttsen F, Farre C, Brennan C, Weber SG, Nolkrantz K, Jardemark K, Chiu DT, Orwar O (2000) Characterization of single-cell electroporation by using patch-clamp and fluorescence microscopy. Biophys J 79:1993-2001.

Shukla R, Wakade AR (1991) Functional aspects of calcium channels of splanchnic neurons and chromaffin cells of the rat adrenal medulla. J Neurochem 56:753-758.

Smith C, Moser T, Xu T, Neher E (1998) Cytosolic Ca^{2+} acts by two separate pathways to modulate the supply of release-competent vesicles in chromaffin cells. Neuron 20:1243-1253.

Sontag JM, Sanderson P, Klepper M, Aunis D, Takeda K, Bader MF (1990) Modulation of secretion by dopamine involves decreases in calcium and nicotinic currents in bovine chromaffin cells. J Physiol 427:495-517.

Tomlinson A, Coupland RE (1990) The innervation of the adrenal gland. IV. Innervation of the rat adrenal medulla from birth to old age. A descriptive and quantitative morphometric and biochemical study of the innervation of chromaffin cells and adrenal medullary neurons in Wistar rats. J Anat 169:209-236.

Travis ER, Wightman RM (1998) Spatio-temporal resolution of exocytosis from individual cells. Annu Rev Biophys Biomol Struct 27:77-103.

Troyer KP, Wightman RM (2002) Temporal separation of vesicle release from vesicle fusion during exocytosis. J Biol Chem 277:29101-29107.

Voets T, Neher E, Moser T (1999) Mechanisms underlying phasic and sustained secretion in chromaffin cells from mouse adrenal slices. Neuron 23:607-615.

Wakade AR (1981) Studies on secretion of catecholamines evoked by acetylcholine or transmural stimulation of the rat adrenal gland. J Physiol 313:463-480.

Wakade AR, Wakade TD (1982) Secretion of catecholamines from adrenal gland by a single electrical shock: electronic depolarization of medullary cell membrane. Proc Natl Acad Sci U S A 79:3071-3074.

Wakade AR, Wakade TD (1983) Contribution of nicotinic and muscarinic receptors in the secretion of catecholamines evoked by endogenous and exogenous acetylcholine. Neuroscience 10:973-978.

Watanabe A, Tasaki I, Singer I, Lerman L (1967) Effects of tetrodotoxin on excitability of squid giant axons in sodium-free media. Science 155:95-97.

Wightman RM, Jankowski JA, Kennedy RT, Kawagoe KT, Schroeder TJ, Leszczyszyn DJ, Near JA, Diliberto EJ, Jr., Viveros OH (1991) Temporally resolved catecholamine spikes correspond to single vesicle release from individual chromaffin cells. Proc Natl Acad Sci U S A 88:10754-10758.

Chapter IV

Quantifying Adenosine Production from Ectonucleotidases in Spinal Nociceptive Circuits

Introduction

Neurons and glia throughout the nervous system release adenosine 5'-triphosphate (ATP) spontaneously and in response to diverse pathological insults, including tissue damage, inflammation, hypoxia and nerve injury (Nakamura and Strittmatter, 1996, Arcuino et al., 2002, Matsuka et al., 2008, Gourine et al., 2010). In the somatosensory system, ATP excites and sensitizes nociceptive DRG neurons and can activate spinal microglia (Dussor et al., 2009). The excitatory effects of extracellular ATP can be terminated by a cascade of ectonucleotidases that hydrolyze ATP to adenosine (Dunwiddie et al., 1997, Zimmermann, 2008), although the speed at which these ectonucleotidases work in any region of the nervous system is unknown. Adenosine can signal through the adenosine A_1 receptor (A_1R) to inhibit neurotransmission and nociception (Sawynok and Liu, 2003, Zylka, 2011).

Recently, two ectonucleotidases in nociceptive neurons that hydrolyze extracellular AMP to adenosine were identified. These enzymes include the trans-membrane isoform of prostatic acid phosphatase (PAP, also known as ACPP) and ecto-5'-nucleotidase (NT5E). PAP and NT5E are extensively co-localized in nociceptive DRG neurons and on axon terminals located in lamina II of the dorsal spinal cord (Zylka et al., 2008, Sowa et al., 2010b). PAP deficient (*Pap*$^{-/-}$) and NT5E deficient (*Nt5e*$^{-/-}$) mice have similar behavioral phenotypes, including enhanced nociceptive sensitization following nerve injury and following peripheral inflammation. Mice lacking A_1R likewise show enhanced sensitization in

models of chronic pain (Wu et al., 2005). Humans with null mutations in *Nt5e* develop very painful arterial calcifications (St Hilaire et al., 2011), suggesting loss of an adenosine generating ectonucleotidase exacerbates an already painful condition in humans (Zylka and Sowa, 2011). While these and other data suggest adenosine tonically inhibits nociceptive circuits (Keil and DeLander, 1996, Tian et al., 2010), the time frame over which adenosine is produced and the molecular source of adenosine (from ectonucleotidases and/or directly released from cells) are unknown (Wall and Dale, 2008).

Several studies suggest ectonucleotidases inhibit nociception by generating adenosine from endogenously released nucleotides. Notably, pharmacological inhibitors of ectonucleotidases reduce adenosine production from adenosine 5'-monophosphate (AMP) in dorsal spinal cord and reduce adenosine release in dorsal spinal cord synaptosomes (Sweeney et al., 1989, Patterson et al., 2001). Moreover, AMP hydrolysis in spinal lamina II was reduced, but not eliminated, in *Pap*$^{-/-}$ and *Nt5e*$^{-/-}$ single knockout mice (Zylka et al., 2008, Sowa et al., 2010b). Lastly, intrathecal injection of soluble (non-membrane bound) PAP or NT5E protein had long-lasting (2-3 days) antinociceptive effects that were entirely dependent on A_1R activation (Zylka et al., 2008, Sowa et al., 2009, Sowa et al., 2010a, Sowa et al., 2010c).

Here, we generated mice lacking PAP and NT5E to investigate the combined importance of these enzymes in nociceptive mechanisms. Then, we used FSCV to measure adenosine levels at sub-second resolution in the spinal microdomain (lamina II) where these enzymes are located (Swamy and Venton, 2007, Cechova and Venton, 2008). As previously outlined,, certain criteria are necessary to confirm an electrochemical signal (Marsden et al., 1988, Phillips and Wightman, 2003). Pharmacological verification was obtained by using dipyridamole, an adenosine transporter blocker. Our data indicate PAP and NT5E rapidly hydrolyze nucleotides to adenosine and generate inhibitory adenosine transients in spinal nociceptive circuits. Furthermore, any residual AMP hydrolysis is

performed by alkaline phosphatase, a group of ectonucleotidases found ubiquitously throughout the body. Finally, adenosine transients were observed for the first time anywhere in the central nervous system. The implications of this signal to adenosinergic tone and antinociception are discussed.

Experimental

Animals

All procedures and behavioral experiments involving vertebrate animals were approved by the Institutional Animal Care and Use Committee at the University of North Carolina at Chapel Hill. Wild-type (WT) C57BL/6 mice were purchased from Jackson Laboratories or bred in house from C57BL/6J stock. *Pap*$^{-/-}$ (Vihko et al., abstract from Proceedings of the AACR, 2005, 96th Annual Meeting, Anaheim, CA) (Zylka et al., 2008), *Nt5e*$^{-/-}$ (Thompson et al., 2004) mice were backcrossed to C57BL/6J mice for > 10 generations. dKO mice were generated by breeding backcrossed *Nt5e*$^{-/-}$ and *Pap*$^{-/-}$ mice.

Slice Preparation

Transverse (800-900 μm, used in field recordings) and sagittal (400 μm, used in FSCV experiments) spinal cord slices were prepared as previously described from 1-2 month old mice (Wang and Zylka, 2009). Briefly, mice were anesthetized with urethane (1.5 g/kg, i.p.) and the lumbar spinal cord was quickly dissected and sliced on a Vibratome 3000EP at 4°C. The dissection buffer contained the following (in mM): 87 NaCl, 2.5 KCl, 1.25 NaH_2PO_4, 25 $NaHCO_3$, 75 sucrose, 10 glucose, 1.5 ascorbic acid, 0.5 $CaCl_2$, 7 $MgCl_2$. The slices were then incubated at 37°C for 45 minutes and then at room temperature in regular artificial cerebrospinal fluid (aCSF) that contained (in mM): 125 NaCl, 2.5 KCl, 1.25 NaH_2PO_4, 26 $NaHCO_3$, 25 glucose, 2.5 $CaCl_2$, 1.5 $MgCl_2$. For cyclic voltammetry experiments, the slices were incubated for one hour or less before the experiments were

carried out. All solutions were bubbled with 95% O_2/5% CO_2 for the duration of the dissection and incubation steps.

Fast-Scan Cyclic Voltammetry of Adenosine

Disk-shaped carbon-fiber microelectrodes were fabricated as previously described (Cahill et al., 1996). Briefly, a single 6 µm diameter T-650 carbon fiber (Thornell, Amoco Corp. Greenville, SC) was aspirated into a glass capillary (1.2 mm x 0.68 mm, AM Systems, Carlsborg, WA) which was then sealed on a vertical pipette puller (model PE-21, Narishige Group, Japan). Electrodes were then cut with a surgical blade, sealed with epoxy, and polished at 30º on a K. T. Brown micro-pipette beveller (model BV-10, Sutter Instruments, Novato, CA). Before use, electrodes were soaked in a mixture of isopropanol and activated carbon for at least 20 minutes (Bath et al., 2000). To detect adenosine, the electrode's potential was held at -0.4 V between each scan, and was ramped from -0.4 V to 1.5 V at a scan rate of 400 V/s every 100 ms. The peak at 1.0 V was used to quantify the peak concentrations of adenosine because it is unique to adenosine and not observed with ATP, ADP or AMP (Swamy and Venton, 2007). A Ag/AgCl reference electrode was used for all experiments. FSCV data was collected using a custom LABVIEW program, Tar Heel CV. Two computer interface boards (National Instruments PCI 6052 and PCI 6711, Austin, TX) were used to apply the triangular waveform, digitize the resulting current, and to control pressure ejection synchronization with the waveform application through a homemade breakout box. A Chem-Clamp Voltammeter (Dagan Corporation, Minneapolis, MN) was used to control the electrode potential and measure the resulting current, which was filtered with a built-in analog low pass Bessel filter at 10 kHz. To make electrical contact with the head stage, a stainless steel wire was inserted into the back of the microelectrode which was backfilled with an electrolyte mixture of 4 M potassium acetate and 0.15 M potassium chloride.

FSCV data were viewed in the form of color plots with sequentially stacked cyclic voltammograms shown over time (abscissa), plotted against the electrode potential displayed on the ordinate where the switching potential (1.5 V) is in the middle. The current is displayed in false color, with oxidative currents being shown in green and reductive currents being shown in blue and black. From these plots, the current at a specific potential can be plotted against time to examine how the adenosine concentration changes. These current traces are converted to concentration from calibrations performed in a flow injection apparatus which allows for a bolus of adenosine ranging in concentration from 1-10 μM or 10 μM AMP to be introduced to the electrode surface.

To detect the production of adenosine by PAP and NT5E, 100 μM AMP was pressure ejected five times at 5 minute intervals using a Picospritzer® III (Parker Instrumentation, Pinebrook, NJ) for 1 s at 20 psi from a micropipette inserted into sagittal slices, approximately 100 μm from the carbon fiber microelectrode. To minimize tissue damage, electrodes were inserted at 30° from the slice surface with the disk facing down, approximately 50 μm below the surface of the slice. AMP solutions were freshly prepared for each experiment to overcome the possible confound of degradation into adenosine. Furthermore, the absence of adenosine in the pressure ejection pipette was confirmed before and after each experiment by ejections onto the electrode above the slice (confirmed by the absence of current at 1.0 V). For experiments carried out at pH 5.6, five consecutive ejections at 5 minute intervals were performed 10 minutes after application of pH 5.6 buffer. The buffer used for experiments at pH 5.6 contained in mM: 10 Tris Maleate, 140 NaCl, 4 KCl, 2 $MgCl_2$, 2 $CaCl_2$, 5 Glucose, and pH adjusted to 5.6 with NaOH. When detecting spontaneous adenosine transients, the carbon fiber was inserted into the slice without any stimuli applied to the slice. For adenosine assignment, each event had a distinguishable cyclic voltammogram with a current peak at 1.0 V that was more than 5 times the standard deviation of the baseline noise.

Pharmacology

Dipyridamole and MLS-0038949 were used as received. Stock solutions were prepared in DMSO. The stock solution was then diluted into the recording buffer and perfused across the slice at a flow rate of ~2 mL/min.

Statistical Analysis

Statistical analysis was performed in GraphPad Prism (GraphPad Software, Inc., San Diego, CA, USA). Student's t-test (paired), or one-way ANOVA were used to test for significant differences between data sets. Data were considered significant at the 95 % confidence level and are reported as the mean ± SEM. The number of slices is indicated by n, unless noted otherwise.

Results

Determination of Adenosine Production from PAP and NT5E in Lamina II with Fast-Scan Cyclic Voltammetry

Before beginning experiments with animals that lack PAP, NT5E, or both ecotnucleotdases, developing a method for measuring the production of adenosine from AMP was necessary. The voltammetry of adenosine has already been well described elsewhere (Swamy and Venton, 2007). This method allows for detection of just adenosine without interference from metabolites like inosine. Furthermore, the adenosine cyclic voltammogram has peaks at both 1.0 and 1.5 V while the precursors for adenosine such as AMP and ATP only show a peak at 1.5 V.

While typical methods of stimulation such as applying a current from a bipolar stimulation electrode proved unsuccessful, injecting the substrate of these enzymes and measuring the production of adenosine with a carbon-fiber microelectrode gave reproducible results in WT animals. Pressure ejection from pulled capillaries allowed for a localized

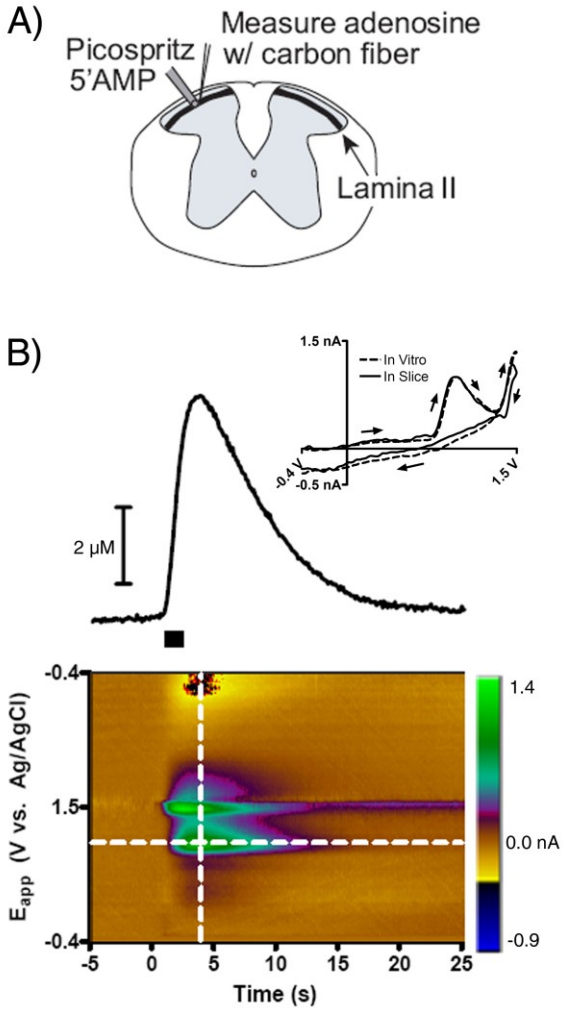

Figure 4.1. Method for monitoring adenosine production from ectonucleotidases. (A) Cartoon showing placement of pulled capillary and carbon-fiber microelectrode in lamina II of the spinal cord. (B) Representative color plot (below) and concentration versus time trace (above) from the pressure ejection of 100 µM AMP for 1 s at time t=0 s. The color plot shows the horizontal line for where the concentration versus time plot was extracted from, and the vertical line shows where the cyclic voltammogram in the inset was taken from. The cyclic voltammogram obtained from this experiment matches that obtained in vitro.

delivery of 100 μM AMP ~100 μm from the carbon-fiber multiple times (up to 20 ejections). Figure 4.1 shows a representative example of how this experiment is carried out. A cartoon of a spinal cord slice showing the placement of the pulled capillary and the carbon-fiber microelectrode into lamina II of the spinal cord is shown in Figure 4.1A. Below in Figure 4.1B, a representative color plot from the pressure ejection of AMP at time t = 0 s for 1 s at 20 psi is seen, and the concentration versus time plot is seen above it, showing a rapid production of adenosine which peaks about 4 s after the ejection and then shows the diffusion of adenosine away from the electrode. As shown by the horizontal dotted line in the color plot, the peak at 1.0 V was used to quantify the amount of adenosine being produced, because it is distinct to adenosine and cannot be attributed to the AMP being applied to the slice. Lastly, the cyclic voltammogram from the vertical dotted line in the color plot is seen as the inset next to the concentration versus time plot. The cyclic voltammogram from the pressure ejection has the distinct shape of adenosine previously described, and is also comparable to that seen *in vitro*. Furthermore, pressure ejection of AMP directly onto the electrode in buffer solution, or in agarose, produced no peak at 1.0 V (data not shown).

Once the method for determination of adenosine production in the spinal cord was complete, experiments were performed in order to determine the contributions of PAP and NT5E to the hydrolysis of AMP in lamina II of the spinal cord. In WT slices, adenosine levels peaked within ~4 s at a concentration of 4.34 ± 0.57 μM at pH 7.4 (Figure 4.2A, E, F). Adenosine production and peak levels (4.13 ± 0.55 μM) were not impaired in *Pap*$^{-/-}$ slices at pH 7.4 (Figure 4.2B, E, F). However, adenosine production and peak levels were significantly impaired in *Pap*$^{-/-}$ slices at pH 5.6 compared to WT slices (0.72 ± 0.05 μM verses 1.66 ± 0.06 μM, respectively, Figure 4.2G, H). In addition, adenosine production and peak levels were significantly impaired in *Nt5e*$^{-/-}$ and dKO slices at neutral and acidic pH

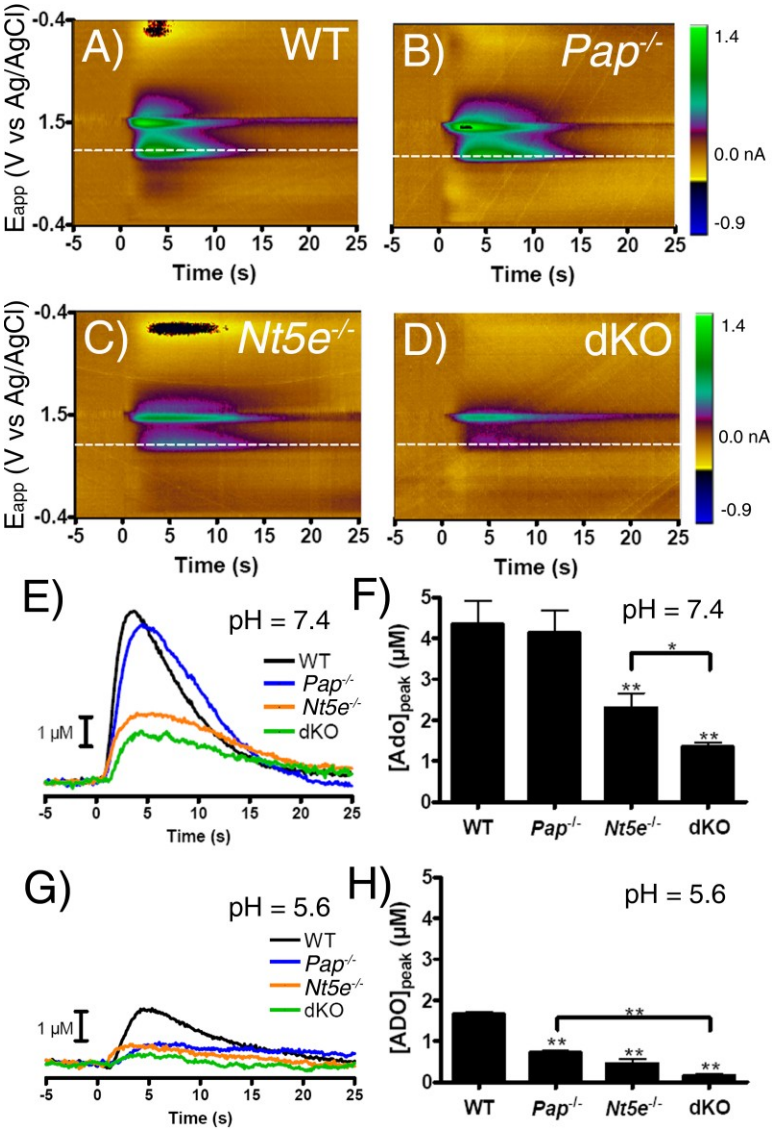

Figure 4.2. Adenosine production is impaired in spinal nociceptive circuits of *Pap*$^{-/-}$, *Nt5e*$^{-/-}$ and dKO mice. (A-D) Color plots for the 1 s pressure ejection of 100 µM AMP into lamina II of (A) WT, (B) *Pap*$^{-/-}$, (C) *Nt5e*$^{-/-}$, and (D) dKO slices at pH 7.4. (E) Current extracted at 1.0 V from the dashed horizontal lines in A-D), converted to concentration of adenosine and plotted versus time. (F) Peak adenosine production following pressure ejection of AMP into lamina II at pH 7.4 (n = 5 for each genotype). (G) Current extracted at 1.0 V from representative experiments performed at pH 5.6. (H) Peak adenosine production following pressure ejection of AMP into lamina II at pH 5.6 (n = 5 for each genotype). (F, H) One way ANOVAs with Bonferroni's post-hoc tests were used to compare each genotype to WT and to compare between genotypes. *$p < 0.05$, **$p < 0.005$. Data presented as means ± SEM.

(Figure 4.2C-H). Notably, peak adenosine levels at pH 7.4 were significantly lower in dKO slices than in *Nt5e*$^{-/-}$ slices (1.34 ± 0.11 μM verses 2.30 ± 0.36 μM, respectively), unmasking a contribution of PAP to adenosine production at neutral pH, (Figure 4.2F). Lastly, at pH 5.6, almost no adenosine was produced after pressure ejecting AMP into lamina II of dKO slices (Figure 4.2G, H). Taken together, these direct measures with gene knockout mice indicate PAP and NT5E rapidly generate adenosine at neutral and acidic pH and together are the main adenosine-generating ectonucleotidases in spinal nociceptive circuits.

Remarkably, some adenosine was still produced in dKO spinal slices at pH 7.4 (Figure 4.2F), suggesting there is at least one more adenosine-generating enzyme. The presence of this third enzyme could not have been anticipated without first studying *Pap/Nt5e* dKO mice. AMP hydrolysis and adenosine production were largely eliminated in lamina II at pH 5.6 in dKO mice, making it unlikely this enzyme is another acid phosphatase. However, this enzyme could have a neutral to alkaline pH optimum given that adenosine is produced at pH 7.4 (albeit at levels that are only ~30% of WT levels; Figure 4.2F). Alkaline phosphatases are present in the spinal cord, have such a pH optimum and can hydrolyze ATP, ADP and AMP extracellularly (MacGregor et al., 1995, Zimmermann, 2008).

Determination of Adenosine Production from Alkaline Phosphatases in Lamina II with Fast-Scan Cyclic Voltammetry

To determine whether alkaline phosphatases (of which there are four functional genes in the mouse) or other ectonucleotidases contribute to residual adenosine production in spinal nociceptive circuits, an alkaline phosphatase inhibitor MLS-0038969 was perfused onto WT and dKO slices using the above experimental parameters (Sergienko et al., 2009). Figure 4.3 shows representative examples of these experiments. In WT slices, the peak adenosine concentration was determined to be 6.13 ± 0.64 μM without the alkaline phosphatase inhibitor (Figure 4.3A), and 5.34 ± 0.98 μM with the inhibitor being bath applied

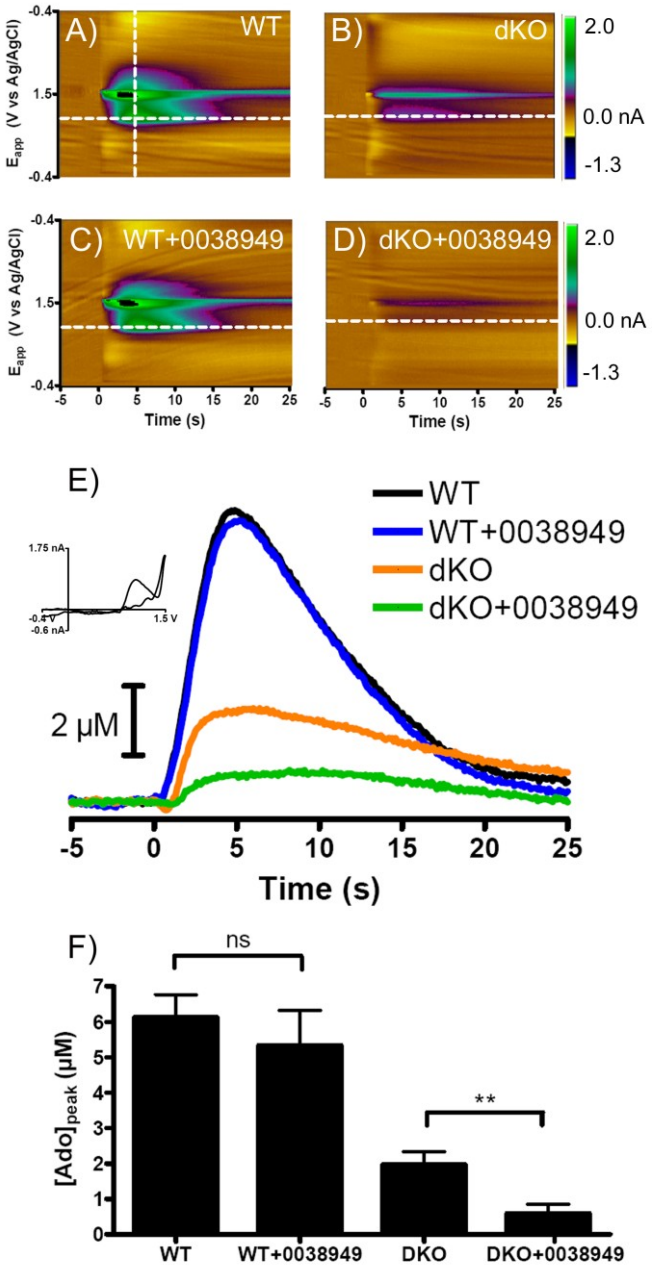

Figure 4.3. Alkaline phosphatase contributes to adenosine production when PAP and NT5E are not present. (A-D) Color plots for the 1 s ejection of 100 µM AMP at 20 psi at time t=0 s into lamina II of (A) WT, (B) DKO, (C) WT with 00038949 on board, and (D) dKO with 00038949 on board. (E) Concentration versus time plots for the data extracted at 1.0 V from the horizontal lines in A-D. The inset shows the cyclic voltammogram taken from the vertical line in A. (F) Peak adenosine concentration for all experiments upon pressure ejection of AMP into lamina II with and without alkaline phosphatase inhibitor present (n = 5 for each genotype). Paired student's t-tests were used to compare genotypes before and after drug application. **p<0.005. Data presented as mean ± SEM.

(Figure4.3C), values which are not statistically different (Figure 4.3F, $p>0.05$, $n = 5$, paired student's t-test). In dKO slices, however, the peak adenosine concentration from the application of AMP was determined to be 1.97 ± 0.35 μM before application of drug (Figure 4.3B), while it was 0.59 ± 0.26 μM (Figure 4.3D), a significant decrease of about 70% in the amount of adenosine being produced down to almost none (Figure 4.3F, $p<0.005$, $n = 5$, paired student's t-test). These data show that while the ectonucleotidases PAP and NT5E produce the majority of adenosine from AMP in spinal nociceptive circuits, alkaline phosphatase does provide a significant role in AMP hydrolysis when these more active enzymes are absent.

Pharmacological Verification of Adenosine Signal

In order to have further verification that the signal observed upon the application of AMP into lamina II of the spinal cord is indeed adenosine, a highly selective adenosine transporter blocker, dipyridamole (DIP), was used to observe its effect on the signal (Thorn and Jarvis, 1996). AMP was pressure ejected into lamina II of the spinal cord, as described above. After a stable signal was obtained, 25 μM DIP was bath applied to the slice, and adenosine production was monitored. Figure 4.4A shows an example from one of these experiments. After application of DIP, the peak adenosine concentration about 4 s upon pressure ejection of AMP is nearly double that of the signal before drug application. While it might be expected that the falling phase of the signal would be affected as when cocaine is applied to a slice when cocaine or a dopamine transporter blocker is applied (Jones et al., 1995), this experiment is different because the adenosine transporter is probably already saturated by applying and producing such large amounts of adenosine that the falling phase is governed by diffusion. The peak concentration increases because the adenosine that is produced between the pulled capillary and the carbon-fiber is not taken up, and is allowed to be detected. Figure 4.4B shows a summary of the three experiments performed. The

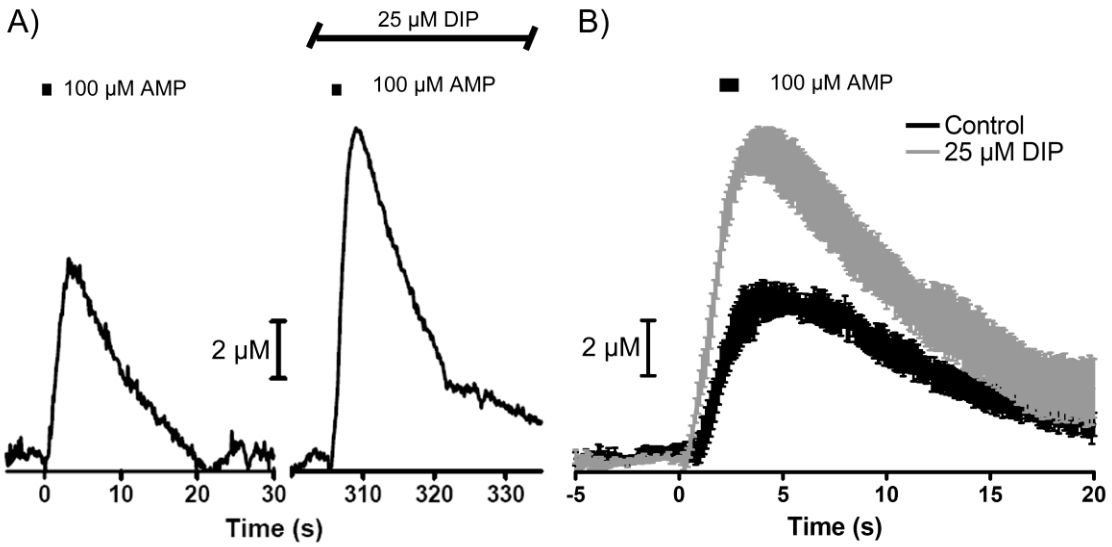

Figure 4.4. A nucleoside transport inhibitor promotes the buildup of ectonucleotidase-generated adenosine. (A) AMP was pressure ejected into lamina II of WT spinal cord slices in the absence or presence of DIP. FSCV was used to measure extracellular adenosine; (B) Average responses ± SEM, from n = 3 slices. DIP significantly increased the concentration of extracellular adenosine for 0.7 to 8 s following AMP addition ($p < 0.005$ by one-way ANOVA), and peak adenosine concentration .increased from 5.77 ± 0.46 μM to 10.86 ± 0.40 μM after application ($p<0.005$, paired student's t-test, n = 3)

traces show the concentration of adenosine before and after DIP application ± SEM. Control experiments showed peak adenosine concentrations of 5.77 ± 0.46 μM, which increased to 10.86 ± 0.40 μM after application, values which are statistically significant from each other ($P<0.005$, paired student's t-test, n=3). These data give pharmacological verification that the signal observed upon application of AMP to the slice is indeed adenosine.

Adenosine Transients Occur Spontaneously and Are Generated by PAP and NT5E

While performing FSCV studies, we unexpectedly observed "adenosine transients," spontaneous and transient increases in adenosine concentration, every time a freshly-polished carbon-fiber microelectrode was placed in lamina II of WT slices (Figure 4.5A). We did not see these transients if microelectrodes were re-used without being re-polished, suggesting debris on the tip interferes with detection of these transients. The peaks at 1.0 V and 1.5 V in color plots and cyclic voltammograms (Figure 4.5) confirmed that these transients contained adenosine. Transient release was observed at a low frequency (0.35 ± 0.04 events/min) in all WT slices (Table 4.1; with 2.5 mM extracellular calcium). These transients were also observed when freshly polished carbon-fiber electrodes were placed into slices from *Pap*$^{-/-}$, *Nt5e*$^{-/-}$ and dKO animals (Figure 4.5B-D).

To ascertain if these events were Ca^{2+} dependent, we chelated intracellular Ca^{2+} by pre-incubating slices in 10 μM BAPTA-AM for 45 minutes and removed extracellular Ca^{2+} from the bath. Under these conditions, adenosine transients were observed in four of the five slices, at a frequency (0.06 ± 0.03 events/min) that was significantly less than when calcium was present in the bath (Table 4.1). PAP and NT5E do not require divalent cations for activity, so this reduction was not likely due to inhibition of PAP or NT5E.

Next, to determine if PAP and NT5E generate adenosine transients, electrodes were placed into *Pap*$^{-/-}$, *Nt5e*$^{-/-}$, and dKO slices and up to 20 consecutive one-minute intervals

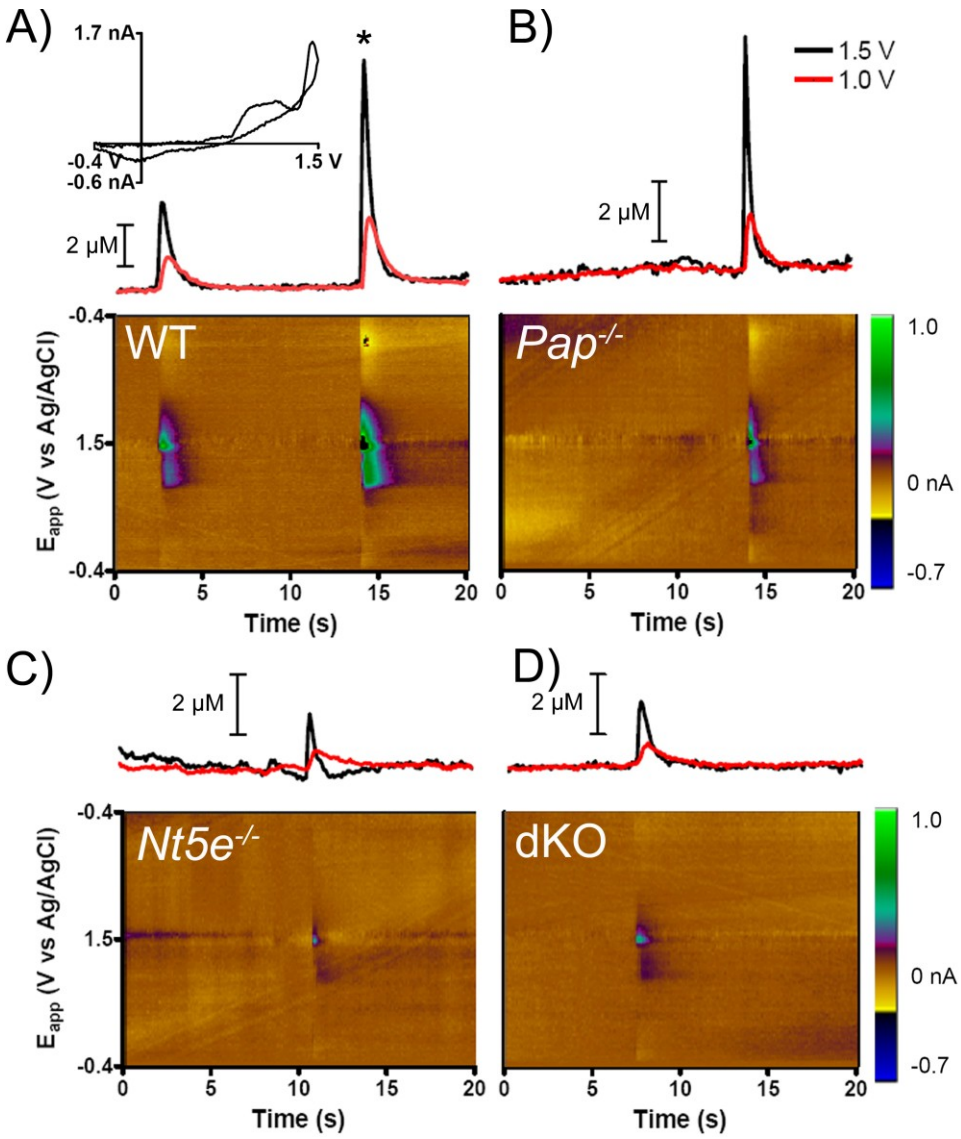

Figure 4.5. Spontaneous adenosine transients detected in lamina II by FSCV. (A-D) Concentration versus time traces (top) and color plots (bottom) in slices containing lamina II from (A) WT, (B) *Pap*$^{-/-}$, (C) *Nt5e*$^{-/-}$, and (D) dKO mice. Scale bars are for the 1.0 V traces. The inset in A shows the cyclic voltammogram for the transient denoted with an asterisk.

Table 4.1. Summary of adenosine transient events in spinal cord lamina II. One-way ANOVA ($p < 0.05$) followed by Newman-Keuls multiple comparison post-hoc test to compare all genotypes relative to WT (2.5 mM Ca^{2+}); *$p < 0.05$, **$p < 0.005$. # Transient time was measured from the onset of the transient until the signal decayed to baseline.

Genotype	$[Ca^{2+}]$ (mM)	$[Ado]_{peak}$ (nM)	Frequency (events/min)	Transient Time (s)#
WT (n = 19)	2.5	570 ± 50	0.35 ± 0.04	1.5 ± 0.1
WT (n = 5)	0.0	410 ± 50	0.06 ± 0.03**	1.8 ± 0.3
Pap$^{-/-}$ (n = 10)	2.5	690 ± 150	0.14 ± 0.04*	1.5 ± 0.1
Nt5e$^{-/-}$ (n = 10)	2.5	360 ± 20	0.14 ± 0.07*	1.5 ± 0.1
dKO (n = 16)	2.5	380 ± 40	0.10 ± 0.03**	1.2 ± 0.1

were recorded, background subtracted and corrected to account for background drift of the electrode over time (Figure 4.6A, experiments with WT slices were interleaved with knockout slices). Unlike WT slices where transients were observed in every (19/19) slice, spontaneous events were observed in a subset of slices from *Pap*$^{-/-}$ (8/10 slices), *Nt5e*$^{-/-}$ (6/10 slices) and dKO (9/16 slices) mice. Furthermore, in slices from *Pap*$^{-/-}$, *Nt5e*$^{-/-}$ and dKO mice where transients were observed, the frequency was significantly lower than in WT slices (Figure 4.6B). This reduction is unlikely to be due to deficits in synaptic transmission since evoked field excitatory postsynaptic potential (fEPSP) amplitudes were not significantly different between WT and mutant backgrounds (Figure 4.6C). Collectively, these findings (summarized in Table 4.1) indicate PAP and NT5E generate a majority of all adenosine transients, presumably through hydrolysis of nucleotides that are released by neurons and/or glia. Moreover, the observation that transient frequency can be reduced in single and dKO mice suggests these transients can be dynamically modulated by manipulating ectonucleotidase activity.

Discussion

Nucleotides cause pain by exciting and sensitizing nociceptive neurons. While the duration of nucleotide signaling can be limited by purinergic receptor desensitization and nucleotide hydrolysis, surprisingly, it is unknown how rapidly specific ectonucleotidases break down nucleotides in any region of the nervous system. The speed at which hydrolysis occurs could affect the balance between the excitatory effects of nucleotides and the inhibitory effects of adenosine. While it has been previously found that PAP and NT5E were co-expressed in nociceptive neurons and could hydrolyze AMP (Zylka et al., 2008, Sowa et al., 2010b), it was not shown that either enzyme could generate adenosine directly in nociceptive circuits or how fast these enzymes generate adenosine. Moreover, since studies

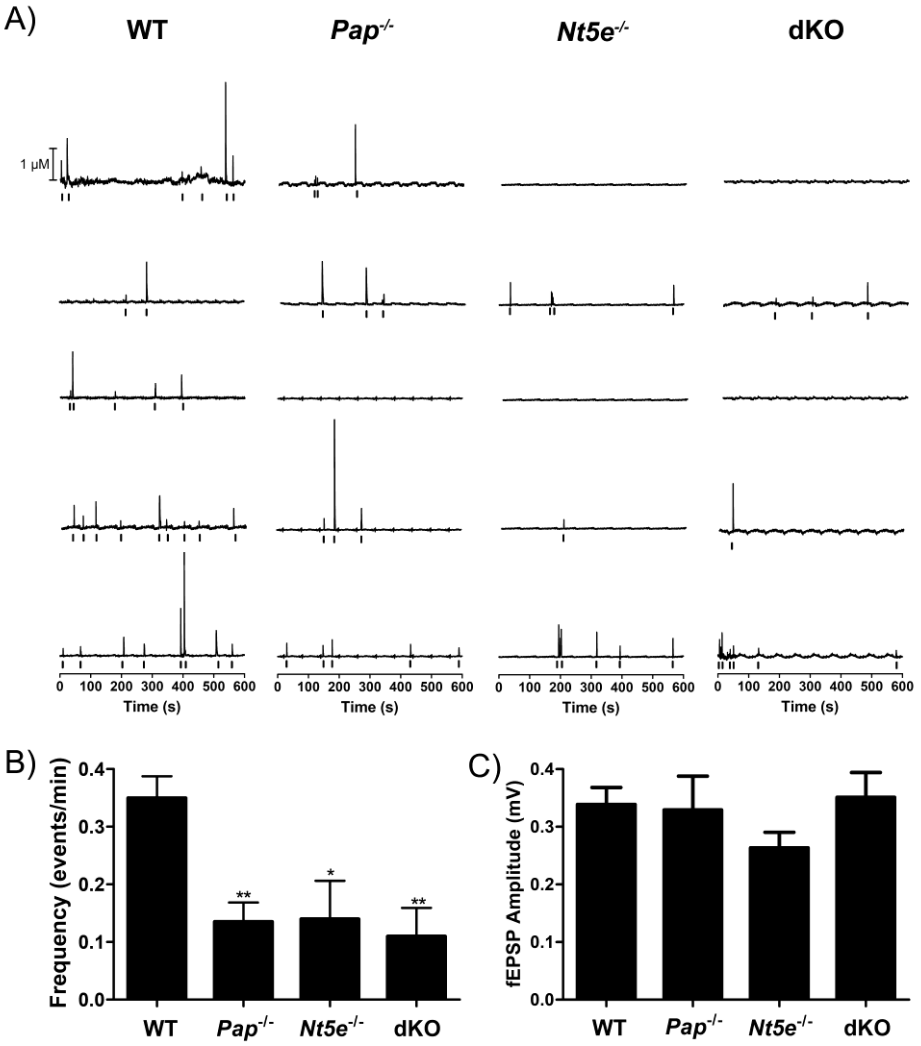

Figure 4.6. Spontaneous adenosine transients in lamina II are reduced in frequency in *Pap*$^{-/-}$, *Nt5e*$^{-/-}$ and dKO mice. (A) Representative traces from each genotype showing adenosine concentration versus time, calculated from FSCV currents measured at 1.5 V. Traces were background subtracted every 60 s and baseline corrected to compensate for electrode drift over time (which creates a visible 60 s oscillation in the baseline). Raster plots below each trace mark each adenosine transient. Adenosine transients were considered to be events if the peak at 1.0 V was more than five times the standard deviation of the noise. (B) Adenosine transient frequency in WT (0.35 ± 0.04 events/min; n=19 slices), *Pap*$^{-/-}$ (0.14 ± 0.04 events/min; n=10 slices), *Nt5e*$^{-/-}$ (0.14 ± 0.07 events/min; n=10 slices), and dKO (0.11 ± 0.05 events/min; n=16 slices) mice. One-way ANOVAs with Bonferroni's post-hoc tests were used to compare each genotype to WT and to compare between genotypes. *P < 0.05, **P < 0.005. (C) Baseline fEPSP amplitude in WT, *Pap*$^{-/-}$, *Nt5e*$^{-/-}$, and dKO mice (n=5 / genotype). There were no significant differences between WT and mutant mice. Data presented as means ± SEM.

were focused on *Pap* and *Nt5e* single knockout mice, it could not be predicted *a priori* if these enzymes had redundant or non-redundant functions.

To resolve these issues, we generated *Pap/Nt5e* dKO mice—the first double knockout of any pair of ectonucleotidases. Our analysis revealed that PAP and NT5E together generate the majority of all adenosine from AMP in nociceptive axon terminals. In addition, we were the first to use FSCV to study the speed at which ectonucleotidases generate adenosine and the first to use FSCV in the pain field. This technique is particularly powerful, because the small probe size allowed us to monitor adenosine production in the spinal microdomain where these enzymes are located. To our surprise, we found that PAP and NT5E very rapidly generate adenosine from pressure ejected AMP and from endogenously released nucleotides.

Our conclusions are supported by an array of sophisticated *in vitro* experiments. Indeed, we found that dKO animals had pronounced deficits in hydrolyzing AMP to adenosine, AMP → adenosine-dependent antinociception, and AMP → adenosine-dependent synaptic inhibition. While a pH preference for these enzymes was evident in former histochemical and FSCV experiments (Sowa et al., 2009, Sowa et al., 2010b), both enzymes contribute additively to nucleotide hydrolysis under physiologically relevant *in vivo* conditions. PAP and NT5E are likely to encounter wide extracellular pH fluctuations under normal physiological and pathological conditions. For example, excitatory synapses become transiently acidified following glutamate release (DeVries, 2001), synaptic vesicle pH can reach pH 5.6 (Miesenbock et al., 1998), and pathological conditions lead to prolonged acidification and nucleotide release (Birdsong et al., 2010).

This method is novel and brings new light to the field of adenosine production because it is currently unknown how rapidly ectonucleotidases generate adenosine in any tissue or cell of the body. This lack of knowledge reflects technical limitations in existing biochemical and biosensor based methods, all of which sample adenosine levels over

minutes to hours (Sweeney et al., 1989, Patterson et al., 2001, Swamy and Venton, 2007, Cechova and Venton, 2008, Goldman et al., 2010). And, enzyme histochemistry detects inorganic phosphate following AMP hydrolysis, not adenosine. As such, enzyme histochemistry is an indirect way to measure adenosine production. Since FSCV has a high temporal and spatial resolution, it is an excellent way to elucidate the speed at which these enzymes produce adenosine. This marks the first time FSCV was used to monitor adenosine generation by ectonucleotidases and the first time FSCV was used in the pain field.

Unexpectedly, our experiments also revealed that at least one more adenosine generating ectonucleotidase is present in nociceptive circuits. This finding could not have been predicted from studying *Pap* or *Nt5e* single knockouts, and suggests nociceptive circuits have a highly redundant molecular apparatus for eliminating nucleotides while simultaneously generating adenosine. We hypothesized that the other ectonucleotidase was tissue nonspecific alkaline phosphatase (TNALP), an enzyme which can hydrolyze AMP to adenosine which is found throughout the body (Narisawa et al., 2007). Using a novel, nonspecific alkaline phosphatase inhibitor, we were able to pharmacologically verify that the remaining adenosine generation signal which was observed in dKO mice was due to TNALP.

FSCV allowed us to measure rapid changes in adenosine concentration in a micron-sized region of spinal cord. The temporal and spatial resolution of this method far surpasses all previously used methods for measuring adenosine (including direct approaches like enzyme biosensors or microdialysis coupled with HPLC and indirect approaches like quantifying signaling downstream of adenosine receptors) (Sweeney et al., 1989, Li and Perl, 1994, Patterson et al., 2001, Swamy and Venton, 2007, Cechova and Venton, 2008, Goldman et al., 2010). Unexpectedly, we detected spontaneous adenosine transients in spinal lamina II, the termination zone for nociceptive afferents. This is the first time

adenosine transients were detected in any region of the nervous system. The duration of these events was remarkably short (lasting 1.5 ± 0.1 s on average in WT mice; Table 4.1), suggesting adenosine is rapidly generated/released within lamina II, precisely where PAP and NT5E are found (Zylka et al., 2008, Sowa et al., 2010b). Remarkably, transients were detected in all WT slices but only ~50% of all *Pap*$^{-/-}$, *Nt5e*$^{-/-}$ and dKO slices. And, within the subset of *Pap*$^{-/-}$, *Nt5e*$^{-/-}$ and dKO slices where transients were observed, the frequency of adenosine transients was reduced by more than half. These data strongly suggest that PAP and NT5E generate adenosine transients in lamina II by rapidly hydrolyzing endogenously released nucleotides. Rapid generation of adenosine is consistent with ectonucleotidases being in close proximity to nucleotide release sites (Joseph et al., 2003).

Nucleotides like ATP are released from several cell types by point-source burst release, which occurs spontaneously at a low frequency (0.38 ± 0.18 bursts/min in rat astrocytes) (Arcuino et al., 2002). Intriguingly, adenosine transients occur at a similar frequency (0.35 ± 0.04 events/min; Table 1), possibly reflecting the pulsatile availability of nucleotide substrate. Several distinct mechanisms of ATP release have been reported in neurons, glia and other cell types, including from vesicles (exocytosis), connexin 43 hemichannels, P2X7 ion channels and volume activated anion channels (VAACs) (Sabirov et al., 2001, Coco et al., 2003, Pascual et al., 2005, Suadicani et al., 2006, Pangrsic et al., 2007, Kang et al., 2008, Sawada et al., 2008, Fields and Ni, 2010). Many of these mechanisms are kinetically fast and Ca^{2+} dependent. Future studies will be needed to determine which cells release ATP and which molecular mechanisms underlie nucleotide release in nociceptive circuits.

Our data also suggests it might be possible to dynamically regulate adenosine transient frequency through physiological and genetic factors. Indeed, we found adenosine transients were reduced in frequency in WT slices under zero Ca^{2+} conditions and in dKO slices; however, transients did not disappear (Table 4.1). Similarly, capsaicin-evoked

adenosine release from synaptosomes (isolated from dorsal spinal cord) was reduced in Ca^{2+}-free conditions and when nonselective ectonucleotidase inhibitors were used [19]. Since adenosine transients were not eliminated in dKO mice, there must be additional mechanisms underlying their generation. These mechanisms could include: 1) hydrolysis of extracellular nucleotides by ectonucleotidase(s) other than PAP and NT5E and/or 2) direct release of adenosine from cells, such as by exocytosis or reverse transport through equilibrative nucleoside transporters (Sweeney et al., 1989, Wall and Dale, 2008).

Physiological Significance of Pulsatile Adenosine

Our physiological and behavioral data suggest that ectonucleotidases, and the adenosine transients they generate, endow nociceptive circuits with a way to transform pulsatile or sustained nucleotide release into an inhibitory adenosinergic signal. Notably, we found that transients were generated in all WT slices but only in ~50% of all *Pap*$^{-/-}$, *Nt5e*$^{-/-}$ and dKO slices, suggesting more "failures" when ectonucleotidases are eliminated. Moreover, the frequency of these events was significantly reduced in slices from all three mutant genotypes. The failure to generate transients, combined with reduced transient frequency likely explains why excitatory neurotransmission was not inhibited after treating dKO slices with DIP. These data suggest that PAP and NT5E generate adenosine endogenously at a level that is sufficient to activate A_1R and inhibit excitatory neurotransmission in lamina II. However, in the absence of these enzymes, less adenosine is tonically produced, causing unimpeded excitatory neurotransmission and enhanced nociceptive responses.

In addition, adenosine transients and the enzymes that generate these transients appear to be biochemically "tuned" to dynamically activate A_1R. In particular, transients have a peak adenosine concentration of 530 ± 60 nM as measured by FSCV (Table 4.1), and could be slightly higher given that analyte concentration is distance dependent with respect

to its point of release/production (Wightman et al., 1995). Extracellular adenosine concentration in hippocampus was similarly ~300-1500 nM (Dunwiddie and Diao, 2000). This concentration range is remarkably similar to the concentration range that half-maximally stimulates A_1R (760 nM-3.1 μM) (Gerwins et al., 1990, Ragazzi et al., 1991, Dunwiddie and Diao, 1994). Since the peak adenosine concentration of each transient falls within the most sensitive region of the A_1R dose-response curve, small increases or decreases in transient frequency, especially when integrated over time, could have profound effects on A_1R signaling. Lastly, ectonucleotidases can "channel" adenosine directly to A_1R (Cunha et al., 1998), which could further maximize the signaling effects of enzymatically produced adenosine.

Adenosine has a tonic inhibitory effect on excitatory neurotransmission in the spinal cord and brain (Keil and DeLander, 1996, Dunwiddie et al., 1997, Dunwiddie and Diao, 2000, Tian et al., 2010), although the molecular origins of this inhibitory tone are unknown. Since PAP and NT5E rapidly generate adenosine from nucleotides and deletion of PAP and NT5E reduced the frequency of adenosine transients, we next hypothesized that PAP and NT5E might generate the inhibitory adenosine tone in nociceptive circuits. Field excitatory post synaptic potentials (fEPSPs) were measured in lamina II of the spinal cord, and were inhibited when DIP was on board, indicating that a buildup of adenosine could be causing this inhibition. Furthermore, the dampening of the fEPSPs with DIP on board was significantly smaller in dKO mice (Street et al., 2011). Indeed, FSCV data shows that DIP significantly elevated extracellular adenosine levels for an extended time period when AMP was pressure ejected into lamina II (Figure 4.4), indicating DIP promotes the buildup of ectonucleotidase-generated adenosine outside cells.

Conclusion

Here, FSCV was used to directly determine the contributions of the enzymes PAP, NT5E, and alkaline phosphatase to the hydrolysis of AMP into adenosine in spinal nociceptive circuits. Furthermore, the first ever adenosine transients, spontaneously occurring fluctuations in adenosine concentration, were reported, and their production was determined to also be dependent on PAP and NT5E. These findings help to confirm that PAP, NT5E, and alkaline phosphatase are the main ectonucleotidases in lamina II of the spinal cord and directly hydrolyze AMP, and that alkaline phosphatases perform the remainder of the function, especially when PAP and NT5E are not present. Finally, adenosine transients are the first direct measure of adenosine being produced in the extracellular space in tissue, and could have implications in determining the origin of an adenosine tone and its contribution to antinociception.

References

Arcuino G, Lin JH, Takano T, Liu C, Jiang L, Gao Q, Kang J, Nedergaard M (2002) Intercellular calcium signaling mediated by point-source burst release of ATP. Proc Natl Acad Sci U S A 99:9840-9845.

Bath BD, Michael DJ, Trafton BJ, Joseph JD, Runnels PL, Wightman RM (2000) Subsecond adsorption and desorption of dopamine at carbon-fiber microelectrodes. Anal Chem 72:5994-6002.

Birdsong WT, Fierro L, Williams FG, Spelta V, Naves LA, Knowles M, Marsh-Haffner J, Adelman JP, Almers W, Elde RP, McCleskey EW (2010) Sensing muscle ischemia: coincident detection of acid and ATP via interplay of two ion channels. Neuron 68:739-749.

Cahill PS, Walker QD, Finnegan JM, Mickelson GE, Travis ER, Wightman RM (1996) Microelectrodes for the measurement of catecholamines in biological systems. Anal Chem 68:3180-3186.

Cechova S, Venton BJ (2008) Transient adenosine efflux in the rat caudate-putamen. J Neurochem 105:1253-1263.

Coco S, Calegari F, Pravettoni E, Pozzi D, Taverna E, Rosa P, Matteoli M, Verderio C (2003) Storage and release of ATP from astrocytes in culture. J Biol Chem 278:1354-1362.

Cunha RA, Sebastiao AM, Ribeiro JA (1998) Inhibition by ATP of hippocampal synaptic transmission requires localized extracellular catabolism by ecto-nucleotidases into adenosine and channeling to adenosine A1 receptors. J Neurosci 18:1987-1995.

DeVries SH (2001) Exocytosed protons feedback to suppress the Ca2+ current in mammalian cone photoreceptors. Neuron 32:1107-1117.

Dunwiddie TV, Diao L (1994) Extracellular adenosine concentrations in hippocampal brain slices and the tonic inhibitory modulation of evoked excitatory responses. J Pharmacol Exp Ther 268:537-545.

Dunwiddie TV, Diao L (2000) Regulation of extracellular adenosine in rat hippocampal slices is temperature dependent: role of adenosine transporters. Neuroscience 95:81-88.

Dunwiddie TV, Diao L, Proctor WR (1997) Adenine nucleotides undergo rapid, quantitative conversion to adenosine in the extracellular space in rat hippocampus. J Neurosci 17:7673-7682.

Dussor G, Koerber HR, Oaklander AL, Rice FL, Molliver DC (2009) Nucleotide signaling and cutaneous mechanisms of pain transduction. Brain Res Rev 60:24-35.

Fields RD, Ni Y (2010) Nonsynaptic communication through ATP release from volume-activated anion channels in axons. Sci Signal 3:ra73.

Gerwins P, Nordstedt C, Fredholm BB (1990) Characterization of adenosine A1 receptors in intact DDT1 MF-2 smooth muscle cells. Mol Pharmacol 38:660-666.

Goldman N, Chen M, Fujita T, Xu Q, Peng W, Liu W, Jensen TK, Pei Y, Wang F, Han X, Chen JF, Schnermann J, Takano T, Bekar L, Tieu K, Nedergaard M (2010) Adenosine A1 receptors mediate local anti-nociceptive effects of acupuncture. Nat Neurosci 13:883-888.

Gourine AV, Kasymov V, Marina N, Tang F, Figueiredo MF, Lane S, Teschemacher AG, Spyer KM, Deisseroth K, Kasparov S (2010) Astrocytes control breathing through pH-dependent release of ATP. Science 329:571-575.

Jones SR, Garris PA, Kilts CD, Wightman RM (1995) Comparison of dopamine uptake in the basolateral amygdaloid nucleus, caudate-putamen, and nucleus accumbens of the rat. J Neurochem 64:2581-2589.

Joseph SM, Buchakjian MR, Dubyak GR (2003) Colocalization of ATP release sites and ecto-ATPase activity at the extracellular surface of human astrocytes. J Biol Chem 278:23331-23342.

Kang J, Kang N, Lovatt D, Torres A, Zhao Z, Lin J, Nedergaard M (2008) Connexin 43 hemichannels are permeable to ATP. J Neurosci 28:4702-4711.

Keil GJ, 2nd, DeLander GE (1996) Altered sensory behaviors in mice following manipulation of endogenous spinal adenosine neurotransmission. Eur J Pharmacol 312:7-14.

Li J, Perl ER (1994) Adenosine inhibition of synaptic transmission in the substantia gelatinosa. J Neurophysiol 72:1611-1621.

MacGregor GR, Zambrowicz BP, Soriano P (1995) Tissue non-specific alkaline phosphatase is expressed in both embryonic and extraembryonic lineages during

mouse embryogenesis but is not required for migration of primordial germ cells. Development 121:1487-1496.

Marsden CA, Joseph MH, Kruk ZL, Maidment NT, O'Neill RD, Schenk JO, Stamford JA (1988) In vivo voltammetry--present electrodes and methods. Neuroscience 25:389-400.

Matsuka Y, Ono T, Iwase H, Mitrirattanakul S, Omoto KS, Cho T, Lam YY, Snyder B, Spigelman I (2008) Altered ATP release and metabolism in dorsal root ganglia of neuropathic rats. Mol Pain 4:66.

Miesenbock G, De Angelis DA, Rothman JE (1998) Visualizing secretion and synaptic transmission with pH-sensitive green fluorescent proteins. Nature 394:192-195.

Nakamura F, Strittmatter SM (1996) P2Y1 purinergic receptors in sensory neurons: contribution to touch-induced impulse generation. Proc Natl Acad Sci U S A 93:10465-10470.

Narisawa S, Harmey D, Yadav MC, O'Neill WC, Hoylaerts MF, Millan JL (2007) Novel inhibitors of alkaline phosphatase suppress vascular smooth muscle cell calcification. J Bone Miner Res 22:1700-1710.

Pangrsic T, Potokar M, Stenovec M, Kreft M, Fabbretti E, Nistri A, Pryazhnikov E, Khiroug L, Giniatullin R, Zorec R (2007) Exocytotic release of ATP from cultured astrocytes. J Biol Chem 282:28749-28758.

Pascual O, Casper KB, Kubera C, Zhang J, Revilla-Sanchez R, Sul JY, Takano H, Moss SJ, McCarthy K, Haydon PG (2005) Astrocytic purinergic signaling coordinates synaptic networks. Science 310:113-116.

Patterson SL, Sluka KA, Arnold MA (2001) A novel transverse push-pull microprobe: in vitro characterization and in vivo demonstration of the enzymatic production of adenosine in the spinal cord dorsal horn. J Neurochem 76:234-246.

Phillips PEM, Wightman RM (2003) Critical guidelines for validation of the selectivity of in-vivo chemical microsensors. TrAC 22:509-514.

Ragazzi E, Wu SN, Shryock J, Belardinelli L (1991) Electrophysiological and receptor binding studies to assess activation of the cardiac adenosine receptor by adenine nucleotides. Circ Res 68:1035-1044.

Sabirov RZ, Dutta AK, Okada Y (2001) Volume-dependent ATP-conductive large-conductance anion channel as a pathway for swelling-induced ATP release. J Gen Physiol 118:251-266.

Sawada K, Echigo N, Juge N, Miyaji T, Otsuka M, Omote H, Yamamoto A, Moriyama Y (2008) Identification of a vesicular nucleotide transporter. Proc Natl Acad Sci U S A 105:5683-5686.

Sawynok J, Liu XJ (2003) Adenosine in the spinal cord and periphery: release and regulation of pain. Prog Neurobiol 69:313-340.

Sergienko E, Su Y, Chan X, Brown B, Hurder A, Narisawa S, Millan JL (2009) Identification and characterization of novel tissue-nonspecific alkaline phosphatase inhibitors with diverse modes of action. J Biomol Screen 14:824-837.

Sowa NA, Street SE, Vihko P, Zylka MJ (2010a) Prostatic acid phosphatase reduces thermal sensitivity and chronic pain sensitization by depleting phosphatidylinositol 4,5-bisphosphate. J Neurosci 30:10282-10293.

Sowa NA, Taylor-Blake B, Zylka MJ (2010b) Ecto-5'-nucleotidase (CD73) inhibits nociception by hydrolyzing AMP to adenosine in nociceptive circuits. J Neurosci 30:2235-2244.

Sowa NA, Vadakkan KI, Zylka MJ (2009) Recombinant mouse PAP has pH-dependent ectonucleotidase activity and acts through A(1)-adenosine receptors to mediate antinociception. PLoS One 4:e4248.

Sowa NA, Voss MK, Zylka MJ (2010c) Recombinant ecto-5'-nucleotidase (CD73) has long lasting antinociceptive effects that are dependent on adenosine A1 receptor activation. Mol Pain 6:20.

St Hilaire C, Ziegler SG, Markello TC, Brusco A, Groden C, Gill F, Carlson-Donohoe H, Lederman RJ, Chen MY, Yang D, Siegenthaler MP, Arduino C, Mancini C, Freudenthal B, Stanescu HC, Zdebik AA, Chaganti RK, Nussbaum RL, Kleta R, Gahl WA, Boehm M (2011) NT5E mutations and arterial calcifications. N Engl J Med 364:432-442.

Street SE, Walsh PL, Sowa NA, Taylor-Blake B, Guillot TS, Vihko P, Wightman RM, Zylka MJ (2011) PAP and NT5E inhibit nociceptive neurotransmission by rapidly hydrolyzing nucleotides to adenosine. Mol Pain 7:80.

Suadicani SO, Brosnan CF, Scemes E (2006) P2X7 receptors mediate ATP release and amplification of astrocytic intercellular Ca2+ signaling. J Neurosci 26:1378-1385.

Swamy BE, Venton BJ (2007) Subsecond detection of physiological adenosine concentrations using fast-scan cyclic voltammetry. Anal Chem 79:744-750.

Sweeney MI, White TD, Sawynok J (1989) Morphine, capsaicin and K+ release purines from capsaicin-sensitive primary afferent nerve terminals in the spinal cord. J Pharmacol Exp Ther 248:447-454.

Thompson LF, Eltzschig HK, Ibla JC, Van De Wiele CJ, Resta R, Morote-Garcia JC, Colgan SP (2004) Crucial role for ecto-5'-nucleotidase (CD73) in vascular leakage during hypoxia. J Exp Med 200:1395-1405.

Thorn JA, Jarvis SM (1996) Adenosine transporters. Gen Pharmacol 27:613-620.

Tian L, Ji G, Wang C, Bai X, Lu Y, Xiong L (2010) Excitatory synaptic transmission in the spinal substantia gelatinosa is under an inhibitory tone of endogenous adenosine. Neurosci Lett 477:28-32.

Wall M, Dale N (2008) Activity-dependent release of adenosine: a critical re-evaluation of mechanism. Curr Neuropharmacol 6:329-337.

Wang H, Zylka MJ (2009) Mrgprd-Expressing Polymodal Nociceptive Neurons Innervate Most Known Classes of Substantia Gelatinosa Neurons. J Neurosci 29:13202-13209.

Wightman RM, Schroeder TJ, Finnegan JM, Ciolkowski EL, Pihel K (1995) Time course of release of catecholamines from individual vesicles during exocytosis at adrenal medullary cells. Biophys J 68:383-390.

Wu WP, Hao JX, Halldner L, Lovdahl C, DeLander GE, Wiesenfeld-Hallin Z, Fredholm BB, Xu XJ (2005) Increased nociceptive response in mice lacking the adenosine A1 receptor. Pain 113:395-404.

Zimmermann H (2008) Ectonucleotidases in the Nervous System. In: Purinergic Signalling in Neuron–Glia Interactions, pp 113-130: John Wiley & Sons, Ltd.

Zylka MJ (2011) Pain-relieving prospects for adenosine receptors and ectonucleotidases. Trends Mol Med 17:188-196.

Zylka MJ, Sowa NA (2011) NT5E mutations and arterial calcifications. N Engl J Med 364:1579; author reply 1579-1580.

Zylka MJ, Sowa NA, Taylor-Blake B, Twomey MA, Herrala A, Voikar V, Vihko P (2008) Prostatic acid phosphatase is an ectonucleotidase and suppresses pain by generating adenosine. Neuron 60:111-122.

Chapter V

High Performance Liquid Chromatography for Quantifying Total Tissue Neurotransmitter Content

Introduction

Over the last century, chromatography has become an integral part of analytical chemistry and a useful method for separating complex mixtures (Hadden, 1971). In this chapter, the use of reversed phase high performance liquid chromatography (RP-HPLC) to analyze total tissue content of brain samples for neurotransmitters and their metabolites will be discussed.

Liquid chromatography separates mixtures based upon their polarity. In RP-HPLC, the stationary phase is non-polar while the mobile phase can vary in polarity depending on the analytes being separated. The stationary phase is typically bonded to a solid support, often small (~5 μm diameter) silica particles or gels for other applications. For most separations, the stationary phase consists of long chain alkanes (typically C_5-C_{30}), although various different types of substitutions can be made for different types (ion separation and size exclusion, for example). The time it takes for an analyte to elute from a column is called its retention time (t_R), a compound specific property which is dependent upon the make-up of the mobile phase. Polar compounds elute faster since they spend more time in the mobile phase, while non-polar compounds elute later because they interact more with the stationary phase. For this reason, RP-HPLC is best utilized for separating non-polar compounds because the analytes will spend more time in the stationary phase.

The t_R of analytes which elute later can be reduced by adding an organic modifier to the mobile phase. Examples of organic modifiers include methanol, acetonitrile, and isopropyl alcohol. The concentration of organic modifier is of great importance when considering a separation of similar compounds. As the concentration of these organic modifiers increases in the mobile phase, more highly retained species will elute faster, spending more time with the non-polar portion of the mobile phase. Biological separations depend on the ability of the use of aqueous mobile phases since the biogenic amines as well as the metabolites of interest are often water soluble. Water based separations are also useful because they can be coupled to other separation methods such as capillary electrophoresis for 2-D separations, as well as sensitive detection methods such as electrospray ionization for tandem mass spectrometry (Zhang et al., 2008, Zhao and Suo, 2008). Typically, small amounts of an organic modifier are used in mobile phases for separations (5-20%). Organic modifiers can be added to the mobile phase at a constant amount (isocratic elution), or starting at a small amount, and gradually increased over time (gradient elution). Isocratic elution suffers from poor resolution for less retained species, and cause band broadening for more highly retained species. Gradient elution is a useful tool for decreasing the t_R of highly retained species, which decreases band broadening of highly retained species, and increasing the resolution of less retained analytes.

Electrochemical detection (ECD) can be used to monitor the current which arises from species which are eluting from a column and are oxidized or reduced at the electrode surface. ECD is a good choice for analyzing brain tissue punches because it is an extremely selective method, and thus insensitive to the brain matrix (Ramstrom et al., 2009). While there are many compounds in the brain which absorb light in the UV-Vis region, or produce complex mass spectra, there are only a select few which are oxidizable at potentials allowed by the solvent window for water making the chromatogram simpler, and easier to interpret. One disadvantage of ECD is that gradient elutions cannot be used since

the increase in organic modifier with time changes the charging of the electrode's double-layer, causing the baseline to shift. The simplicity of the chromatograms associated with ECD makes it a desirable choice for analyzing biogenic amines in response to pharmacological, genetic, or environmental changes (Lahdesmaki et al., 2002, Vriend and Dreger, 2006, Filipov et al., 2007).

In this chapter, RP-HPLC with ECD is used to study the total content of biogenic amines as well as their metabolites in tissue samples. Various different strains of animals, as well as genetically altered animals are studied herein, and the comparisons made between the different groups allows for insight into the different biological mechanisms which can be related to data observed with fast-scan cyclic voltammetry (FSCV) as well as in behavioral experiments. Specifically, norepinephrine (NE) and dopamine (DA) content were analyzed in the bed nucleus of the stria terminalis (BNST), nucleus accumbens (NAc) and dorsolateral striatum of an animal used as a model for post-traumatic stress disorder (PTSD), Lewis rats, were compared to the more commonly used Sprague Dawley laboratory rat. Also, DA as well as the DA metabolite 3,4-Dihydroxyphenylacetic acid (DOPAC), were analyzed in the NAc and dorsolateral striatum of mice lacking the maternal copy of the *Ube3a* gene (*Ube3a*$^{m-/p+}$) and compared to WT animals as a model for Angelman Syndrome. Finally, 5-hydroxytryptamine (5-HT, serotonin) content was determined in the substantia nigra reticulata (SNr) in WT animals before and after acute treatment with citalopram, a serotonin transporter (SERT) blocker.

Experimental

HPLC Instrumentation, Materials, and Chemicals

An Agilent HP 1050 pump (Santa Clara, CA) was used for mixing all mobile phases and flowing the mobile phase through the system, and a Waters Atlantis C-18 column was used for all separations (5 µm, 4.6 x 250 mm, Milford, MA). A modified version of the

methods first described by Mefford was used to analyze standard and tissue samples (Mefford, 1981). The mobile phase consisted of a citric acid buffer containing (in mM) 100 citric acid, 1.0 sodium hexyl sulfate, 0.1 EDTA, and was adjusted to pH=3 with NaOH. Buffers were filtered with a 0.2 µm vacuum filter and were prepared with HPLC grade water. HPLC grade methanol at a concentration of 5-10% served as the organic modifier. 10-20 µL injections of analytes were detected with a thin-layer radial electrochemical flow cell (Bioanalytical Systems, West Lafayette, IN) with the working electrode being held at + 700 or + 800 mV relative to a Ag/AgCl reference electrode. Hydroquinone (HQ) was utilized as the internal standard. Analyte stock solutions were made to be 1-10 mM in 0.1 N $HClO_4$, and standard mixture solutions were made 1-10 µM by diluting stock solutions in 0.1 N $HClO_4$. Response ratios of catecholamines and their metabolites were determined daily.

Tissue Sample Collection for Sprague Dawley and Lewis Rats

Rats (Jackson Laboratories, Bar Harbor, ME, USA) were anesthetized with urethane (1.5 mg/kg), decapitated, and the brain was rapidly removed and placed into ice cold aCSF containing (in mM) 126 NaCl, 2.45 KCl, 25 $NaHCO_3$, 1.2 $MgCl_2$, 2.4 $CaCl_2$, 1.2 NaH_2PO_4, 20 HEPES, and 11 glucose saturated with 95% O_2 / 5% CO_2. The brain was then mounted, sliced into 300-500 µm thick sections, patted dry, and frozen over dry ice before excising the region of interest. The tissue was then massed and 200-300 µL of 0.1 N $HClO_4$ containing 1 µM HQ was added to the tissue. The mixture was then homogenized with a wand sonicator (Fisher Scientific, Pittsburgh, PA), and centrifuged at 6000 rpm for 10 min. The supernatant was removed, and filtered with a 0.2 µm syringe filter (Millex-LG, Millipore, Billerica, MA) before being injected onto the column.

Tissue Sample Collection for Ube3a$^{m-/p+}$ Mice

Mice were deeply anesthetized with sodium pentobarbital and brains were snap frozen in methylbutane on dry ice. Brains were serially sectioned on a cryostat, until reaching the rostral pole of the (NAc). Tissue punches (pooled from both hemispheres) were taken from the NAc and dorsolateral striatum (17 and 15 gauge, respectively) and massed. Punches were stored at -80°C until use. The tissue was then mixed with 200 µL of 0.1 N HClO4 containing 1 µM HQ. The mixture was then homogenized with a wand sonicator (Fisher Scientific, Pittsburgh, PA), and centrifuged at 6000 rpm for 10 min. The supernatant was removed, and filtered with a 0.2 µm syringe filter (Millex-LG, Millipore, Billerica, MA) before being injected onto the column.

Tissue Sample Collection for Mice Before and After Citalopram Administration

Wild-type C57-BL/6J mice (Jackson Laboratories, Bar Harbor, ME, USA) were taken as naïve, or administered with citalopram (DOSAGE HERE). Mice were then anesthetized with ether, decapitated, and the brain was rapidly removed and placed into ice cold aCSF containing (in mM) 126 NaCl, 2.45 KCl, 25 $NaHCO_3$, 1.2 $MgCl_2$, 2.4 $CaCl_2$, 1.2 NaH_2PO_4, 20 HEPES, and 11 glucose saturated with 95% O_2 / 5% CO_2. The brain was then mounted, sliced into 300-500 µm thick sections, patted dry, and frozen over dry ice before excising the region of interest. The tissue was then massed and 200-300 µL of 0.1 N $HClO_4$ containing 1 µM HQ was added to the tissue. The mixture was then homogenized with a wand sonicator (Fisher Scientific, Pittsburgh, PA), and centrifuged at 6000 rpm for 10 min. The supernatant was removed, and filtered with a 0.2 µm syringe filter (Millex-LG, Millipore, Billerica, MA) before being injected onto the column.

Chromatographic Data Analysis

The determination of peak areas for HPLC total tissue content analysis was performed using custom-written Igor programs. These programs were designed in the Jorgenson Lab at UNC-CH. The peak area of the analyte was taken as a ratio to that of an internal standard, hydroquinone (HQ) at a known concentration, adjusted for differential detector response. The ratio was then used to calculate a mass or number of moles of analyte in the extraction solution which was normalized by the mass of tissue taken (represented as μg neurotransmitter/ g tissue or nmoles neurotransmitter/ g tissue). Again, n indicates the number of animals used; however, replicate extractions and injections were performed to reduce random error in the chromatographic measurements.

Statistical Analysis

Statistical analysis was performed in GraphPad Prism (GraphPad Software, Inc., San Diego, CA, USA). Student's t-tests were used to test for significant differences between data sets. Data were considered significant at the 95 % confidence level and are reported as the mean ± SEM. The number of slices is indicated by n, unless noted otherwise.

Results

Separation of the analytes of interest were performed on a reversed phase C-18 column using a citric acid buffer, an ion pairing agent, sodium hexylsulfate, and methanol as the organic modifier (5%). Figure 5.1 shows a representative chromatogram for the separation of 10 μM standard solution containing norepinephrine, hydroquinone (the internal standard), dopamine, DOPAC, and 5-HT using electrochemical detection. Note the long time that it takes for DOPAC and 5-HT to elute from the column. In studies where norepinephrine, an analyte which elutes from the column very quickly, are not present the amount of organic modifier can be increased in order to allow DOPAC and 5-HT to elute

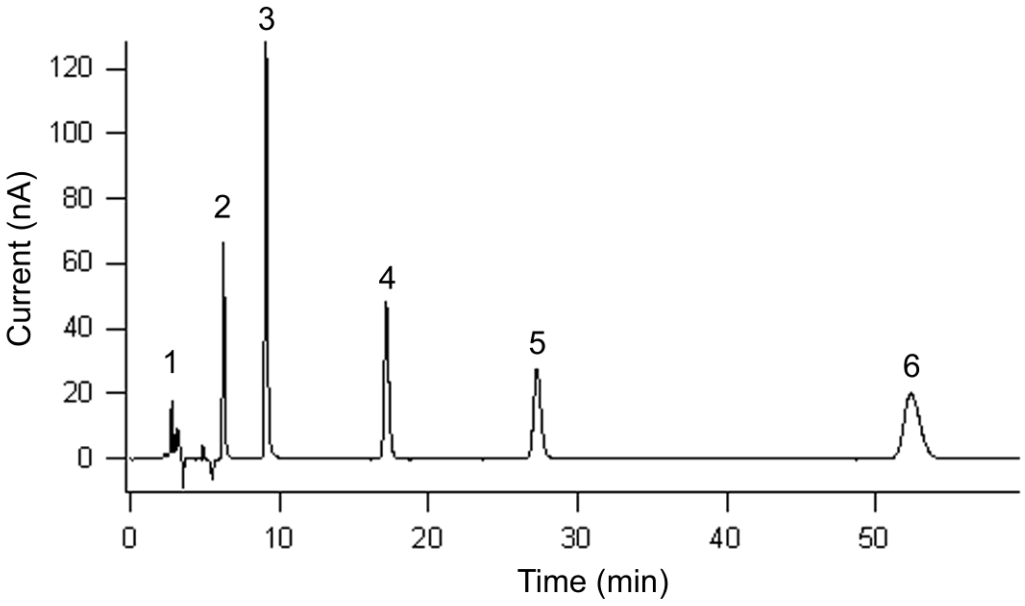

Figure 5.1. Chromatogram of a standard mixture of analytes. A mixture of the analytes of interest (5 µM each) was separated on an Atlantis C18 column (Waters) with a citric acid (100 mM) buffer, pH = 3 as the mobile phase. Sodium hexylsulfate (1 mM) was used as an ion pairing agent, and EDTA (0.1 mM) was added to the mobile phase. Methanol (5%) was used as the organic modifier. ECD was performed at a carbon electrode held at 700 mV vs. Ag/AgCl. Peak identification: 1 – solvent front, 2 – NE, 3 – HQ, 4 – DA, 5 – DOPAC, 6 – 5-HT.

more quickly, decreasing longitudinal diffusion and sharpening the observed peak. A chromatogram such as this can be used to determine the elution order of the analytes of interest, the retention time of each analyte for identification during analysis of brain samples, and for determining the response ratio of the electrochemical detector between the analytes and the internal standard. Response ratios were determined during each experiment before analysis of brain tissue samples.

Tissue samples were collected from rodents in various regions of interest. Figure 5.2 shows coronal brain slices from The Allen Institute for Brain Science Mouse Brain Atlas indicating the areas from which samples were taken. The nucleus accumbens (Figure 5.2A), dorsolateral straitum (Figure 5.2B), BNST (Figure 5.2C), and SNr (Figure 5.2D) were the regions of interest during different studies. While Figure 5.2 shows the anatomy for the mouse brain, the rat has similar anatomical landmarks and tissue punches were taken from similar areas in the Sprague Dawley and Lewis rats. Locations were chosen based on the optimal coordinates that were used during fast-scan cyclic voltammetry experiments for the study of the release of the neurotransmitters of interest.

Upon homogenization of the tissue, and extraction of neurotransmitters and metabolites into the perchloric acid solution, the samples were analyzed using the same method as for the standard solutions. Due to the high selectivity of electrochemical detection, very few peaks are observed on the chromatograms, and are often confined to just the internal standard and the analytes of interest. This makes identification of the analytes based on retention time alone possible. Figure 5.3 shows representative chromatograms from the dorsolateral striatum from a *Ube3a*$^{m+/p+}$ mouse showing the peaks for dopamine and DOPAC (Figure 5.3A), from the BNST of a Sprague Dawley rat showing the peaks for NE and dopamine (Figure 5.3B), and from the SNr of a WT mouse before citalopram administration showing the peaks for dopamine and 5-HT (Figure 5.3C). Note

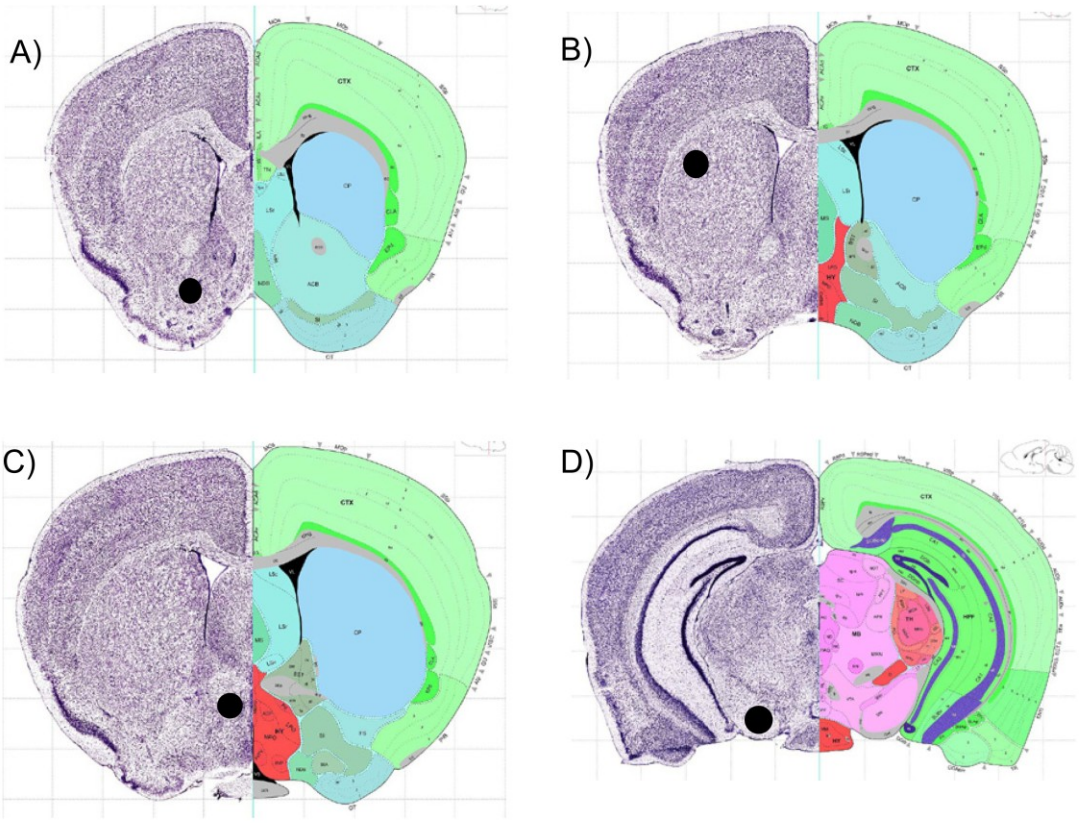

Figure 5.2. Location of punches taken in various brain regions in the mouse brain. Black circles denote the regions from which punches were taken from the (A) nucleus accumbens (AP +1.1 mm from bregma), (B) dorsolateral striatum (AP +0.5 mm from bregma), (C) bed nucleus of the stria terminalis (AP +0.25 from bregma), and (D) substantia nigra reticulate (AP -3.0 mm from bregma). Images are modified from The Allen Institute for Brain Science Mouse Brain Atlas (Science, 2009).

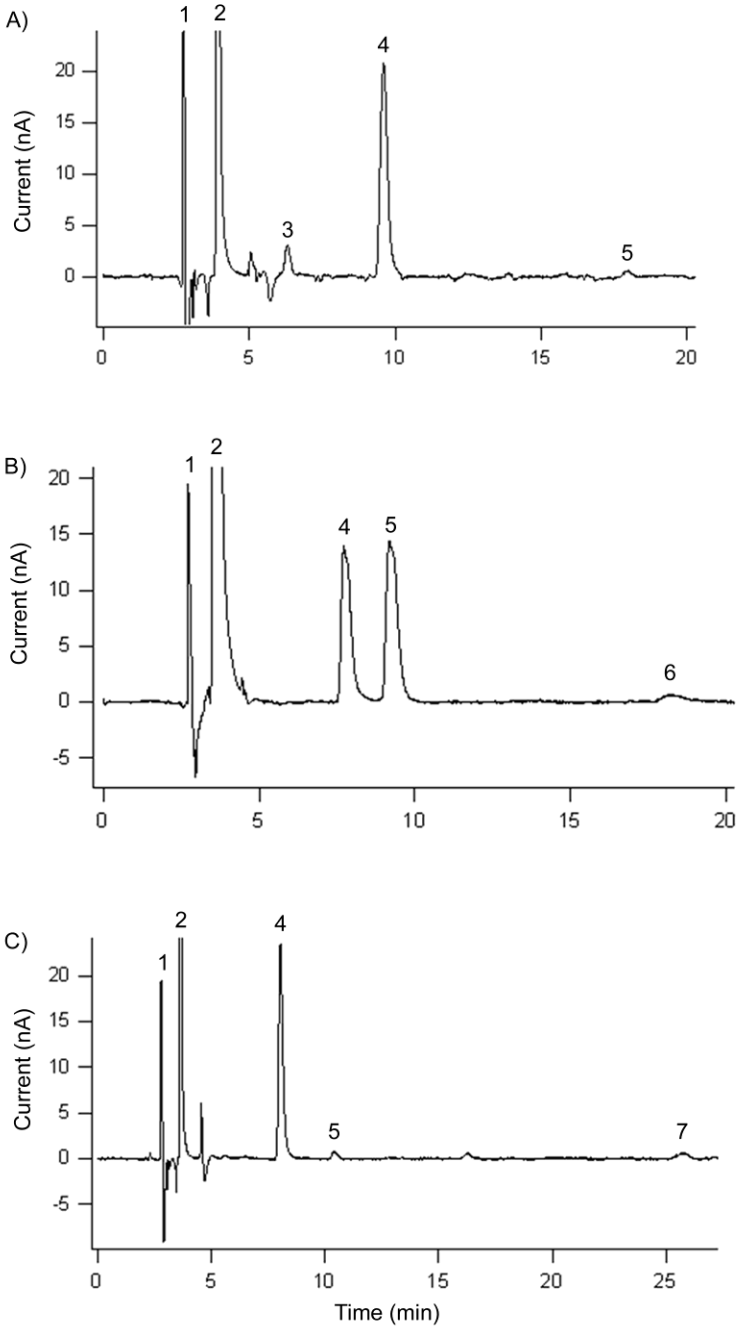

Figure 5.3. Representative chromatograms from tissue samples. Extractions from tissue samples were separated on an Atlantis C18 column (Waters) with a citric acid (100 mM) buffer, pH = 3 as the mobile phase. Sodium hexylsulfate (1 mM) was used as an ion pairing agent, and EDTA (0.1 mM) was added to the mobile phase. (A) BNST sample (1.1 mg) from a Lewis rat with methanol (5%) as the organic modifier. (B) Dorsolateral striatum sample (7.4 mg) from a WT mouse with methanol (10 %) as the organic modifier. (C) SNr sample (1.6 mg) from a WT mouse with methanol (12%) as the organic modifier. ECD was performed at a carbon electrode held at 700 mV vs. Ag/AgCl. Peak identification: 1 – solvent front, 2 – AA, 3 – NE, 4 – HQ, 5 – DA, 6 – DOPAC, 7 – 5-HT.

that the relative sizes of peaks between the chromatograms will differ greatly depending on the mass of the tissue being used, as well as the tissue preparation procedure used before slicing and excising of the tissue of interest.

Tissue Content of Catecholamines in Sprague Dawley and Lewis Rats

Using the above stated methods, total tissue content of dopamine in the dorsolateral striatum and NAc, and total tissue content of dopamine and NE in the BNST was performed on two strains of rats, Sprague Dawley, and Lewis rats. Table 5.1 summarizes the findings. The total content of dopamine was determined to be significantly higher in the dorsolateral striatum of Lewis rats compared to Sprague Dawley rats (3.87 ± 0.30 and 5.20 ± 0.18 µg/g respectively, $n = 5$ for each strain, $p < 0.01$, student's t-test). In the NAc, however, the difference between the dopamine content of the two strains fell short of significance (5.25 ± 0.96 µg/g for Sprague Dawley rats and 6.06 ± 0.32 µg/g for Lewis rats, $n = 5$ for each strain, $p = 0.45$, student's t-test). This is because of the high variability in the dopamine content in the Sprague Dawley animals. In the BNST, both the norepinephrine and the dopamine total content were significantly higher when comparing the two strains. The norepinephrine content was determined to be 4.55 ± 0.84 µg/g in Sprague Dawley rats and 10.86 ± 1.52 µg/g in Lewis rats ($n = 5$ for each strain, $p < 0.01$, student's t-test). The dopamine content was determined to be 1.06 ± 0.32 µg/g in Sprague Dawley rats and 3.15 ± 0.46 µg/g in Lewis rats ($n = 5$ for each strain, $p < 0.01$, student's t-test). These data show the significant difference that changing the kind of animal being used has on neurotransmitter content in areas with high amounts of catecholaminergic innervation.

Tissue Content of Catecholamines in Ube3a$^{m-/p+}$ Mice

Total dopamine and DOPAC content were determined for wild-type (WT) and *Ube3a*$^{m-/p+}$ mice. These regions were selected due to differences which were observed in

Table 5.1. Total neurotransmitter tissue content of Sprague Dawley and Lewis rats. T-tests were performed to compare the neurotransmitter content between different strains of rats in each brain region. Data are presented as mean ± SEM (μg/g). n = 5 for all values, **p < 0.01.

Region (Neurotransmitter)	Sprague Dawley	Lewis
dl striatum (DA)	3.87 ± 0.30	5.20 ± 0.18**
NAc (DA)	5.25 ± 0.96	6.06 ± 0.32
BNST (NE)	4.55 ± 0.84	10.86 ± 1.52**
BNST (DA)	1.06 ± 0.32	3.15 ± 0.46**

behavioral experiments performed in the lab of Ben Philpot in the Department of Cell and Molecular Physiology at the University of North Carolina at Chapel Hill which showed decreased cocaine motor activity (indicating a decrease in dopamine release in the dorsolateral striatum) as well as a decreased reward threshold upon electrical stimulation (indicating a decrease in dopamine release in the NAc). Furthermore, FSCV data collected by Elyse Dankoski in these regions showed a decrease in dopamine release upon high frequency electrical stimulation in both of these regions (data not shown). DOPAC content as well as the ratio of DOPAC: DA was determined to see if the ubiquitin produced by the *Ube3a* gene played a role in the breakdown of the dopamine metabolite. Table 5.2 summarizes the data collected for the animals in both brain regions. The data are represented as nmol/g in these studies so that the DOPAC: DA ratio could be determined.

T-tests of the data showed that the dopamine content was the same between the WT and *Ube3a*$^{m-/p+}$ mice in the dorsolateral striatum (46.93 ± 5.60 and 40.96 ± 4.63 nmol/g, respectively). The same was true for the DOPAC content (3.37 ± 0.93 and 3.15 ± 0.64 nmol/g, respectively), and the DOPAC:DA ratio (0.07 ± 0.02 and 0.07 ± 0.01, respectively). Similar data were observed in the NAc of the WT and *Ube3a*$^{m-/p+}$ mice for dopamine (23.72 ± 2.49 and 25.13 ± 2.52 nmol/g, respectively), DOPAC (1.98 ± 0.51 and 2.46 ± 0.55, respectively), and the DOPAC: DA ratio (0.09 ± 0.03 and 0.10 ± 0.02, respectively). These data indicate that although differences in the behavioral and FSCV data exist, there is no differences in the total amount of dopamine synthesized or stored in the cells, and that the breakdown of the DOPAC metabolite is not affected by the deletion of the maternal copy of the *Ube3a* gene ($p > 0.05$ for all brain regions and analytes, $n = 5$ or 6, student's t-test).

Tissue Content of 5-HT in WT Mice during Citalopram Administration

WT mice were used to determine the total tissue content of 5-HT in the SNr in naïve animals as well as animals which were treated with an acute administration (30 minutes

Table 5.2. Total dopamine and DOPAC content of WT and *Ube3a*$^{m-/p+}$ mice. T-tests were performed to compare genotypes for each analyte in each brain region. Data are represented as mean ± SEM (nmol/g).

Region (Neurotransmitter)	WT	*Ube3a*$^{m-/p+}$
dl stiatum (DA)	46.93 ± 5.60 (n = 5)	40.96 ± 4.63 (n = 6)
dl striatum (DOPAC)	3.37 ± 0.93 (n = 5)	3.15 ± 0.64 (n = 6)
dl striatum (DOPAC:DA)	0.07 ± 0.02 (n = 5)	0.07 ± 0.01) (n = 6)
NAc (DA)	23.72 ± 2.49 (n = 5)	25.13 ± 2.52 (n = 5)
NAc (DOPAC)	1.98 ± 0.51 (n = 5)	2.46 ± 0.55 (n = 5)
NAc (DOPAC:DA)	0.09 ± 0.03 (n = 5)	0.10 ± 0.02 (n = 5)

before sacrifice) of citalopram (5 mg/kg), a SERT blocker. Furthermore, animals which were chronically injected with either vehicle or citalopram (5 mg/kg) for 14 days were also analyzed for total 5-HT content in the SNr. Upon normalization of the data for the tissue mass, the 5-HT content for the naïve animals was determined to be 2.04 ± 0.29 μg/g, while the 5-HT content was found to be 2.21 ± 0.40 μg/g for animals acutely treated with citalopram. Animals which were chronically administered with vehicle has 5-HT content of 2.04 ± 0.28 μg/g while chronic administration of citalopram led to tissue content of 2.55 ± 0.21 μg/g 5-HT. Performing a one-way ANOVA of the data to compare the groups using a Newman-Keuls post-hoc test to compare individual group, no significant difference was observed between the groups (Table 5.3, $p > 0.05$ for all, $n = 5$ or 6 for each, one-way ANOVA). These data indicate that acute administration of citalopram has no significant effect on the synthesis or storage of 5-HT in the SNR.

Discussion

HPLC-ECD is a simple, inexpensive, and useful tool for the determination of total tissue content of various neurotransmitters in many different brain regions. Interpretation of the data is simple when electrochemical detection is used, because the chromatograms only contain peaks for analytes which can be oxidized at or below the potential applied to the working electrode in the amperometric detector while interfering species such as proteins go undetected. Coupling this detection scheme with an internal standard and normalization with the mass of the tissue used allows for comparisons between genetically different animals, as well as animals before and after administration of a drug which changes the release or uptake properties of neurotransmitters of interest. The data contained in this chapter show how a method which has been in use since the 1980s can still be used today to answer interesting questions about the synthesis and storage of neurotransmitters in the brain today (Mefford, 1981).

Table 5.3. 5-HT content in the SNr before and after treatment with SERT inhibitor citalopram. One-way ANOVA with Newman-Keuls post-hoc test was performed to compare groups ($p > 0.05$ for all comparisons). Data are represented as mean ± SEM (µg/g).

Treatment	5-HT Content in SNr (µg/g)
Naïve	2.04 ± 0.29 (n = 5)
Acute Citalopram	2.21 ± 0.18 (n = 5)
Chronic Vehicle	2.04 ± 0.28 (n = 6)
Chronic Citalopram	2.55 ± 0.21 (n = 6)

Tissue Content of Catecholamines in Sprague Dawley and Lewis Rats

Drug abuse remains a complex public health issue for which there is no real cure and many different physiological mechanisms which play a key role. Furthermore, relapse is a common problem among addicts, and stress disorders are often found to be a recurring problem with patients who show high rates of relapse. Research into the comorbidity of these disorders has highlighted the role of adrenergic systems and the endogenous opioid system as targets for the link joining the two (Van Bockstaele et al., 2001, Smith and Aston-Jones, 2008). The BNST receives the largest projection of norepinephrine in the central nervous system, and serves as a relay between the cognitive-emotive brain centers and reward and stress nuclei, modulating critical aspects of addiction (McElligott and Winder, 2009). Given these important inputs, the BNST plays a key role in the reinstatement of seeking, conditioned place aversion to opiate withdrawal, anxiety-like behavior, and the affective component of pain (Poulin et al., 2009). Furthermore, plasticity within the BNST can be modulated by chronic stress (McElligott et al., 2010).

Lewis rats, in particular, have been used to study anxiety disorders and drug abuse due numerous observed properties such as high levels of self-administration of opiates (Sanchez-Cardoso et al., 2007), high baseline anxiety (Cohen et al., 2006), BNST-dependent generalized expression of fear (Duvarci et al., 2009), and elevated levels of norepinephrine released in the BNST to a stressor as compared to Sprague Dawley rats as measured by microdialysis (Pardon et al., 2002). Both the mesolimbic dopamine pathway and the BNST of naïve Lewis rats have been said to resemble Sprague Dawley rats which are opioid dependent (Beitner-Johnson et al., 1991, Guitart et al., 1992, Guitart and Nestler, 1993). Interestingly, recent studies have indicated that if the BNST of Lewis rats are lesioned, the animals no longer exhibit fear generalization and have lower anxiety (Duvarci et al., 2009). These observations also make them a good animal model for Post-Traumatic

Stress Disorder (PTSD). These previous observations lead to the need for a fundamental study of the total neurotransmitter content in both the BNST as well as the dopaminergic terminals in the striatum. These data indicate that the total amount of catecholamines synthesized and stored in both the dorsolateral striatum and BNST are significantly higher in these brain regions leading to the above mentioned phenotypes. Reasons for these differences could include increase in the amount of tyrosine hydroxylase or phosphorylated tyrosine hydroxylase, the enzyme used during the rate dependent step of catecholamine synthesis, or differences in the amount of enzymes which break down catecholamines after release or uptake, such as monoamine oxidase.

Tissue Content of Catecholamines in Ube3a$^{m-/p+}$ Mice

Angelman syndrome is a neurodevelopmental disorder characterized by intellectual disability, profound language impairment, seizures, and a propensity for a happy disposition (Steffenburg et al., 1996, Peters et al., 2004, Williams et al., 2006). Angelman Syndrome results from loss of function of the maternally-inherited *UBE3A* allele at the 15q11-q13 locus (Kishino et al., 1997). The *Ube3a* gene encodes a HECT domain E3 ubiquitin ligase (UBE3A, also known as E6AP) involved in protein degradation through the ubiquitin-proteasome pathway (Kishino et al., 1997, Sutcliffe et al., 1997). Behavioral experiments performed in the lab of Dr. Ben Philpot in the Department of Cell and Molecular Physiology on mice lacking the maternal copy of the *Ube3a* gene showed a decrease in cocaine induced motor sensitivity, as well as a decrease in the reward threshold of the animals during intracranial self-stimulation experiments (data not shown). Furthermore, FSCV studies showed an increase in the dopamine release in the NAc of the *Ube3a$^{m-/p+}$* animals compared to WT, but no difference in dopamine release in the dorsolateral striatum of the mice upon stimulation of the ventral tegmental area (VTA) or substantia nigra (SN) (data not shown).

These observations lead to the total tissue content analysis of *Ube3a*$^{m-/p+}$ as compared to WT animals to help determine the role UBE3A plays in these dopaminergic systems. Content analysis showed no difference between the two genotypes in terms of the dopamine or DOPAC content as well as no differences in the ratio of the DOPAC: DA. These findings support the assertion that UBE3A plays an integral, pathway-specific role in the release of dopamine in the mouse model of Angelman Syndrome. This role, however, is not directly associated with the synthesis or storage of dopamine in these presynaptic terminals. This is supported by the observation that there is no difference in the amount of tyrosine hydroxylase (TH) as determined by Western Blot (data not shown), or the total amount of TH positive cells in the VTA and SN (data not shown). This example shows how HPLC total tissue content determination can be used to discount possible hypotheses for observations in differences in catecholamine release in the striatum of genetically different animals, specifically, an Angelman Syndrome mouse model.

Tissue Content of 5-HT in Mice during Citalopram Administration

Serotonin is an important neurotransmitter that is involved in a myriad of functions including sleep, motivated social behaviors and most famously, depression (Petty et al., 1996). Selective serotonin reuptake inhibitors (SSRIs), such as citalopram are a common pharmacological treatment for depression, although the exact mechanism of their therapeutic action remains ambiguous (De Montigny, 1981, Sharp and Cowen, 2011). Furthermore, it has been hypothesized that changes in phasic and tonic levels of 5-HT, typically modulated by the 5-HT1a receptor, could be effected by SSRIs such as citalopram (Best et al., 2011). Recently, FSCV of 5-HT release in the SNr was completed by stimulation of the dorsal raphe nucleus (DRN) and the medial forebrain bundle (MFB) allowing for real-time measurement with a method with high spatial and temporal resolution (Hashemi et al., 2009, Hashemi et al., 2011). In these studies, acute administration of

citalopram showed an increase in the maximal measured concentration of 5-HT in the extrasynaptic space as well as a slowing of the uptake of 5-HT.

Work has since moved into studying the mechanisms of 5-HT release in the SNr in mice as opposed to rats. In order to study if acute treatment of animals with citalopram changes the synthesis or packaging of 5-HT in the SNr, HPLC determination of total tissue content was performed pre and post administration of citalopram. The data showed no difference in 5-HT content in the SNr 30 minutes post-injection. These data are supported by previously reported values which showed that while pharmacological administration of drugs changed binding of 5-HT to SERT, no change was seen in total tissue content of 5-HT (Callaghan et al., 2006). While there is an upward trend in the content of animals administered with citalopram chronically, these findings fall short of statistical significance and could be due to the location of the punches and the small size of the region. Given these observations, we can conclude that the changes in phasic 5-HT release are not due to differences in synthesis or packaging of 5-HT given acute administration of an SSRI, but rather the blockage of SERT itself. Furthermore, chronic inhibition of SERT does not lead to long-term changes in intracellular mechanisms governing the total content of 5-HT in the SNr.

Conclusion

In this chapter, a simple analytical tool, HPLC-ECD, is used in order to answer fundamental questions about the synthesis, storage, and total tissue content of neurotransmitters in various brain regions under different conditions. Differences in dopamine and norepinephrine content were observed when comparing different strains of rats showing the fundamental difference between the two, and these results were put into context in terms of how they are used as a model system for Post-Traumatic Stress Disorder and drug addiction. In a stark contrast, no differences were observed in mice lacking the

maternal copy of the *Ube3a* gene, a model mouse for Angelman Syndrome, although differences had been observed between the animals in both behavioral and FSCV experimentation. Lastly, 5-HT content in the SNr was determined to be no different between animals before or after treatment with citalopram, showing that this method can also be used not only to compare genetically different animals, but also for animals pre- and post-drug administration. Experiments such as these should always be conducted when studying genetically different animals and making comparisons so that data can be properly interpreted.

References

Beitner-Johnson D, Guitart X, Nestler EJ (1991) Dopaminergic brain reward regions of Lewis and Fischer rats display different levels of tyrosine hydroxylase and other morphine- and cocaine-regulated phosphoproteins. Brain Res 561:147-150.

Best J, Nijhout HF, Reed M (2011) Bursts and the efficacy of selective serotonin reuptake inhibitors. Pharmacopsychiatry 44 Suppl 1:S76-83.

Callaghan PD, Farrand K, Salem A, Hughes P, Daws LC, Irvine RJ (2006) Repeated administration of the substituted amphetamine p-methoxyamphetamine produces reductions in cortical 5-HT transporter binding but not 5-HT content, unlike 3,4-methylenedioxyamethamphetamine. Eur J Pharmacol 546:74-81.

Cohen H, Zohar J, Gidron Y, Matar MA, Belkind D, Loewenthal U, Kozlovsky N, Kaplan Z (2006) Blunted HPA axis response to stress influences susceptibility to posttraumatic stress response in rats. Biol Psychiatry 59:1208-1218.

De Montigny C (1981) Enhancement of the 5-HT neurotransmission by antidepressant treatments. J Physiol (Paris) 77:455-461.

Duvarci S, Bauer EP, Pare D (2009) The bed nucleus of the stria terminalis mediates inter-individual variations in anxiety and fear. J Neurosci 29:10357-10361.

Filipov NM, Stewart MA, Carr RL, Sistrunk SC (2007) Dopaminergic toxicity of the herbicide atrazine in rat striatal slices. Toxicology 232:68-78.

Guitart X, Beitner-Johnson D, Marby DW, Kosten TA, Nestler EJ (1992) Fischer and Lewis rat strains differ in basal levels of neurofilament proteins and their regulation by chronic morphine in the mesolimbic dopamine system. Synapse 12:242-253.

Guitart X, Nestler EJ (1993) Second messenger and protein phosphorylation mechanisms underlying opiate addiction: studies in the rat locus coeruleus. Neurochem Res 18:5-13.

Hadden N (1971) Basic liquid chromatography. [s.l.]: Varian Aerograph.

Hashemi P, Dankoski EC, Petrovic J, Keithley RB, Wightman RM (2009) Voltammetric detection of 5-hydroxytryptamine release in the rat brain. Anal Chem 81:9462-9471.

Hashemi P, Dankoski EC, Wood KM, Ambrose RE, Wightman RM (2011) In vivo electrochemical evidence for simultaneous 5-HT and histamine release in the rat substantia nigra pars reticulata following medial forebrain bundle stimulation. J Neurochem 118:749-759.

Kishino T, Lalande M, Wagstaff J (1997) UBE3A/E6-AP mutations cause Angelman syndrome. Nat Genet 15:70-73.

Lahdesmaki J, Sallinen J, MacDonald E, Kobilka BK, Fagerholm V, Scheinin M (2002) Behavioral and neurochemical characterization of alpha(2A)-adrenergic receptor knockout mice. Neuroscience 113:289-299.

McElligott ZA, Klug JR, Nobis WP, Patel S, Grueter BA, Kash TL, Winder DG (2010) Distinct forms of Gq-receptor-dependent plasticity of excitatory transmission in the BNST are differentially affected by stress. Proc Natl Acad Sci U S A 107:2271-2276.

McElligott ZA, Winder DG (2009) Modulation of glutamatergic synaptic transmission in the bed nucleus of the stria terminalis. Prog Neuropsychopharmacol Biol Psychiatry 33:1329-1335.

Mefford IN (1981) Application of high performance liquid chromatography with electrochemical detection to neurochemical analysis: measurement of catecholamines, serotonin and metabolites in rat brain. J Neurosci Methods 3:207-224.

Pardon MC, Gould GG, Garcia A, Phillips L, Cook MC, Miller SA, Mason PA, Morilak DA (2002) Stress reactivity of the brain noradrenergic system in three rat strains differing in their neuroendocrine and behavioral responses to stress: implications for susceptibility to stress-related neuropsychiatric disorders. Neuroscience 115:229-242.

Peters SU, Beaudet AL, Madduri N, Bacino CA (2004) Autism in Angelman syndrome: implications for autism research. Clin Genet 66:530-536.

Petty F, Davis LL, Kabel D, Kramer GL (1996) Serotonin dysfunction disorders: a behavioral neurochemistry perspective. J Clin Psychiatry 57 Suppl 8:11-16.

Poulin JF, Arbour D, Laforest S, Drolet G (2009) Neuroanatomical characterization of endogenous opioids in the bed nucleus of the stria terminalis. Prog Neuropsychopharmacol Biol Psychiatry 33:1356-1365.

Ramstrom M, Zuberovic A, Gronwall C, Hanrieder J, Bergquist J, Hober S (2009) Development of affinity columns for the removal of high-abundance proteins in cerebrospinal fluid. Biotechnol Appl Biochem 52:159-166.

Sanchez-Cardoso P, Higuera-Matas A, Martin S, del Olmo N, Miguens M, Garcia-Lecumberri C, Ambrosio E (2007) Modulation of the endogenous opioid system after morphine self-administration and during its extinction: a study in Lewis and Fischer 344 rats. Neuropharmacology 52:931-948.

Science AIfB (2009) Allen Mouse Brain Atlas [Internet]. In: http://mousebrain-maporg(Science, A. I. f. B., ed) Seattle (WA): Allen Institute for Brain Science.

Sharp T, Cowen PJ (2011) 5-HT and depression: is the glass half-full? Current Opinion in Pharmacology 11:45-51.

Smith RJ, Aston-Jones G (2008) Noradrenergic transmission in the extended amygdala: role in increased drug-seeking and relapse during protracted drug abstinence. Brain Struct Funct 213:43-61.

Steffenburg S, Gillberg CL, Steffenburg U, Kyllerman M (1996) Autism in Angelman syndrome: a population-based study. Pediatr Neurol 14:131-136.

Sutcliffe JS, Jiang YH, Galijaard RJ, Matsuura T, Fang P, Kubota T, Christian SL, Bressler J, Cattanach B, Ledbetter DH, Beaudet AL (1997) The E6-Ap ubiquitin-protein ligase (UBE3A) gene is localized within a narrowed Angelman syndrome critical region. Genome Res 7:368-377.

Van Bockstaele EJ, Menko AS, Drolet G (2001) Neuroadaptive responses in brainstem noradrenergic nuclei following chronic morphine exposure. Mol Neurobiol 23:155-171.

Vriend J, Dreger L (2006) Effects of haloperidol and melatonin on the in situ activity of nigrostriatal tyrosine hydroxylase in male Syrian hamsters. Life Sci 78:1707-1712.

Williams CA, Beaudet AL, Clayton-Smith J, Knoll JH, Kyllerman M, Laan LA, Magenis RE, Moncla A, Schinzel AA, Summers JA, Wagstaff J (2006) Angelman syndrome 2005: updated consensus for diagnostic criteria. Am J Med Genet A 140:413-418.

Zhang MY, Kagan N, Sung ML, Zaleska MM, Monaghan M (2008) Sensitive and selective liquid chromatography/tandem mass spectrometry methods for quantitative analysis of 1-methyl-4-phenyl pyridinium (MPP+) in mouse striatal tissue. J Chromatogr B Analyt Technol Biomed Life Sci 874:51-56.

Zhao XE, Suo YR (2008) Simultaneous determination of monoamine and amino acid neurotransmitters in rat endbrain tissues by pre-column derivatization with high-performance liquid chromatographic fluorescence detection and mass spectrometric identification. Talanta 76:690-697.

Chapter VI

Surface Analysis of Nafion Coated Ag/AgCl Reference Electrodes

Introduction

Fast-scan cyclic voltammetry (FSCV) is a powerful tool for studying *in vivo*, sub-second neurotransmitter dynamics (Ewing and Wightman, 1984, Kuhr et al., 1984, Hashemi et al., 2009, Park et al., 2009). Miniaturization of the electronics associated with FSCV has allowed correlation of transient dopamine concentration fluctuations with behavior in freely moving rats (Cheer et al., 2007, Owesson-White et al., 2008). These behavioral experiments necessitate a 'survival' surgery in which an electrical stimulating electrode, a guide cannula and a Ag/AgCl reference electrode are permanently implanted into the brain of a rat. After a recovery period (typically 4 days), the rat is placed in an operant chamber and a fresh carbon-fiber electrode is lowered into the brain for voltammetric recordings of dopamine during behavior. These recordings often yield cyclic voltammograms where the oxidation and reduction potentials associated with dopamine redox processes are 'shifted' with respect to *in vitro* recordings. This electrochemical shift, typically of + 0.2 to 0.3 V, can have dramatic effects on the voltammetric measurements. First, the identification of the species electrolyzed, which is based upon the position of the voltammetric peaks is confounded. Second, the sensitivity of the responses is altered because the voltammetric response to adsorbed species depends upon the potential limit of the voltage scan (Takmakov et al., 2010). These electrochemical shifts arise from a drift in response of the chronically implanted reference electrode because they are not seen with acute implantation (Garris and Wightman, 1994, Robinson et al., 2003).

Deterioration of probes permanently implanted in the brain is commonly seen in a variety of experiments (Rousche and Normann, 1998, Williams et al., 1999, Nicolelis et al., 2003), and the brain's response towards implanted devices has been well-documented (Stensaas and Stensaas, 1976, Smith et al., 1986, Szarowski et al., 2003, Polikov et al., 2005). When a foreign body is inserted into the tissue, a dense network of glial cells encapsulates the device, isolating it from the tissue in a process called gliosis or glial scarring (Kreutzberg, 1996, Turner et al., 1999, Biran et al., 2005). For FSCV measurements, the electrochemical shift affects the quantification of dopamine levels and reproducibility of substrate identity. In the past, we have offset the potential shift. While this approach is effective, it is desirable to prevent the shift from occurring so that the potentials employed in the brain are accurate.

Past research has focused on strategically shaping, texturing, coating or optimizing materials for devices to reduce tissue responses (Edell et al., 1992, Yuen and Agnew, 1995, Rousche et al., 2001, Nicolelis et al., 2003, George et al., 2005). In 1994, Moussy *et al.* found that the rapid subcutaneous degradation of Ag/AgCl could be prevented with Nafion modifications to the reference electrode surface (Moussy and Harrison, 1994). Here, their method was optimized and applied it to *in vivo* neurochemical FSCV by coating sintered Ag/AgCl electrodes with Nafion, and surface analysis of the electrodes was performed in order to analyze the surface after various implantation times in the brain. Scanning electron microscopy and energy dispersive x-ray spectroscopy (SEM-EDS) were performed to image the electrodes, and analyze the changes on the surface. SEM imaging showed buildup of tissue on uncoated electrodes while Nafion coated electrodes remained clean. Furthermore, EDS showed a gradual decrease in the Nafion coating over implantation time along with a more dramatic decrease in relative chlorine on the surface of bare electrodes, indicating a possible mechanism for the fouling of electrodes *in vivo*.

Experimental

Animals and Surgery

Surgery for voltammetric measurements of dopamine were performed as previously described (Phillips et al., 2003). Briefly, male Sprague-Dawley rats aged 90-120 days (275-350 g) (Charles River Labs., Raleigh, NC, USA) were anesthetized with urethane (1.5 g kg^{-1} rat weight) and affixed into a stereotaxic frame (Kofp instruments). Flat-skull surgical techniques were employed using coordinates from a stereotaxic atlas (Paxinos and Watson, 2007). A guide cannula (Bioanalytical Systems, West Lafayette, IL) was implanted above the nucleus accumbens (NAc) (stereotaxic coordinates relative to bregma: 2.2 mm anterior, 1.7 mm lateral) and a bipolar stimulating electrode (Plastics One, Roanoke, VA) was lowered into the medial forebrain bundle (MFB) (stereotaxic coordinates relative to bregma: 1.8 mm posterior, 1.7 mm lateral, 8.5 mm ventral). Reference electrodes (prepared as described below) were implanted in the contralateral hemisphere. Electrodes were stabilized with skull screws and cranioplastic cement. After voltammetry and impedance experiments, acetone was applied to the cement around the reference electrode in order to soften it. A small crater was drilled around the reference electrode pin so that it could be removed carefully from the tissue minimizing tissue damage. All surgical procedures were approved by the University of North Carolina Institutional Animal Care and Use Committee and in concordance with the NIH Guide for the Care and Use of Animals.

Fast-Scan Cyclic Voltammetry

Carbon-fiber microelectrodes were used for voltammetric recordings of dopamine. T-650 carbon fibers (Thornel, Amoco Corp., Greenville, SC) were aspirated into glass capillaries (AM Systems, Sequim, WA), pulled on a vertical pipette puller (model PE-22, Narishige Group, Tokyo, Japan), and cut to a length of 50-100 μm. An electrochemical waveform was applied to the electrode that scanned from -0.4 V to 1.3 V at a rate of 400 V

s^{-1} at 10 Hz. The holding potential of -0.4 V between voltammetric scans allows for adsorption of dopamine to the electrode. Waveform application, current monitoring, and stimulus application were performed using a customized version of the TH-1 software (ESA, Chelmsford, MA) written in LabVIEW (National Instruments, Austin, TX) with a custom built potentiostat (UEI, University of North Carolina Chemistry Department Electronics Facility) for waveform application. A DAC/ADC card (NI 6251 M, National Instruments) and a triggering card (NI 6711, National Instruments) were used to interface between the software and the instrument and the timing of the electrical stimulation with the waveform application.

Flow Injection Analysis

Flow injection analysis was used for *in vitro* calibration experiments (Kristensen et al., 1986). The carbon-fiber microelectrode was placed in the output of a six-port HPLC loop injector mounted on a two-position actuator (Rheodyne model 7010 valve and 5701 actuator), operated by a 12 V DC solenoid valve kit (Rheodyne, Rohnert Park, CA, USA). The apparatus enabled the introduction of a rectangular pulse of analyte to the microelectrode surface using a syringe infusion pump (Harvard Apparatus model 940, Hollison, MA, USA) at a flow rate of 2 mL/min. The flow injection buffer was constituted with the following: Trizma hydrochloride (15 mM), NaCl (140 mM), KCL (3.25 mM), $2H_2O$ CaCl (1.2 mM), H_20 NaH_2PO_4 (1.25 mM), Mg Cl_2 (1.2 mM) and Na_2 SO_4 (2.0 mM) all purchased from Sigma-Aldrich (St. Louis, MO, USA).

Nafion Coatings

Reference electrodes were fabricated using a modified procedure originally described by Moussy *et al.* (Moussy and Harrison, 1994). Sintered Ag/AgCl reference electrodes (E255A, In Vivo Metric, Healdsburg, CA) were mounted and soldered into conductive pins. The entirety of the electrode was dipped in 5% Nafion solution (Liquion-1105-MeOH, Ion Power, DE) for 10 seconds using a slow agitating motion. This coating

was allowed to dry for 30 minutes and the process was repeated for a total of 5 coatings. The electrodes were air dried overnight and then cured at 120 °C for 1 hour. Because of the toxic nature of the methanol solvent, the curing process at 120 °C is essential to ensure full evaporation of the methanol from the thick Nafion membrane.

SEM-EDS

Scanning electron microscopy and energy dispersive x-ray spectroscopy (SEM-EDS) was performed on an S-4700 Cold Cathode Field Emission Scanning Electron Microscope (Hitachi, Pleasanton, CA). SEM images were collected under high vacuum, using an excitation voltage of 20 kV. EDS data were collected using a Si (Li) detector and quantified using the INCA PentaFET -x3 software (Oxford Instruments, Concord, MA), and calibrated using 99% Cu. EDS spectra were collected at three distinct 300 x 300 μm locations on each electrode and the values for atomic % fluorine were averaged.

Results and Discussion

Electrochemical Shift in Electrochemical Peaks for Dopamine 4 Days after Implantation

FSCV experiments in behaving rats require a period of recovery after the surgery to implant the reference and stimulating electrodes. Within this 4-day period, chemical or physical processes occur around the reference electrode surface such that when dopamine is measured with a fresh carbon-fiber microelectrode, the oxidation and reduction potentials are 'shifted' with respect to their *in vitro* positions. Figure 6.1 illustrates this type of response in a freely moving rat that had undergone surgery 4 days previously. The color plot in panel (i) displays cyclic voltammograms collected at 10 Hz for 15 seconds in the NAc during an electrical stimulation (at 5 seconds) of the MFB. The time of the electrical stimulation is indicated with the black bar under the color plot. This electrically evoked response has previously been characterized anatomically, physiologically, chemically and

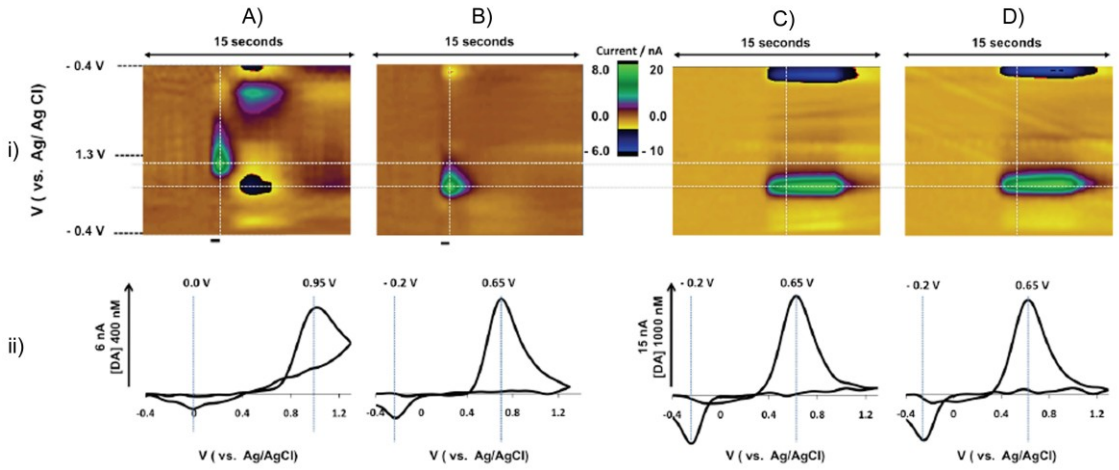

Figure 6.1. Chronically implanted references electrodes shift over time. (i) Color plots with potential on the y-axis plotted against time on the x-axis and the current response represented in false color. These plots represent (A) the signal obtained in the NAc of a freely-moving rat upon MFB stimulation (black bar under the color plot denotes the stimulation time and duration) 4 days after initial surgery. (B) The same signal after a - 0.3 V 'offset', (C) an *in vitro* injection of dopamine (1 μM) vs. a fresh Ag/AgCl reference electrode and (D) an *in vitro* injection of dopamine (1 μM) vs. the Ag/AgCl electrode explanted from the rat used in signal (A). (ii) (A)-(D) Representative cyclic voltammograms taken from the vertical white dashed lines.

pharmacologically to arise from neuronal release of dopamine (Kuhr et al., 1984). However, the peaks for this substance recorded *in vivo* do not occur at the same potential as those for authentic dopamine (1 μM) measured *in vitro* (Figure 6.1C) using a freshly fabricated Ag/AgCl electrode. This is also apparent in the corresponding cyclic voltammograms shown in panel (ii) of Figure 1. *In vivo*, the oxidation occurs at around 0.95 V instead of 0.65 V and the reduction occurs at 0.0 V instead of -0.2 V showing that a process at the implanted reference electrode has offset the potential of the applied waveform. Moreover, this change in waveform seems to enhance sensitivity to the pH changes that occur after the stimulation, making it more difficult to distinguish smaller dopamine signals. We have previously compensated for this by applying a counter potential offset as illustrated in Figure 6.1B where the horizontal white dashed lines show the position of the maximum oxidation with respect to the *in vitro* signal. In this example, the waveform was offset by -300 mV, which shifts the oxidation response to 0.65 V and the reduction to -0.2 V. This response then matches the *in vitro* response (Figure 6.1C).

Interestingly, the potential of this 'shifted' reference electrode is not permanently altered. To establish this, we removed the reference electrode from the rat's brain and used it as a reference electrode *in vitro* for dopamine measurements. Figure 6.1D shows that despite the shifted electrochemical response *in vivo,* the reference electrode yields an

electrochemically characteristic dopamine cyclic voltammogram that is not offset *in vitro.* Thus, the mechanisms leading to the electrochemical shifts are specific to the local environment around the reference electrode *in vivo*.

Prevention of Electrochemical Shift with Nafion-Coated Ag/AgCl Reference Electrodes

In our previous work, and in the example showed in Figure 6.1, we constructed Ag/AgCl reference electrodes by electroplating AgCl onto a silver wire (Phillips et al., 2003).

Because this resulted in a thin chloride layer, it may be particularly susceptible to an alteration in chemical composition when implanted in the brain. Thus, we used commercially available, sintered Ag/AgCl electrodes (E255A, In Vivo Metric, Healdsburg, CA). The Ag/AgCl is sintered in a mesh matrix, and a Ag wire is forced into the matrix to create the electrode that has a much thicker AgCl coating than the homemade reference electrodes. However, despite the thicker chloride layer, these electrodes also showed a potential shift of similar magnitude *in vivo* 4 days after implantation.

Moussy *et al.* previously described Nafion coatings on Ag/AgCl reference electrodes that prevented the degradation of their electrochemical performance (Moussy and Harrison, 1994). We have previously utilized Nafion extensively in our electrochemical recordings (Kristensen et al., 1987, Wiedemann et al., 1990, Hashemi et al., 2009) therefore we optimized their coating technique in an attempt to stabilize the potential of our reference electrodes. The sintered electrodes were used because their rough surface is ideal for adherence of polymer coatings. The electrodes were dipped 5 times in 5% Nafion solution for 10 seconds with a slow agitating motion and each coating was allowed to dry for 30 minutes. These electrodes were dried in air overnight and then cured at 120 °C for 1 hour. To test their stability we performed experiments where we implanted both Nafion and uncoated reference electrodes into the brains of rats who were then allowed to recover for 7, 14, and 28 days. After these periods, the rats were anesthetized, an acute reference electrode and carbon fiber electrode were implanted into their brain and dopamine release was compared with recordings using each of the 3 reference electrodes (acute, Nafion-coated, permanently implanted and bare, permanently implanted).

Figure 6.2A (i) shows a color plot of the dopamine response in the NAc of an anesthetized animal upon MFB stimulation when the potential was applied versus the acutely implanted Ag/AgCl reference electrode. Figures 6.2B (i) and 2C (i) show

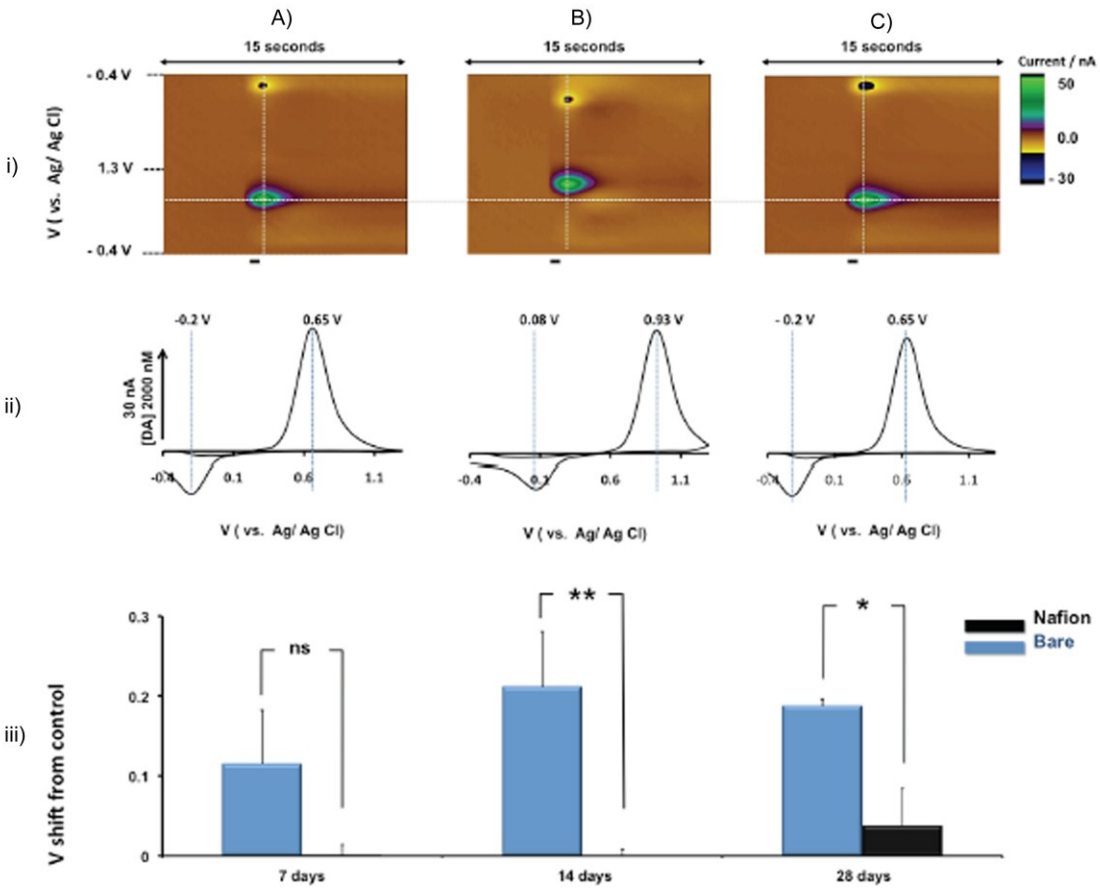

Figure 6.2. Nafion coatings prevent electrochemical shifts upon chronic implantation. (i) Color plots with potential on the y-axis plotted against time on the x-axis and the current response represented in false color. These plots represent (A) a dopamine signal in the NAc of an anesthetized rat upon MFB stimulation (stimulation time and duration noted by black bar under the plot) vs. an acutely implanted Ag/AgCl reference electrode, (B) a dopamine signal in the same rat vs. a bare electrode implanted for 7 days, (C) a dopamine signal in the same vs. a Nafion-coated electrode implanted for 7 days. (ii) (A) –(C) Representative cyclic voltammograms taken from the vertical white dashed lines. (iii) Averaged volts shifted from an acutely implanted Ag/AgCl reference electrode for bare (blue) and Nafion-coated (black) electrodes for 7, 14 and 28 days (n=6 per group (18 in total ± SEM). Results were analyzed using a two-way ANOVA showing a significant difference in potential shift between Bare and Nafion electrodes ($p<0.001$) and post-tests to compare groups at the different time points, *$p<0.05$, **$p<0.01$.

comparisons of this same response, at the same carbon-fiber microelectrode in the same rat, however, vs. bare (B) and a Nafion-coated (C) chronically implanted reference electrodes that had been implanted for 7 days. Panel (ii) shows the corresponding cyclic voltammograms. As before, the bare electrode displays shifted oxidation and reduction peaks (0.93 V and 0.08 V respectively); however, the Nafion-coated reference electrode prevents this effect. The positions of the oxidation and reduction peaks are maintained and correlate not only with the acutely implanted reference electrode, as indicated by the horizontal white dashed line, but also to an *in vitro* experiment (0.65 V and -0.2 V respectively). This effect is maintained over multiple days. Figure 6.2 (iii) shows a histogram that compares dopamine potential shifts between acutely implanted reference electrodes and bare (blue) and Nafion-coated (black) electrodes that have been implanted into the brain for 7, 14 and 28 days (n=6 for each group (18 in total) ± SEM). The bare electrodes display shifts in all cases, most robustly after 28 days as evidence by the small error margin. The Nafion coated electrode reduces this shift however. We analyzed the shifts in peak potential using a two-way ANOVA, with appropriate post-tests, and found that Nafion coatings had a significantly different behavior than the bare electrodes on potential over time ($P<0.001$). Using the post-tests, it was determined that there was no significant difference between the groups after 1 week implantation ($p>0.05$), but a significant difference after two and four weeks of implantation ($p<0.01$ and $p<0.05$, respectively). We can therefore increase the stability of the reference electrodes robustly and significantly for up to 28 days using this technique.

Surface Analysis of Chronically Implanted Reference Electrodes

To test the idea of whether or not cells adsorb to the bare electrode surface to a larger extent that to the Nafion surface, scanning electron microscopy (SEM) and energy dispersive x-ray spectroscopy (EDS) was performed on reference electrodes after they were

removed from tissue. Figure 6.3 shows SEM images of bare (i) and Nafion coated (ii) electrodes before implantation (A), after 7 days (B), 14 days (C), or 28 days (D) in the rat brain. Before implantation, there is a clear visual difference between the bare electrode and the Nafion coated electrodes. The bare electrodes have a coarse appearance due to the sintered Ag/AgCl surface, while the Nafion coated electrodes are smooth. The non-polar coating gives the surface a shiny appearance and is easily distinguishable from the Ag/AgCl. As implantation time is increased, a build-up of large plaques is apparent on the bare electrode surface; this is particularly striking after 28 days (B) and is highlighted with the focused image in (C). In contrast, the Nafion-coated surfaces (ii) remain free of plaques. This is consistent with the histological data that shows that the cells remain intact in the tissue and indeed with the voltammetric data that shows no electrochemical shifts. However, as implantation time is increased up to 28 days (B), the Nafion-coated electrode resembles a bare electrode, showing that the Nafion coating has degraded. The 28-day marker is again consistent with the voltammetric data that shows a small percentage of electrodes that shift after 28 days and with the histological data that shows a rough surface lesion around the Nafion-coated electrode's implant site in tissue.

We next chemically analyzed three distinct sites on the electrode's surface with EDS. EDS displays high spatial resolution with an ability to measure the atoms present microns below the outermost surface. Hence, we can observe the Ag present under the Nafion coatings. Figure 6.4 shows representative EDS spectra for (A) a bare electrode before implantation, (B) a Nafion coated electrode before implantation, (C) a bare electrode after 14 days implantation, and (D) a Nafion coated electrode after 14 days implantation. Peaks were quantified as the atomic percent of each atom observed. The Nafion coated electrodes display the same peaks positions as the bare electrodes (Ag doublet at 3 keV, Cl peaks at 0.1 and 2.8 keV), and in addition have peaks for carbon (peak at 0.3 keV), sulfur

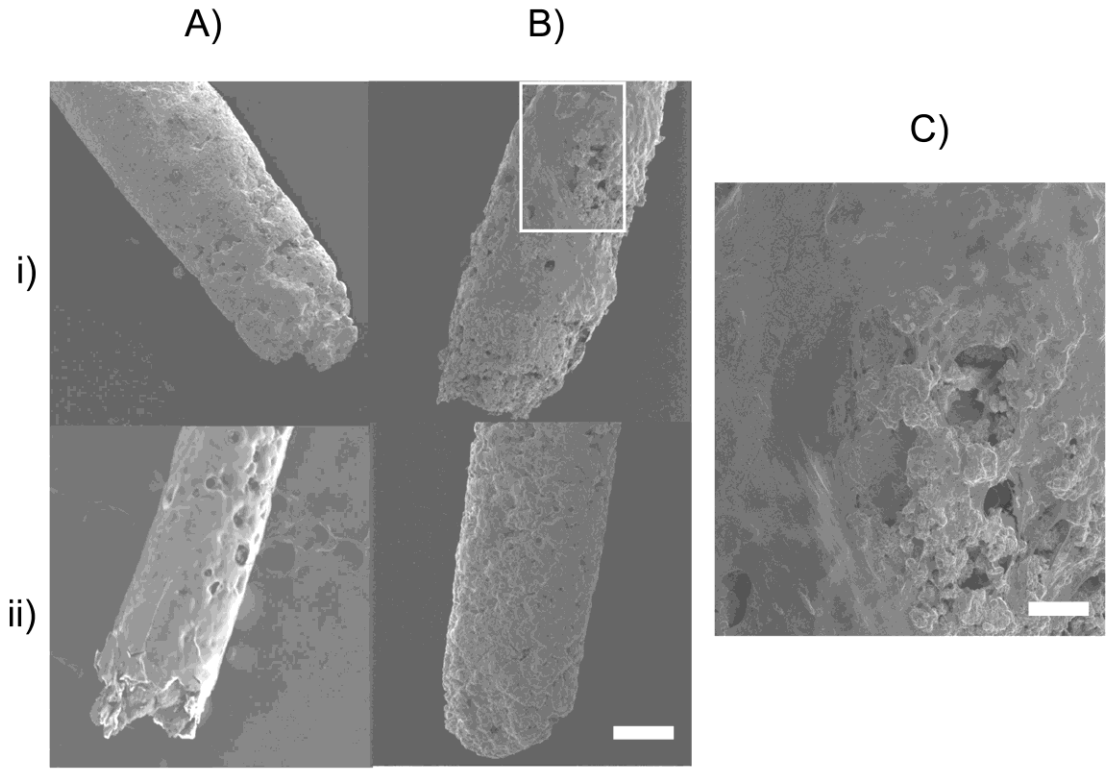

Figure 6.3. SEM images of chronically implanted electrodes. Representative scanning electron microscopy images of bare (i) and Nafion-coated (ii) electrodes before implantation in the brain (A) and after 28 days implantation (B) in the brain and (C) zoomed section as outlined by the white box. Scale bar A-B 500 μM, scale bar (C) 100 μm.

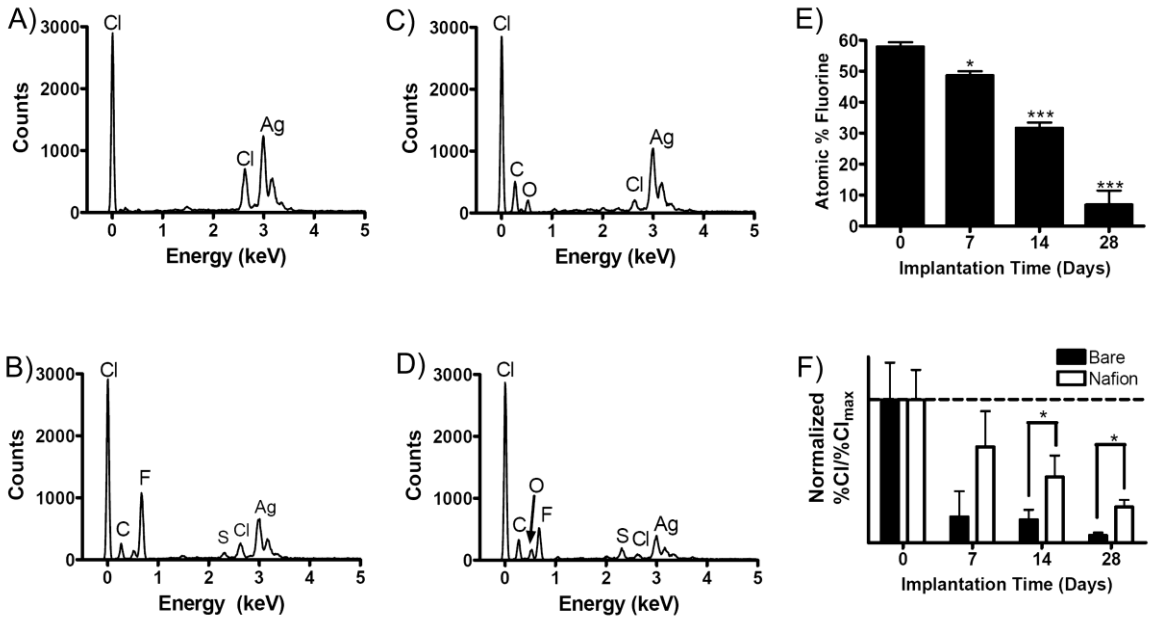

Figure 6.4. EDS spectra of chronically implanted electrodes. Representative EDS spectra for Ag/AgCl reference electrodes uncoated before brain implantation (A), Nafion-coated before brain implantation (B), uncoated after 2 weeks brain implantation (C), and Nafion-coated after 2 weeks brain implantation (D). Peaks are labeled indicating the atom they represent. (E) Atomic percent fluorine on the surface of Nafion-coated electrodes after 0, 7, 14, and 28 days brain implantation (*$p<0.05$, ***$p<0.001$, one-way ANOVA with appropriate post-hoc test compared to 0 days). (F) Normalized, atomic percent chlorine on the surface of Nafion-coated (white) and bare (black) electrodes after 0, 7, 14, and 28 days brain implantation (student's t-test were performed on unpaired data, *$p<0.05$ was taken as significant).

(peak at 2.3 keV) and fluorine (peak at 0.7 keV), key components of the non-polar per-fluorinated coating. After 14 days, additional peaks can be observed on the bare electrodes including carbon and oxygen (peak at 0.6 keV). This confirms that the compositions of the hard plaques apparent in Figure 6.3 are organic, providing yet more evidence that cells are adsorbing to the bare electrode surface. We can quantify the Nafion levels on the electrode surface by measuring the atomic percent of fluorine as implant time was increased. Figure 6.2E shows that the content of fluorine on the surface of the electrode is around 60% before implantation. After 7 days, the content is around 50% ($p<0.05$ compared to pre-implantation). At 14 days, the fluorine content is around 30% ($p<0.001$ compared to pre-implantation) and dramatically lower after 28 days at around 7% ($p<0.001$ compared to pre-implantation). These data quantifiably support the visual observation from Figure 6.3 that the Nafion coating becomes unviable after 28 days.

Conclusion

These studies support the notion that the Nafion coatings on reference electrodes are stable up to 28 days in the rat brain. Voltammetric signals both in vitro and in vivo show that electrochemical shift of the signal can be eliminated by coating the reference electrodes with a thick layer of Nafion to protect it. Cell adsorption onto the reference electrodes is consistent with the loss of chlorine on the surface and subsequently with the electrochemical shift. Viable Nafion coatings prevent cell adsorption, maintaining the chlorine layer, hence preventing electrochemical shifts.

Dr. Parastoo Hashemi is gratefully acknowledged for her contribution to the work of studying the voltammetric signal before and after Nafion coating the electrodes.

References

Biran R, Martin DC, Tresco PA (2005) Neuronal cell loss accompanies the brain tissue response to chronically implanted silicon microelectrode arrays. Exp Neurol 195:115-126.

Cheer JF, Aragona BJ, Heien ML, Seipel AT, Carelli RM, Wightman RM (2007) Coordinated accumbal dopamine release and neural activity drive goal-directed behavior. Neuron 54:237-244.

Edell DJ, Toi VV, McNeil VM, Clark LD (1992) Factors influencing the biocompatibility of insertable silicon microshafts in cerebral cortex. IEEE Trans Biomed Eng 39:635-643.

Ewing AG, Wightman RM (1984) Monitoring the stimulated release of dopamine with in vivo voltammetry. II: Clearance of released dopamine from extracellular fluid. J Neurochem 43:570-577.

Garris PA, Wightman RM (1994) Different kinetics govern dopaminergic transmission in the amygdala, prefrontal cortex, and striatum: an in vivo voltammetric study. J Neurosci 14:442-450.

George PM, Lyckman AW, LaVan DA, Hegde A, Leung Y, Avasare R, Testa C, Alexander PM, Langer R, Sur M (2005) Fabrication and biocompatibility of polypyrrole implants suitable for neural prosthetics. Biomaterials 26:3511-3519.

Hashemi P, Dankoski EC, Petrovic J, Keithley RB, Wightman RM (2009) Voltammetric detection of 5-hydroxytryptamine release in the rat brain. Anal Chem 81:9462-9471.

Kreutzberg GW (1996) Microglia: a sensor for pathological events in the CNS. Trends Neurosci 19:312-318.

Kristensen EW, Kuhr WG, Wightman RM (1987) Temporal characterization of perfluorinated ion exchange coated microvoltammetric electrodes for in vivo use. Anal Chem 59:1752-1757.

Kristensen EW, Wilson RL, Wightman RM (1986) Dispersion in Flow-Injection Analysis Measured with Microvoltammetric Electrodes. Analytical Chemistry 58:986-988.

Kuhr WG, Ewing AG, Caudill WL, Wightman RM (1984) Monitoring the stimulated release of dopamine with in vivo voltammetry. I: Characterization of the response observed in the caudate nucleus of the rat. J Neurochem 43:560-569.

Moussy F, Harrison DJ (1994) Prevention of the rapid degradation of subcutaneously implanted Ag/AgCl reference electrodes using polymer coatings. Anal Chem 66:674-679.

Nicolelis MA, Dimitrov D, Carmena JM, Crist R, Lehew G, Kralik JD, Wise SP (2003) Chronic, multisite, multielectrode recordings in macaque monkeys. Proc Natl Acad Sci U S A 100:11041-11046.

Owesson-White CA, Cheer JF, Beyene M, Carelli RM, Wightman RM (2008) Dynamic changes in accumbens dopamine correlate with learning during intracranial self-stimulation. Proc Natl Acad Sci U S A 105:11957-11962.

Park J, Kile BM, Wightman RM (2009) In vivo voltammetric monitoring of norepinephrine release in the rat ventral bed nucleus of the stria terminalis and anteroventral thalamic nucleus. Eur J Neurosci 30:2121-2133.

Paxinos G, Watson C (2007) The Rat Brain in Stereotaxic Coordinates: Elsevier.

Phillips PE, Robinson DL, Stuber GD, Carelli RM, Wightman RM (2003) Real-time measurements of phasic changes in extracellular dopamine concentration in freely moving rats by fast-scan cyclic voltammetry. Methods Mol Med 79:443-464.

Polikov VS, Tresco PA, Reichert WM (2005) Response of brain tissue to chronically implanted neural electrodes. J Neurosci Methods 148:1-18.

Robinson DL, Venton BJ, Heien ML, Wightman RM (2003) Detecting subsecond dopamine release with fast-scan cyclic voltammetry in vivo. Clin Chem 49:1763-1773.

Rousche PJ, Normann RA (1998) Chronic recording capability of the Utah Intracortical Electrode Array in cat sensory cortex. J Neurosci Methods 82:1-15.

Rousche PJ, Pellinen DS, Pivin DP, Jr., Williams JC, Vetter RJ, Kipke DR (2001) Flexible polyimide-based intracortical electrode arrays with bioactive capability. IEEE Trans Biomed Eng 48:361-371.

Smith GM, Miller RH, Silver J (1986) Changing role of forebrain astrocytes during development, regenerative failure, and induced regeneration upon transplantation. J Comp Neurol 251:23-43.

Stensaas SS, Stensaas LJ (1976) The reaction of the cerebral cortex to chronically implanted plastic needles. Acta Neuropathol 35:187-203.

Szarowski DH, Andersen MD, Retterer S, Spence AJ, Isaacson M, Craighead HG, Turner JN, Shain W (2003) Brain responses to micro-machined silicon devices. Brain Res 983:23-35.

Takmakov P, Zachek MK, Keithley RB, Walsh PL, Donley C, McCarty GS, Wightman RM (2010) Carbon microelectrodes with a renewable surface. Anal Chem 82:2020-2028.

Turner JN, Shain W, Szarowski DH, Andersen M, Martins S, Isaacson M, Craighead H (1999) Cerebral astrocyte response to micromachined silicon implants. Exp Neurol 156:33-49.

Wiedemann DJ, Basse-Tomusk A, Wilson RL, Rebec GV, Wightman RM (1990) Interference by DOPAC and ascorbate during attempts to measure drug-induced changes in neostriatal dopamine with Nafion-coated, carbon-fiber electrodes. J Neurosci Methods 35:9-18.

Williams JC, Rennaker RL, Kipke DR (1999) Long-term neural recording characteristics of wire microelectrode arrays implanted in cerebral cortex. Brain Res Brain Res Protoc 4:303-313.

Yuen TG, Agnew WF (1995) Histological evaluation of polyesterimide-insulated gold wires in brain. Biomaterials 16:951-956.